GLOBAL NET-TO-GROSS UNCERTAINTY ASSESSMENT AT RESERVOIR APPRAISAL STAGE

A DISSERTATION
SUBMITTED TO THE DEPARTMENT OF ENERGY
RESOURCES ENGINEERING
AND THE COMMITTEE ON GRADUATE STUDIES
OF STANFORD UNIVERSITY
IN PARTIAL FULFILLMENT OF THE REQUIREMENTS
FOR THE DEGREE OF
DOCTOR OF PHILOSOPHY

Amisha Maharaja

June 2007

I certify that I have read this dissertation and that, in my opinion, it is fully adequate in scope and quality as a dissertation for the degree of Doctor of Philosophy.

(Andre Journel) Principal Adviser

I certify that I have read this dissertation and that, in my opinion, it is fully adequate in scope and quality as a dissertation for the degree of Doctor of Philosophy.

(Jef Caers)

I certify that I have read this dissertation and that, in my opinion, it is fully adequate in scope and quality as a dissertation for the degree of Doctor of Philosophy.

(Tapan Mukerji)

Approved for the University Committee on Graduate Studies.

Abstract

Net-to-gross (NTG) is the fraction of reservoir volume occupied by hydrocarbon-bearing rocks. It is a global attribute and as such no replicate of it can be found over the reservoir. An estimate of global NTG is obtained from wells, but this estimate depends heavily on the location of the few wells available. If these wells were located elsewhere the NTG estimate would have been different. Wells at reservoir appraisal stage are few because they are expensive, and they tend to be preferentially located in high pay zones. Consequently, any naive estimate of NTG from these wells is likely to over-estimate the global NTG.

Since new wells cannot be drilled from the real reservoir to assess uncertainty, synthetic wells are re-sampled from stochastic realizations of reservoir facies which are conditioned to all available data. Stochastic realizations, however, require a prior knowledge of the structural model and of a global NTG, which are both highly uncertain at appraisal stage. Hence, we propose to consider alternative structural models, and to randomize the global NTG value corresponding to each structural model. The structural model is randomized by considering alternate geological interpretations that fit all existing data. The global NTG associated with each particular geological interpretation is randomized by considering a probability distribution of global NTG value, which represents both the possible range of NTG values and the prior probability of those NTG values. Such a distribution can be obtained by pooling together NTG values of previously discovered reservoirs that are deemed analogous to the newly discovered reservoir. This prior probability distribution is then updated into a posterior probability distribution given the NTG estimate observed from the actual reservoir data.

To perform this update, the prior NTG distribution is first discretized into M classes. For each class a representative facies realization is simulated from each geological scenario. All such realizations must honor all available data. Synthetic data sets are re-sampled from this realization by following the initial drilling strategy. The NTG estimates computed from these synthetic data sets provide the likelihood of observing the initial NTG estimate in a simulated reservoir with that global NTG. Then using Bayes rule, the prior probability of the global reservoir NTG being in any given class m is updated given the observed NTG estimate. Repeating this procedure for all prior global NTG classes provides the posterior probability distribution of global NTG. This posterior global NTG distribution is a model of uncertainty specific to the reservoir under study and to a particular geological scenario. Posterior distributions corresponding to different geological scenarios can be combined into a single posterior, but this calls for a prior probability of occurence of each scenario.

Tests on a synthetic reservoir reveal that both initial NTG estimate and prior NTG distribution have a large impact on the posterior NTG distribution. A biased NTG estimate would result in non-representative posterior uncertainty intervals. Due to its exhaustive coverage, incorporating seismic data helps correct the bias due to preferential well location. In addition, using a prior NTG distribution based on relevant historical information helps obtaining more representative posterior NTG uncertainty models. Posterior statistics also depend on the discretization of the prior NTG distribution. An early sensitivity analysis should be performed to determine the appropriate level of discretization.

Application of the workflow to an actual deep-water reservoir showed that the impact of the geological scenario on the posterior NTG distribution is larger when the facies geometries are very different. The range of the posterior distribution is always smaller than that of the prior distribution. The shape of the prior distribution impacts the posterior probability. With each additional well the posterior uncertainty intervals shrink, indicating that more data reduces uncertainty. The case study also revealed challenges encountered in practice, such as re-sampling from domains of varying thickness and deducing facies proportions from a global NTG value in the multiple facies case.

The proposed workflow is demanding because it requires more decisions and modeling effort than any of the existing approaches. But in return it provides more informed models of NTG uncertainty reflecting a company's geological expertise and historical information. These valuable sources of information must be incorporated when assessing NTG uncertainty, especially at appraisal stage when well data is sparse and the stakes are high. There is no such thing as an objective or true model of uncertainty since each model is necessarily a result of multiple subjective decisions that go into building that model.

Acknowledgements

First and foremost, my deepest gratitude goes to Prof. André Journel, who has been my advisor throughout my graduate studies. I was trained as a geologist, but had a penchant for numbers. His article on stochastic modeling and geostatistics in an AAPG publication inspired me to pursue a degree in geostatistics at Stanford. It has been an honor to have him as my advisor. I greatly appreciate his research guidance and mentorship.

Second, I would like to thank Prof. Jef Caers, who has had a strong influence on me since the very beginning. He is one of the best teachers I have ever had. His comments and suggestions for improving my Ph.D. research were greatly appreciated.

This research would not have been possible without the financial support of Chevron Energy Technology Corporation. I am also thankful to Chevron for providing the data set for my thesis. Special thanks goes to Dr. Sebastien Strebelle for his advise, constant support, and enthusiam.

I would like to acknowledge the pivotal role that Dr. Guillaume Caumon played in this research, while he was a post-doc at Stanford. His advise and tutoring with Gocad during my two month stay in Nancy has been essential for the completion of this thesis.

I would like to thank all my professors at Stanford, especially Steve Graham and the ERE professors - Margot Gerritsen, Roland Horne, Lou Durlofsky, Tony Kovscek, and Khalid Aziz. I am honored to have learnt petroleum engineering from such a world class faculty. I am also thankful to Ginni Savalli and Thuy Nguyen of the ERE department; their hard work and dedication has ensured a smooth stay at Stanford.

The SCRF research group has been my home for the past five years. It has provided a thriving environment for research and passionate discussions. I have met many wonderful and talented people here during these years, and it has been a privilege to have been a part of this group. Melton Hows, Sunderrajan Krishnan, Joe Voelker, Burch Arpat, Tuanfeng Zhang, Jenya Polyakova have all enriched my Stanford experience. Special thanks goes to Jianbing Wu and Nicolas Remy for their help and guidance with SGeMS.

I would especially like to thank my friends Scarlet Castro, Lisa Stright, and Whitney Trainor for their friendships. Each one of you are amazing individuals and I have been fortunate to have met you.

Special thanks goes to my dear friend and mentor, Minoo Mehta, who has encouraged me to fly higher and push my boundaries. I would not have been at Stanford without his encouragement and support.

My love and gratitude goes to my family, especially to my parents, Chetna and Dipak Maharaja. I owe my academic achievement to their love and efforts towards my education and development since my first day at school. I thank my brother Arpit for his love and support. I have been lucky to have four loving grandparents, who often have had more faith in me than I did myself. I will especially miss Sudha ba and Shanti dada (daddu), both of whom I lost during the last year of my Ph.D. To my parents and grandparents, I dedicate this thesis.

I would also like to thank the Boucher family for their love and companionship. We have had some really great times while hiking, biking, skiing, snowshoeing and camping together. I am fortunate to have such a wonderful new family and I look forward to many more good times ahead.

Last, but not the least, my deepest love goes to Alexandre Boucher, who has been my partner for most of my time at Stanford, and luckily for me, will be my partner for life. He has been there for me, during the ups and the downs, and I thank him for his steady love, support and encouragement.

Contents

List of Tables

List of Figures

Chapter 1

Global uncertainty assessment

1.1 Introduction

When a new hydrocarbon reservoir is discovered, many factors influence the decision of whether to develop or abandon that reservoir. These factors include the Hydrocarbons in Place (HIP), the location of the reservoir (e.g. deep water or shallow water), the type of hydrocarbon (e.g. oil or gas), the demand for that hydrocarbon, the price of the hydrocarbon, etc. Many of these factors are determined by the existing economic conditions, while others are a direct result of the geological setting. Due to the high costs and risks associated with hydrocarbon exploration, it is not enough that the exploration well confirms the presence of hydrocarbons. To justify the costs of developing a newly discovered reservoir, it is crucial to know early on the spatial and uncertainty distribution of HIP in the reservoir.

HIP or more specifically Oil in Place (OIP) is given by:

$$OIP = V * NTG * \phi * S_o \tag{1.1}$$

where V is the reservoir volume, NTG is the net-to-gross ratio, ϕ is the average porosity of the reservoir quality rock, and S_o is the oil saturation. To obtain the uncertainty about OIP, one must assess the uncertainty about each of these quantities and combine them accounting for any dependence between them. Net-to-gross (NTG)

is defined as the ratio of volume of pay rock to the gross reservoir volume. Pay rock, also referred to as net pay, pay sand or pay zone, is defined as the local reservoir interval that contains economically producible hydrocarbons. The overall interval in which pay sections occur is the gross pay; the smaller portions of the gross pay that meet local criteria for pay (such as minimum porosity, permeability and hydrocarbon saturation) are net pay.

The first step in reserve computation is to define the gross reservoir volume. Then, the fraction of this gross volume that is occupied by pay rocks is computed, followed by the porosity, permeability and oil saturation of the pay rocks. Reservoir volume is typically obtained from interpretation of 3D seismic data. Major faults and bounding surfaces are identified by tracing amplitude peaks on sections of seismic amplitude. This demarkation is prone to interpretation errors, which is a source of volume uncertainty. The resolution of the seismic data is another issue; surface seismic surveys have limited horizontal and vertical resolutions, both of which decrease with depth.

For reserve computation, discretization of the reservoir volume is an equally consequential decision. Changing the horizontal and vertical grid resolution can affect the reserve estimates. For instance, if the vertical grid size is larger then the vertical well log resolution, then only an averaged facies value can be assigned to the grid blocks that are colocated with the well log; this would result in different facies proportions, hence different NTG estimate. For accurate reserve computation, it is better to adopt a fine grid resolution, both horizontally and vertically. Grid resolution can be guided by the average size of the geological features being modeled. The vertical resolution can also be taken from the smallest vertical resolution of available vertical data, for instance well log data. At appraisal stage, the grid resolution is only limited by the corresponding computation cost associated with simulation of facies and petrophysical properties, which is computationally less expensive than flow simulation.

A major source of uncertainty in volume computation is related to uncertainty in time-to-depth conversion (Sheriff and Geldart, 1995). In simple terms, seismic amplitude is a response of acoustic waves reflected and refracted through the reservoir rocks and fluids. Consequently, the seismic response is originally recorded in the time

domain. Reservoir models are built in the depth domain. To convert seismic signals from time to depth domain, many assumptions must be made about the types and distribution of reservoir rocks and fluids, their acoustic properties such as density and velocity, the nature of overburden, etc. Each of these parameters are highly uncertain. Inaccurate modeling of these parameters leads to inaccurate time-to-depth conversion. Great strides have been made in seismic data processing, however it still remains largely deterministic. Some headway is being made in accounting for some of these sources of uncertainty through a stochastic approach (Clapp, 2001, 2003).

Reservoir volume and NTG have the largest impact on reserve computations, hence the corresponding uncertainties should be carefully assessed before proceeding into elaborate porosity and saturation models. Volume uncertainty is directly related to seismic processing and interpretation, which is beyond the scope of this research. This research focuses on the second most consequential uncertainty, that related to reservoir NTG.

Difference between local and global uncertainty assessment should be noted. Net-to-gross is a global parameter, i.e. it has a single value over the entire reservoir. Unlike a local parameter, it has no replicate. Geostatistical simulation techniques aim at assessing the local uncertainty at any unsampled location in the reservoir, but require global parameters such as the facies global proportions and variograms, which are themselves uncertain. For instance, sequential indicator simulation (Goovaerts, 1997) of two rock types produces a set of simulated images of the spatial distribution of these two rock types, that all globally honor a prior target proportion or NTG value. The variations of NTG observed from one realization to another are just ergodic fluctuations around this target, caused due to the finite size of simulation field. Such ergodic fluctuations do not account for the uncertainty about the target input for NTG. Characterization of local uncertainty is useful for well planning and development. But at the appraisal stage the top priority is to determine if the reservoir is worth the risk, given the uncertainty in OIP which includes that on NTG.

1.2 Literature review

The global NTG of any reservoir is a single, but unknown value. The uncertainty about this NTG value stems from our limited knowledge about it. In subsurface resource exploitation, the direct data provide a very small window into the actual field; these data tend to be sparse and they have a much smaller volume support than the domain to be exploited. Due to this sparse sampling and support difference, the global estimates derived from these data are unlikely to be accurate representations of the true global value, unless the subsurface heterogeneity is extremely simple. Such simple cases are exceptions rather than the rule as proven repeatedly by modern 3D seismic imaging.

The objective of drilling wells during exploration stage is generally to confirm presence or absense of oil-bearing reservoir rocks. Thus, such wells are often preferentially drilled in the high pay zones, as determined from seismic data. The wells may be clustered if they were drilled from the same offshore platform. This combination of sparse and preferentially located data can result in an overly optimistic NTG estimate biased towards higher values. It is critical to correct for the biased well estimate by utilizing other data, such as seismic data which provides a quasi-exhaustive spatial coverage.

A global parameter (a) like NTG by definition has no replicate. We have an estimate ($a^\star$) of this global parameter from local data (d). The classical bootstrap method proposed by Efron (1979) is well-known method for assessing uncertainty about a global parameter estimate $a^\star$. It consists of drawing K independent synthetic data sets $D = d_k; k = 1, \ldots, K$ by re-sampling with replacement from the set of actual observed data d_0. The same estimation algorithm is applied on the K synthetic sets to obtain confidence intervals on the global parameter under study. The goal of this technique is to assess the uncertainty on sample statistics given an alternative, but equivalent, sample group from the same original data. This sampling is done with replacement, hence removing any spatial correlation that may exist between the data. Such procedure is not appropriate in earth sciences as the sequence of data along a well is not random; it was produced by specific geologic events, hence the data are

spatially correlated.

The approach of Haas and Formery (2002) is also founded on the data independence hypothesis. In the case of facies proportions, if the facies data are independently drawn from the reservoir, they may be assumed to follow a multinomial distribution. Let $\mathbf{x}$ be the vector of facies proportions and let $\mathbf{n}$ denote a vector of facies samples observed along the well(s). The distribution $p_{\mathbf{x}}(n)$ follows a multinomial law. Haas and Formery (2002) show analytically that if the prior probability of the facies proportions is uniform or Dirichlet, then the probability distribution of the unknown facies proportions is also Dirichlet. The parameters of this distribution are obtained by Bayes inversion as:

$$f_{\mathbf{n}}(\mathbf{x}) = \frac{p_{\mathbf{x}}(\mathbf{n}) \times f_0(\mathbf{x})}{p_0(\mathbf{n})} \tag{1.2}$$

where, $f_{\mathbf{n}}(\mathbf{x})$ is the pdf of proportion vector $\mathbf{x}$ given $\mathbf{n}$, $f_0(\mathbf{x})$ is the prior pdf of proportion vector $\mathbf{x}$, and $p_0(\mathbf{n})$ is the prior pdf of the number vector $\mathbf{n}$.

Biver et al. (2002) have applied this methodology to assess uncertainty about global facies proportions in a field at the appraisal stage. They propose to account for spatial dependency by declustering the data using a variogram model. However, this is questionable because (1) such variogram model is necessarily arbitrary, (2) the observed proportions do not follow a multinomial distribution if the data are spatially correlated. As discussed earlier, independence hypotheses are not applicable in earth sciences where data are spatially correlated. Ignoring spatial dependency and data redundancy is likely to produce too narrow uncertainty ranges. Bitanov and Journel (2004) have shown that both classical bootstrap and Dirichlet approach could indeed lead to over-optimistic (narrow) confidence intervals. Also, both classical bootstrap and the Dirichlet approaches assume that the data are unbiased, representative of the global NTG value. The estimate of reservoir NTG obtained from wells clearly depends on the location of these wells. If the wells were drilled elsewhere, the estimate would have been different. Moreover, since appraisal stage wells tend to be sparse and preferentially located the estimate from such wells is likely to over-estimate the true global NTG value.

To overcome the limitations of the classical bootstrap method Journel (1993) proposed the spatial bootstrap method to assess global uncertainty. Instead of resampling from the actual observed data, spatial bootstrap involves resampling alternate sets of data from simulated fields. By resampling from a spatially correlated field, the spatial dependency of the data is accounted for when building the uncertainty intervals. Moreover, this method can integrate secondary information such as seismic data during NTG estimation and field simulation stage. Figure 1.1 shows the general workflow for spatial bootstrap.

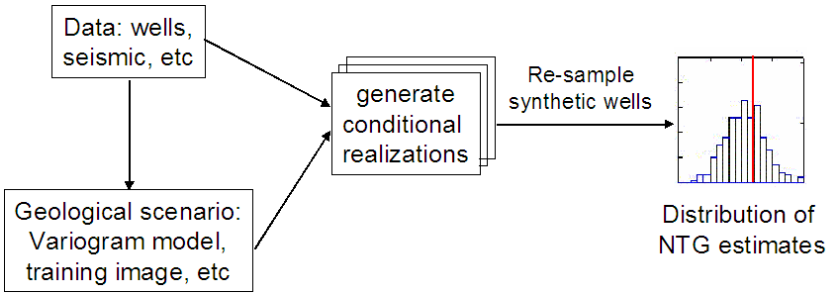

Figure 1.1: NTG uncertainty assessment using spatial bootstrap.

Because it accounts for spatial correlation spatial bootstrap is an attractive method for assessing global uncertainty. However, the uncertainty intervals obtained using this method depend on the spatial correlation model and input global NTG values used for generating the simulated facies realizations. These two input parameters are highly uncertain at appraisal stage when well data is sparse. Norris et al. (1993) use the NTG estimate from the appraisal stage wells as input global NTG for generating multiple facies realizations. They resample synthetic wells from these realizations by freezing the initial well pattern to obtain a distribution of NTG estimates. From this distribution, they retain the p_5, p_{50}, and p_{95} NTG values to generate three facies realizations to be used for reserve computation. They claim that these three stochastic models fully account for geological and sampling uncertainty. This claim is far-fetched because of two reasons: 1) a single geological scenario (in their case a set of indicator variograms) is used for generating the facies realizations, which may not be appropriate given the high geological uncertainty at appraisal stage; 2) the well

estimate might not be representative of the input global NTG value. Had they used a different geological scenario and a different global NTG value for generating the facies realizations, they would have obtained a different NTG distribution. Moreover, they did not use seismic data either when estimating the input NTG or when simulating the facies realizations. Bitanov and Journel (2004) have shown that seismic data can help correct for the bias in well estimate due to preferential well location.

To overcome these limitations of spatial bootstrap, Caumon and Journel (2004) propose to randomize both, the geological scenario and the prior global NTG value corresponding to each scenario. Their workflow still builds on the spatial bootstrap concept but accounts for additional uncertainty related to the geological scenario and the corresponding global NTG. This workflow is described in the next section.

1.3 Workflow for NTG Uncertainty Assessment

As discussed earlier, spatial bootstrap results depend on the geological scenario and the global NTG value used for simulating the realizations from which synthetic data sets are sampled. At appraisal stage we have few direct observations from which to determine a unique geological scenario. Caumon and Journel (2004) propose to retain all reasonable geological interpretations that fit the available data. For any given geological interpretation or scenario, they randomize the global NTG values that this scenario can take.

The workflow initially proposed by Caumon and Journel (2004) and further developed by Maharaja (2006) is presented in Figure 1.2. This workflow can be divided into five main stages which are described below.

1.3.1 Net-to-gross estimation

The first step in net-to-gross (NTG) uncertainty assessment is to obtain a NTG "best" estimate using all available data. We denote the data as the random variable (RV) vector $\mathbf{D}$. The bold face indicates that data are multiple and vectorial, i.e. they include well, seismic, and any other available numerical information. The actual data

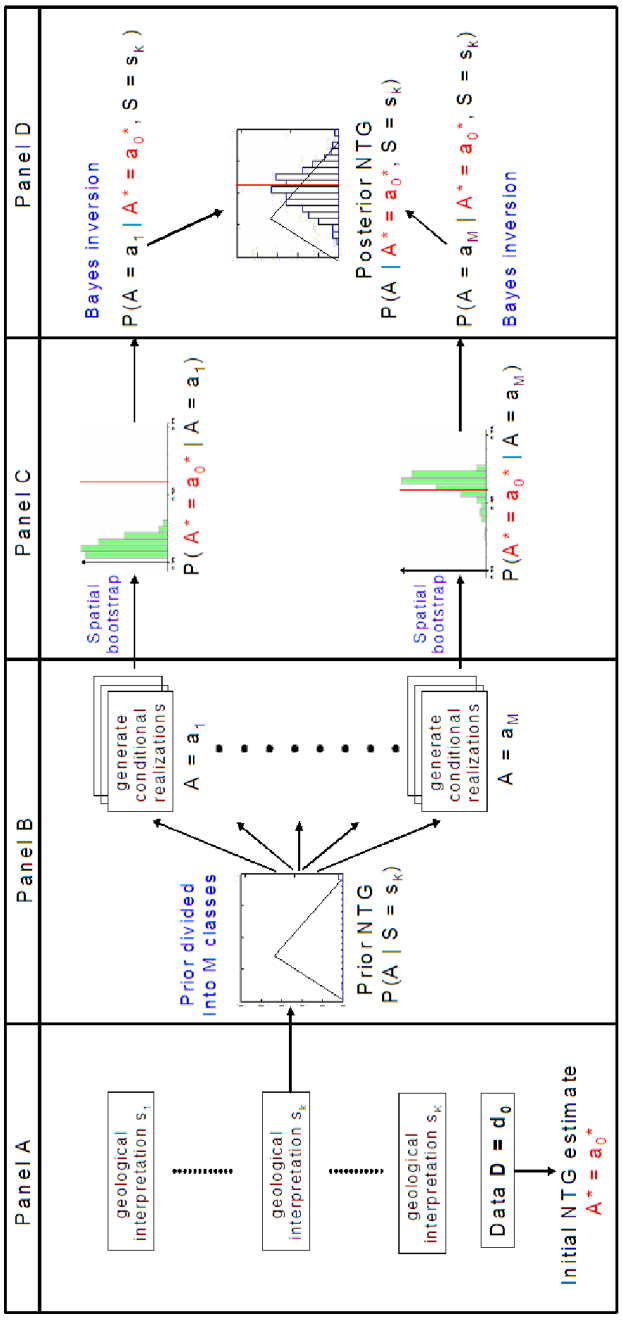

Figure 1.2: Workflow for global net-to-gross uncertainty assessment.

$\mathbf{d}_0$ obtained from the reservoir is one realization of this RV. Other realizations of the data can be obtained by randomizing for example the data location. Since, the NTG estimate depends on the data, it is also cast as a RV $A^\star$. It can be seen as a summary of the data obtained by applying some estimation function Φ. The estimate obtained from the actual data $\mathbf{d}_0$ is one realization of RV $A^\star = a_0^\star = \Phi(\mathbf{d}_0)$. Ideally, a model of uncertainty about A should not be related to a particular estimator of A; i.e. we should retain the entire data set $\mathbf{d}_0$ and not just a summary of that data. However, assessing the likelihood of a large vector of data $\mathbf{d}_0$ is extremely difficult. Obtaining exact replicates of facies along the original wells by resampling from facies realizations requires a very large number of simulations; it is much easier to obtain replicates of a summary of the original data event.

The estimate $a_0^\star$ is a function of both the data and the estimation algorithm used for summarizing the data. One way of randomizing $A^\star$ is to randomize the well location. Another way of randomizing $A^\star$ is by retaining a different estimation algorithm, or by considering alternative well log interpretations and seismic data processing.

NTG is defined as the ratio of volume of pay rock to total rock volume in the reservoir. Direct observation about rock-type comes from cores. The sequence of rocks along a core is divided into facies. Different facies have different proportions of sand and mud. For example floodbasin facies is dominantly mud, while channel facies is dominantly sand. Facies interpretation from sparse cores is necessarily subjective; different geologists would come up with different facies divisions from the same set of cores. This is because facies interpretation is always done with a particular depositional setting in mind. Facies stacking patterns for different depositional environments have been documented. The difficulty is that cores only sample a very small portion of the reservoir. Hence, even the best geologist may not be able to deduce unequivocally a single geological setting from inspecting a few cores. This interpretation uncertainty impacts the NTG uncertainty assessment. Moreover, parts of the core may be missing and the exact depth of the cored interval may not be known accurately.

It is uncommon to have cores from all wells at appraisal stage. Well-logs, which

are an indirect measurement of some rock or petrophysical property, are more prevalent. Examples of well logs include gamma ray and spontaneous potential logs which are indicators of shale content; sonic, neutron and density logs which are proxies for porosity (Bassiouni, 1994). Where available, log response is calibrated using core data. Along with interpretation error, well-log data may also contain measurement errors due to tool malfunctioning, borehole conditions, etc. The uncertainty from these sources is rarely quantified and the data are accepted as is. Recently, Akamine and Caers (2007) have attempted to address the uncertainty in well log data due to interpretation and measurement errors.

A net-to-gross estimate obtained by averaging sand observations at the wells alone is bound to be non-representative of the global NTG value since the wells tend to be preferentially located. A better, more representative NTG estimate may be obtained by using seismic data which provide a quasi-exhaustive spatial coverage of the reservoir. Like well logs, seismic data is also an indirect indicator of facies; hence, it must be calibrated using facies observations at wells. Many different calibration techniques have been proposed and used (Fournier and Derain, 1995; Goovaerts, 1997; Caers and Ma, 2002; Strebelle et al., 2002). The major stumbling block for many of these techniques is that they might not be robust in sparse data situation prevailing in early reservoir assessment. A simpler, but more robust method, would be more suitable for such situation. One such method is Bayes inversion as used by Bitanov and Journel (2004).

In the Bayes inversion method, the colocated facies-impedance pairs are used to compute the likelihood of observing impedance value s_j given a facies category f_i, $P(S = s_j \mid F = f_i)$. The facies proportions computed from wells are used as the prior facies probability, $P(F = f_i)$. Since the well data is sparse, a smoothing function is applied to these likelihoods. For each facies category, Bayes inversion is then applied at each grid location, $\mathbf{u}$, to compute the probability of observing that facies category given the observed impedance value at that location (Equation 1.3). Here, n refers to the number of facies; m is the number of classes used to discretize the impedance distribution. In Equation 1.3, $P(F = f_i)$ is the proportion of facies i and it is obtained from the wells. Hence, Equation 1.3 can be interpreted as the update of well facies

proportions using seismic data.

$$P(F(\mathbf{u}) = f_i \mid S(\mathbf{u}) = s_j\ ) = \frac{P(S = s_j \mid F = f_i) \times P(F = f_i)}{P(S = s_j)} \tag{1.3}$$

where $i = 1, \ldots, n$ and $j = 1, \ldots, m$. By performing Bayes inversion at each grid location for the n facies categories we get n facies probability cubes; the average of these 3D maps is the updated proportion p_i for each facies i (Equation 1.4).

$$p_i = \sum_{\mathbf{u}} P(F = f_i(\mathbf{u}) \mid S = s_j(\mathbf{u})\ ) \tag{1.4}$$

The seismic-derived estimate depends greatly on the quality of seismic data and the quality of calibration data. Quality of seismic data refers to the ability of seismic data to discriminate between the different reservoir facies. The seismic response is a function of contrasts in density and velocity, both of which are controlled not only by lithology, but also by diagenetic alteration, type of pore fluids, etc. For NTG estimation purpose, the smaller the overlap between the different seismic likelihoods $P(S = s_j \mid F = f_i)$ the better the discrimination between facies; hence, better quality seismic.

The overlap between the seismic likelihood distributions also depends on the calibration data from which they are derived. If the calibration data is sparse and biased towards one facies, then the resulting seismic likelihoods would also be biased toward that facies. For example, if all the available wells are located in low impedance (high pay) zones, then the calibration will be biased toward the high pay facies, because the calibration data is dominated by such facies. In the worst case scenario (complete overlap between likelihood histograms), the seismic-derived estimate will revert to the well-derived proportions $P(F = f_i)$ (no update), see Equation 1.3.

The NTG estimate also depends on the calibration algorithm used and the parameters of that algorithm. For example, in Bayes inversion, the resulting estimate depends on the number of seismic classes, the procedure used for smoothing the likelihoods, etc. Note that the conceptual framework presented here does not call for any specific algorithm to calibrate seismic and well data.

1.3.2 Building geological scenarios

The uncertainty about the geological setting at appraisal stage is expressed through the random variable G. The different geological scenarios g_k, with $k = 1, \ldots, K$ are the realizations of this vectorial RV. As discussed in section 1.3.1, the uncertainty about geological setting stems primarily from data sparsity. To account for this uncertainty alternate, competing geological interpretations that fit the available data should be considered until some could be eliminated by subsequently acquired data, see panel A in Figure 1.2.

The level of details to be incorporated in initial geological models depends on the company philosophy and amount of time available for building such models. Some companies may prefer quick-and-dirty models for initial evaluation, while others may insist on building models with already lamina-scale details. Either model is fine as long as it is understood that these models will be used for sampling synthetic data sets; hence, they must be conditioned to all relevant available data, including dense seismic data. Global NTG is an average of sand over the entire reservoir, thus models that capture the large-scale geological heterogeneity are sufficient for NTG uncertainty assessment. More detailed models may be necessary at later stage for well planning and recovery efforts, but most details are an overkill at appraisal stage.

Geostatistical simulation techniques are widely used for generating facies realizations. Each technique requires an input structural model which can be as simple as a variogram (Goovaerts, 1997) or it can be a fully explicit multiple-point model such as a training image (Remy et al., 2008). Geologists are more apt at expressing geological heterogeneity through images, consequently, they might find Tis to be more intuitive than variograms. A training image (Ti) is a conceptual representation of types and spatial distributions of patterns deemed present in the sub-surface. It need not have any local accuracy, hence it can be generated using unconditional Boolean simulation (Lantuejoul, 2002). Local accuracy is achieved by the data conditioning multiple-point simulation (mps) algorithms. Two such mps algorithms, *snesim* (Strebelle, 2002), and *filtersim* (Zhang, 2006), are available in the Stanford Geostatistical Modeling Software (SGeMS) (Remy et al., 2008).

The virtual reservoirs from which synthetic wells are re-sampled are not the conceptual models (variograms and Tis), but the conditional realizations generated using these conceptual models. Thus, the simulation algorithm, the parameters of that algorithm, and the conditioning data jointly define the geological scenario underlying the simulated realizations actually used for resampling. The simulation domain (volume) is also an important element of the geological scenario.

1.3.3 Prior net-to-gross distribution

Along with a structural model, prior global facies proportions are a required input for geostatistical simulation of facies. Since these proportions are uncertain at appraisal stage, they are treated as a random variable A. The true, but unknown, global NTG value of the reservoir a_0 is a realization of this RV. A prior probability distribution of global NTG represents the range of possible NTG values that a specific geological scenario can take $P(A = a|G = g_k)$. Thus, each geological scenario has its associated prior NTG distribution, see panel B in Figure 1.2. Ideally, such a prior distribution is obtained by pooling together NTG values observed from previously discovered reservoirs or outcrops that are deemed analogous to that scenario. This allows each company to capitalize on their past experience and geological expertise. If no database is available to quantitatively obtain a prior distribution, then one may retain different types of distributions based on the available information. For instance, if the geologist has an idea about the range of the global NTG values, then uniform, triangular, and Gaussian distributions can be retained. For the triangular distribution, additional information is required to determine the mode; in that case alternate triangular distributions with different modes may be retained.

By resampling synthetic data sets from virtual reservoirs, spatial bootstrap assesses the uncertainty about the global NTG estimate $a_0^\star$ for a given geological model and global NTG value $A = a_m$. This uncertainty assessment takes the form of a probability distribution $P(A^\star = a_0^\star|G = g_k, A = a_m)$. As such, the global NTG value is an input to the geostatistical algorithm, hence it should be included in the definition of the geological scenario. However, for the convenience of notation, we keep these two

RVs (G and A) separate.

By casting the global NTG as an RV, the problem of global uncertainty assessment is recast as follows: what is the posterior probability of given global NTG value given an observed estimate $P(A = a_m|A^\star = a_0^\star)$. This posterior probability can be obtained using Bayes inversion rule. Spatial bootstrap provides the likelihood of observing an estimate for a given global NTG value and geological scenario. Classical Bayesian approaches assume a Gaussian data likelihood function to update the prior probability into the posterior probability (Biver et al., 1996). Although our methodology also utilizes a Bayesian framework, no prior assumption is made about the type of likelihood function; spatial bootstrap determines that data likelihood function.

1.3.4 Spatial bootstrap

Spatial bootstrap is an important component of the proposed workflow, see panel C in Figure 1.2. It provides the likelihood of observing a NTG estimate for a given geological scenario and global NTG value. Since one does not have the luxury of drilling new wells from the actual reservoir due to economic constraints, synthetic wells are re-sampled from virtual (simulated) representations of the reservoir. Spatial bootstrap is more suitable to earth sciences data sets because data along a well and between wells are spatially correlated. When resampling from a virtual field, this correlation must be honored. This can be achieved by preserving the original drilling strategy applied to a geological representation of that correlation.

The original well pattern can be honored in two ways: 1) by freezing the exact inter-well geometry of the original well configuration and moving this configuration as a whole when re-sampling, or 2) by maintaining a minimum distance between the synthetic wells so that no two wells are closer than the prescribed distance (Caumon et al., 2004). This second constraint does not prevent the wells from being farther away from one another than in the original pattern. The decision of which sampling strategy to mimick in any particular application depends on several things. If the actual wells are known to be drilled in a specific pattern for a known reason (for example to verify the extent of a lobe or determine channel directions),

then this pattern should be honored. If it is not honored then the NTG estimates from the synthetic wells may not have the same level of redundancy as the actual wells, which will result in non-representative uncertainty intervals.

Recall that the goal of spatial bootstrap is to honor a particular structural and redundancy model between and along the wells when building uncertainty intervals. For the same structural model (geological scenario), different well configurations will produce different uncertainty intervals. For instance, consider three wells that are drilled in a curvilinear pattern to hit a channelized section of the reservoir. Because of this channelized pattern these three wells are highly redundant, if the simulated geological scenario does reflect channels. If this well configuration is not repeated during re-sampling, then the synthetic wells will not reflect the redundancy of the actual wells. Along with initial drilling strategy, it is also important to honor the number of wells and number of samples per well when re-sampling from simulated realizations.

Note: Spatial bootstrap, like any other statistical technique, is not suitable for global uncertainty assessment when the range of the phenomenon is much larger than the size of the simulation field. Ergodic fluctutations supersede spatial variability in such cases, see Chiles and Delfiner (1999) for a discussion on ergodicity.

1.3.5 Update prior NTG distribution

Associated with each geological scenario, $G = g_k$, is a prior probability distribution of global NTG $P(A|G = g_k)$, see Figure 1.2, Panel A. That prior NTG distribution is a continuous distribution. For computational reasons, that prior distribution is discretized into M classes resulting in M realizations of the NTG, $a_m, m = 1, \ldots, M$, see Figure 1.2, Panel B. To update the prior probability of each class of global NTG given the observed NTG estimate $a_0^\star$, the workflow proceeds as follows:

- From class m pick a representative global NTG value a_m. Using this global NTG value simulate L facies realizations that honor all available reservoir data.

- Freezing the initial drilling strategy, sample N sets of synthetic wells from each

of the L realizations by randomizing the well locations. Compute a distribution of NTG estimates using these $N * L$ estimates, $a_1^\star, \ldots, a_{NL}^\star$.

- From this distribution retain the likelihood of observing the initial NTG estimate $a_0^\star$ for the given class of true NTG and the given geological scenario, $P(A^\star = a_0^\star \mid A = a_m, G = g_k)$, see Figure 1.2, Panel C. If $a_0^\star \notin [a_1^\star, \ldots, a_{NL}^\star]$, then this likelihood is zero, and the posterior probability of that class of global NTG is also zero.

- Use Bayes rule update the prior probability that the global NTG is in class m given the observed NTG estimate and geological scenario:

$$P(A = a_m | A^\star = a_0^\star, G = g_k) = \frac{P(A^\star = a_0^\star | A = a_m, G = g_k) * P(A = A_m | G = g_k)}{P(A^\star = a_0^\star | G = g_k)} \tag{1.5}$$

The denominator $P(A^\star = a_0^\star \mid G = g_k)$ is obtained by summing the numerator product over all M classes:

$$P(A^\star = a_0^\star \mid G = g_k) = \sum_{m=1}^{M} P(A^\star = a_0^\star \mid A = a_m, G = g_k) * P(A = a_m \mid G = g_k) \tag{1.6}$$

This procedure gives the posterior distribution of global NTG given the initial NTG estimate for a given geological scenario, $P(A = a_m \mid A^\star = a_0^\star, G = g_k)$, see Figure 1.2, Panel D. If desired, the probability distribution for the global NTG given only the initial NTG estimate, $P(A = a_m \mid A^\star = a_0^\star)$, can be obtained using the total probability rule:

$$P(A = a_m \mid A^\star = a_0^\star) = \sum_{k=1}^{K} P(A = a_m \mid A^\star = a_0^\star, G = g_k) * P(G = g_k) \tag{1.7}$$

Equation 1.7 calls for the prior probability of a geological scenario $P(G = g_k)$, which is a difficult and necessarily subjective task. A convenient alternative to using expert knowledge is to assume each scenario to be equally likely, which might be reasonable in sparse data situation.

This workflow has been coded as a plug-in for the gOcad[1] software. The plug-in contains the different modules of the workflow, such as NTG estimation, geostatistical simulation, and spatial bootstrap. The workflow is fully automated; the final posterior NTG distribution and all intermediate results are output in a directory. Note that the conceptual framework does not call for any specific algorithm for NTG estimation or geostatistical simulation.

[1]

Chapter 2

Workflow testing on a synthetic data set

The NTG uncertainty workflow in Figure 1.2 builds on spatial bootstrap. Hence, the results of the workflow are dependent on the parameters of that spatial bootstrap, namely the input geological concept and the global NTG value. It also depends on the initial NTG estimate since the posterior probability of global NTG values is conditional to this initial estimate; thus, the estimation algorithm and its parameters are also important. To understand the impact of various workflow parameters on NTG uncertainty models, we use the synthetic Stanford VI reservoir (Castro et al., 2005).

Synthetic reservoirs are useful for such a global uncertainty study because the true global NTG is known. We can retain different initial data sets (i.e. wells) to study the impact of different initial data configurations and NTG estimates on the posterior NTG uncertainty models. We can also evaluate the impact of different prior NTG distributions as well as the importance of seismic data. Since the prior NTG distribution is discretized into classes when performing the workflow, we also study the impact of such discretization.

2.1 The Stanford VI reservoir runs

Stanford VI is a prograding fluvial reservoir which is later deformed into an asymmetric anticline. It is 3.75 km × 5.0 km × 200 m and contains 150 × 200 × 200 gridblocks of dimensions 25 m × 25 m × 1 m. It consists of three layers with different geological settings and NTG (Table 2.1). A prograding delta in the bottom layer transitions into meandering channels in the middle layer, which themselves transition into low-sinuosity channels in the top layer (Figure 2.1). The top two layers consist of four facies, namely channel sand, point bar sand, channel mud drapes, and floodbasin clays. The bottom layer consists of only channel sands and floodbasin clays. For demonstrating the workflow, only the top layer with low sinuosity channels is retained. The gridblocks of this layer are upscaled to 50 m × 50 m × 2 m so that the top layer has 75 × 100 × 40 gridblocks, which speeds up the computations without compromising learning. For simplicity, channel sand and point bar sand are grouped into a single "sand" facies (NTG=1) and the channel mud drapes and floodbasin clays are combined into "non-sand" (NTG=0). Hence, the NTG in this case is the proportion of sand facies.

Layer	**Global NTG**
top	0.27
middle	0.25
bottom	0.44
overall	0.34

Table 2.1: Global NTG of different layers of Stanford VI reservoir

Seismic data

Acoustic impedance for the Stanford VI reservoir is generated by forward modeling. For details about the petrophysical properties of the various facies and seismic data generation refer to Castro et al. (2005). The original acoustic impedance cube in the depth domain is filtered to mimick realistic seismic quality (Figure 2.2). This filtered cube is used in the workflow for two different tasks: 1) for NTG estimation and 2)

conditioning facies realizations. The time-to-depth conversion is an important source of uncertainty in seismic data processing and it should be accounted for during the geophysical inversion. For this study we ignore that source of uncertainty.

Geological scenario

The geological interpretation is done using the filtered acoustic impedance data. Channels are seen in the horizon slices of seismic data (Figure 2.2); hence, the conceptual geological model retained for the top layer of Stanford VI is also channelized (Figure 2.3). The various channel parameters, such as width, sinuosity, orientation are deduced from the seismic data, while channel thickness is obtained from wells.

Initial wells and NTG estimates

To mimick appraisal stage conditions, we retain three initial wells drilled in a pseudo-linear pattern (Figure 2.4(a)). These wells are approximately 800 meters apart and all three wells hit channelized area of the reservoir. Consequently, the NTG estimate (proportion of sand) obtained from these wells is high at 0.61. Recall that the true global NTG of the Top layer is only 0.27; hence, this is a severe over-estimation of the global value. When seismic data is used for NTG estimation in addition to the three wells, the initial estimate goes down to 0.49. Thus, seismic data is somewhat correcting for the bias due to preferential well location. The magnitude of this correction depends on the quality of seismic data and the calibration data set. The three preferentially located wells have a high proportion of sand; hence, the calibration is biased towards sand. The Bayes inversion technique described in Section 1.3.1 was used for calibrating the well and seismic data. The likelihoods of impedance given sand and non-sand computed from the pairs of facies and impedance data at wells are shown in Figure 2.5. Since the well data is sparse, a smoothing function is applied to these likelihoods.

We also retain another set of three wells which were drilled at random (Figure 2.4(b)). The NTG estimate from these three randomly located wells is 0.17, which is lower than the true global NTG of top layer. After incorporating seismic data,

the NTG estimate goes up to 0.26, which is quite close to the true value (0.27). In this case, seismic data corrects the initial under-estimation. Figure 2.6 shows the likelihoods of impedance given sand and non-sand computed from these wells.

The first set of three wells represent a more realistic drilling strategy; wells are drilled strategically to discover and later to produce oil, never at random. The alternate set of three wells is retained merely to study the impact of different NTG estimates on posterior NTG distribution.

Prior NTG distributions

A prior NTG probability distribution represents the range of NTG values that a specific geological scenario can take. Ideally, such a prior distribution should be obtained from a database of analog reservoirs, which would vary from one company to another and encapsulates each company exploration strategy. Because this is a synthetic case we do not have such database. Suppose we suspect a bias associated to a high initial NTG estimate, therefore we choose a prior NTG distribution with mean lower than this NTG estimate. A triangular distribution with mode 0.35, minimum 0.20, and maximum 0.60 is retained (Figure 2.7). Table 2.2 gives selected summary statistics. In spite of being wide, the prior $[p_{10}, p_{90}]$ interval does not include the true global NTG value of 0.27. The goal of the workflow is to update this prior NTG distribution into a posterior NTG distribution given either NTG estimates of 0.49 and 0.26 observed from the data using the geological concept shown in Figure 2.3.

mean	0.38
median	0.37
minimum	0.20
p_{10}	0.28
p_{90}	0.50
maximum	0.60

Table 2.2: Summary statistics of prior NTG distribution used for Stanford VI study.

The entire workflow is carried-out twice, first with the three preferentially located wells (Figure 2.4(a)), then using the randomly located three wells (Figure 2.4(b)). The

prior NTG distribution is discretized into 10 classes. The median NTG value from each class is retained and a facies realization honoring that NTG value and the well and seimic data is simulated using the multiple-point simulation algorithm *snesim* (Strebelle, 2002). The version of this algorithm available in the SGeMS (Remy et al., 2008) software is used. From each such realization 500 sets of 3 synthetic wells are drilled using the initial drilling strategy. The Bayesian calibration procedure described in Section 1.3.1 is applied to each re-sampled well set; these estimates are pooled together to obtain a distribution of NTG estimates. From this distribution, the probability of the initial NTG estimate $a_0^\star$ is read. Finally, using Bayes inversion rule (Equation 1.5) the probability of the NTG value being in a given global NTG class is computed. All workflow parameters, except for the wells, are the same for both preferentially located and randomly located wells. The results of these runs and other sensitivity studies are presented in the following section.

2.2 Results

2.2.1 Impact of the initial NTG estimate

Figure 2.8 gives the two posterior NTG distributions resulting from using the two different initial estimates: 1) 0.49 which corresponds to three preferentially located wells, and 2) 0.26 which corresponds to three randomly located wells. Table 2.3 gives selected summary statistics of these posterior distributions.

As expected, the mean of the posterior NTG distribution corresponding to the preferentially located wells (first posterior) is higher than that of the randomly located wells (second posterior). The $[p_{10}, p_{90}]$ interval of the first posterior does not include the true global NTG value (0.27) because of the severe over-estimation. Recall that the prior $[p_{10}, p_{90}]$ interval $[0.28, 0.50]$ did not include that true global value. However, starting from the same prior interval $[0.28, 0.50]$ the true value 0.27 is included in the $[p_{10}, p_{90}]$ of the second posterior. Resampling with randomly located wells allows for a larger interval of variability for NTG.

	Preferentially located wells	Randomly located wells
NTG estimate	0.49	0.26
mean	0.39	0.33
median	0.38	0.33
p_{10}	0.29	0.24
p_{90}	0.50	0.41
$p_{90} - p_{10}$	0.21	0.17

Table 2.3: Summary statistics of posterior NTG distributions resulting from using different sets of initial wells. True NTG = 0.27.

2.2.2 Impact of the prior NTG distribution

In the previous runs we used a triangular prior distribution for which the p_{10} value was greater than the true value. This distribution can be called an optimistic prior. The first set of wells are preferentially located in channels; hence, the initial NTG estimate (0.49) from these wells and seismic data is much higher than the true global NTG (0.27) of the top layer of Stanford VI. When the optimistic prior distribution is used together with preferentially located wells, the resulting posterior $[p_{10}, p_{90}]$ interval does not include the true global NTG value. Unfortunately, such compounding of biases is not uncommon at appraisal stage.

This is why historical data is truly important. If we know from prior experience that a channelized reservoir can have a much lower global NTG than what is observed from the wells, particularly preferentially located wells, then we can choose a prior that reflects this. This prior might not even include the observed biased NTG estimate.

To understand the impact of prior NTG distribution we retain a second less optimistic triangular distribution with mode 0.30 and bounds 0.10 and 0.50 (Figure 2.9). The true global NTG value (0.27) is now included in the prior $[p_{10}, p_{90}]$ interval $[0.19, 0.41]$. The workflow is repeated with the three preferentially located wells and this new prior NTG distribution; the corresponding posterior distribution is given in Figure 2.10(a). For comparison, the posterior NTG distribution resulting from the previous triangular distribution is repeated in Figure 2.10(b). Table 2.4 gives some

summary statistics of these two posterior NTG distributions.

	With triangular prior [0.20,0.35,0.60]	With triangular prior [0.10,0.30,0.50]
mean	0.39	0.34
median	0.38	0.34
p_{10}	0.29	0.24
p_{90}	0.50	0.42
$p_{90} - p_{10}$	0.21	0.18

Table 2.4: Summary statistics of posterior NTG distributions resulting from using different prior NTG distributions. The initial NTG estimate in both case is 0.49. True NTG = 0.27.

The new posterior $[p_{10}, p_{90}]$ interval $[0.24, 0.42]$ now contains the true global NTG value 0.27, in spite of the initial over-estimation (0.49). This shows that by taking advantage of an unbiased prior information about NTG, we can bail-out from an initial severe over-estimation due to sparse, preferentially located wells. The new posterior mean (0.34) is still higher than the actual global NTG value (0.27), but it is lower than the posterior mean (0.39) obtained using the first prior NTG distribution. The worflow is repeated for the second set of three randomly located wells with the new prior distribution; the resulting posterior is shown in Figure 2.11. As expected, in this case the posterior mean (0.28) is much closer to the true NTG value (0.27) of top layer of Stanford VI.

2.2.3 Impact of the re-sampling strategy

The initial NTG estimate depends on the strategy for locating the wells. The uncertainty about the initial NTG estimate depends on both the geological scenario and the specific configuration of the initial wells. For example, consider the three wells shown in Figure 2.4(a). These wells are drilled preferentially in a (curvi) linear pattern aimed at hitting the N-S trending channels. To study the impact of this well pattern on posterior NTG distribution the workflow is repeated twice, first by freezing this well pattern when resampling and then by maintaining a minimum interdistance

of 800 m between the three wells. The less optimistic triangular prior (Figure 2.9) with mode of 0.30 was retained for both runs. Figure 2.12 gives the two resulting posterior distributions; Table 2.5 gives some summary statistics.

	Fixed well configuration	Min. well interdistance
mean	0.34	0.37
median	0.34	0.37
p_{10}	0.24	0.29
p_{90}	0.42	0.44
$p_{90} - p_{10}$	0.18	0.15

Table 2.5: Summary statistics of posterior NTG distributions resulting from using different re-sampling strategies.

The posterior distribution resulting from fixed configuration (FC) re-sampling is wider than that resulting from minimum interdistance (MD) re-sampling. In a channelized reservoir with low global NTG (< 0.30), the likelihood of observing a high NTG estimate of 0.49 is higher when the three wells are designed to find channels. Thus, the posterior p_{10} value in the FC case is lower than in the MD case. The posterior p_{90} is larger in the MD case because in channelized reservoir with very high global NTG (> 0.45), a NTG estimate of 0.49 is less likely to be observed when the three wells are designed to find channels.

2.2.4 Impact of seismic data

We saw that incorporating seismic data helps correct for the bias in the NTG estimate obtained from wells. In case of the preferentially located wells the estimate was lowered from 0.61 to 0.49. In the case of the randomly choosen three wells, the initial NTG estimate went up from 0.17 to 0.26. Such correction is significant in both cases, but it is more critical for the severe over-estimation case. To study the impact of seismic data on posterior NTG distribution the workflow is run without using seismic data with both well configurations of Figure 2.4. Figure 2.13 shows the two corresponding posterior NTG distributions and Table 2.6 gives summary statistics.

Note that seismic data was not used for conditioning facies realizations in these runs. The triangular prior with mode of 0.30 was retained for both runs. Compare these distributions to the ones obtained using seismic (Figures 2.10(a) and 2.11(a)).

	Preferentially located wells	Randomly located wells
NTG estimate	0.61	0.17
mean	0.41	0.24
median	0.42	0.23
p_{10}	0.36	0.16
p_{90}	0.46	0.33
$p_{90} - p_{10}$	0.10	0.17

Table 2.6: Summary statistics of posterior NTG distributions resulting from using different sets of initial wells without using seismic data.

The posterior $[p_{10}, p_{90}]$ intervals corresponding to the three preferentially located wells are even farther from the truth. The p_{10} (0.36) is much higher than the true global NTG (0.27); the posterior mean (0.41) is also significantly higher. The posterior statistics in the under-estimation case provided by the three random wells are not so bad. From these results it appears that seismic data is extremely important at appraisal stage, when the wells are few and preferentially located. Ignoring seismic data during NTG estimation, as called by a classical bootstrap approach (Efron, 1979), is not recommended unless seismic is of very poor quality.

2.2.5 Impact of discretization on posterior statistics

Net-to-gross is a continuous variable, hence, its probability distribution is a continuous distribution as well. For computational reasons, the prior distribution is discretized into classes of NTG. Then, from each class, a representative NTG value is chosen to generate facies realizations from which synthetic wells are resampled. The posterior statistics are computed by interpolating between classes; hence, they depend on the number of classes used for discretizing the initial prior distribution. To study the impact of discretization on posterior statistics, we divide the less optimistic triangular

prior with mode 0.30 into 10, 12, 15 and 20 classes respectively. Figure 2.14 shows the four posteriors distributions corresponding to these four classes; Table 2.7 gives their summary statistics.

Nb classes	10	12	15	20
mean	0.34	0.33	0.36	0.37
median	0.34	0.33	0.37	0.38
p_{10}	0.24	0.24	0.27	0.29
p_{90}	0.42	0.42	0.45	0.45
$p_{90} - p_{10}$	0.18	0.18	0.18	0.16

Table 2.7: Summary statistics of posterior NTG distributions resulting from using different classes of NTG. Initial NTG estimate in all four cases is 0.49.

The statistics of the posteriors for 10 and 12 classes are quite similar. However, for 15 and 20 prior classes, the posterior statistics change. The mean of the these two posteriors are higher than the mean in the two previous cases. The posterior $[p_{10}, p_{90}]$ interval widths are comparable, but the intervals are shifted to the right. These differences are attributed to discretization errors. With greater number of classes, the histogram is relatively smoother, i.e. there are no big jumps in posterior probability from one class to another.

2.3 Chapter Summary

Stanford VI is an exhaustively known reservoir. Hence, it can be used to evaluate the impact of various workflow parameters on the global NTG uncertainty. Like all reservoirs in nature, Stanford VI has a unique global NTG value. The uncertainty about that global NTG comes from our limited knowledge (data) about it. If the wells are preferentially located we would likely over-estimate the global NTG. Using seismic data helps correct such initial bias. In case of the three preferentially located wells, the initial global NTG value was severely overestimated; seismic lowered the estimate from 0.61 to 0.49, the true value being 0.27. In real practice, the actual correction depends obviously on the quality of seismic data and the calibration data set.

By utilizing past experience we can obtain a prior NTG distribution that can provide unbiased representative prior uncertainty intervals. It is important to capitalize on such unbiased source of information whenever available. It is also important to freeze initial drilling strategy when re-sampling to mimick and reflect in the bootstrap operation any in-built bias.

Not using seismic data for NTG uncertainty assessment at appraisal stage can be dangerous. Because of its extensive coverage, seismic data not only helps correct the bias in the initial NTG estimation, but also help impart local accuracy to facies realizations. Thus, using seismic data is strongly recommended. The actual magnitude of correction clearly depends on the quality of seismic data and the available calibration data.

Posterior statistics depend on the discretization of the prior NTG distribution. There are no hard-and-fast rules for discretizing the prior NTG distribution. It is a continuous distribution, which is discretized into classes for computational reasons; more classes means more facies simulations. Ideally, it should be discretized into as many classes as can be afforded given the time constraints. Once a decision is made about number of classes, it should be frozen for all subsequent analyses.

Figures

(a) Bottom Layer (b) Middle Layer (c) Top Layer

Figure 2.1: Representive slices showing the channel styles in the three layers of Stanford VI reservoir.

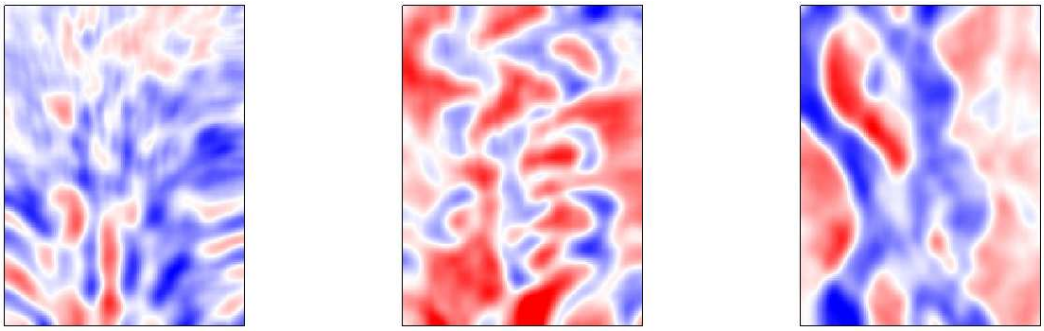

(a) Bottom Layer (b) Middle Layer (c) Top Layer

Figure 2.2: Representive horizontal slices of acoustic impedance in the three layers of Stanford VI reservoir.

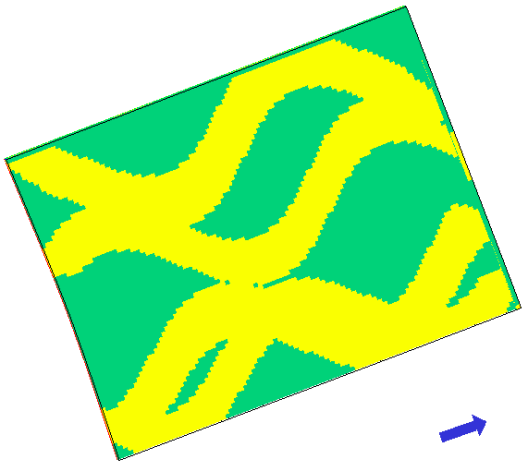

Figure 2.3: Conceptual geological scenario used for the top layer of Stanford VI.

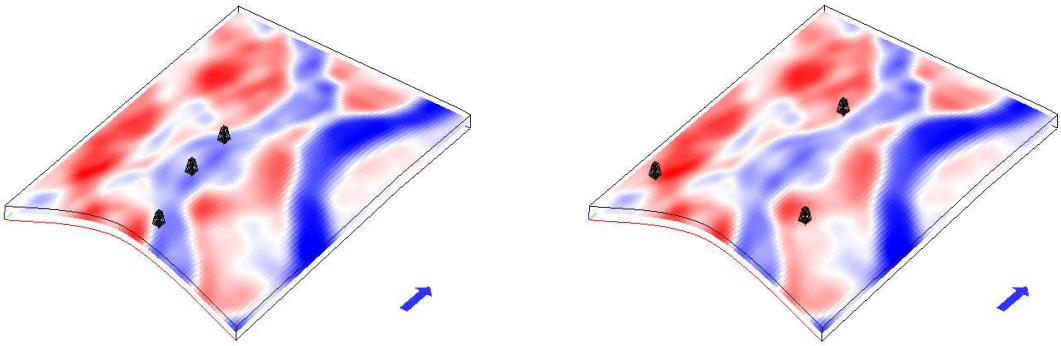

(a) Preferentially located wells

(b) Randomly choosen wells

Figure 2.4: Location of initial wells with a slice of acoustic impedance (vertical exaggeration $\times 3$).

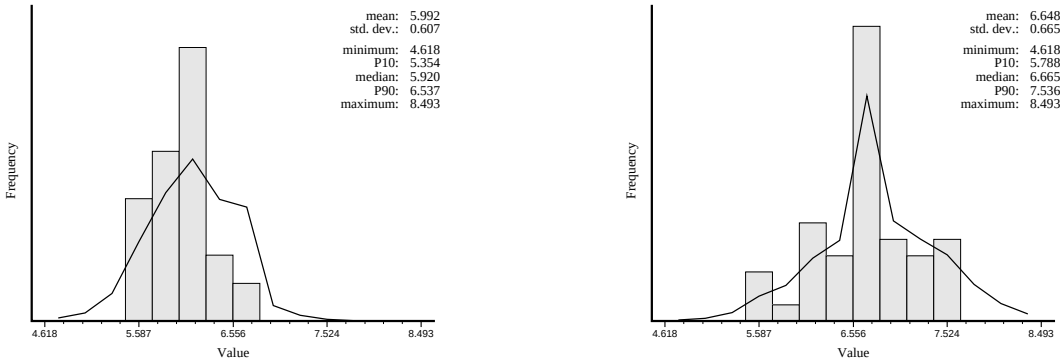

(a) Sand (b) Non-sand

Figure 2.5: Sand and non-sand impedance likelihoods obtained from the three preferentially located wells.

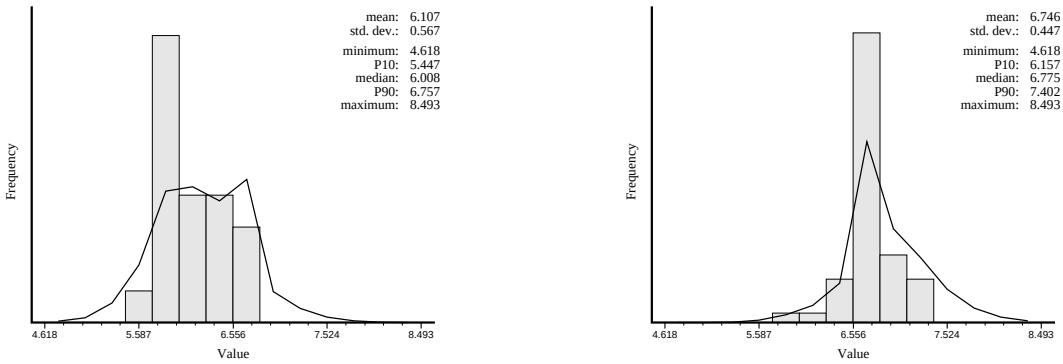

(a) Sand (b) Non-sand

Figure 2.6: Sand and non-sand impedance likelihoods obtained from the three randomly choosen wells.

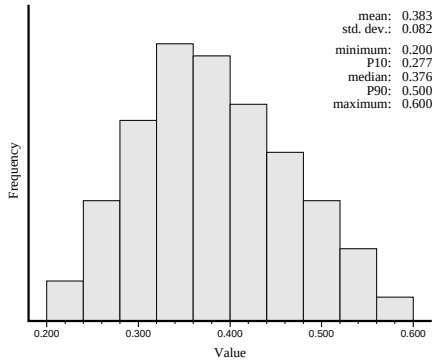

Figure 2.7: Triangular prior NTG distribution used for Stanford VI

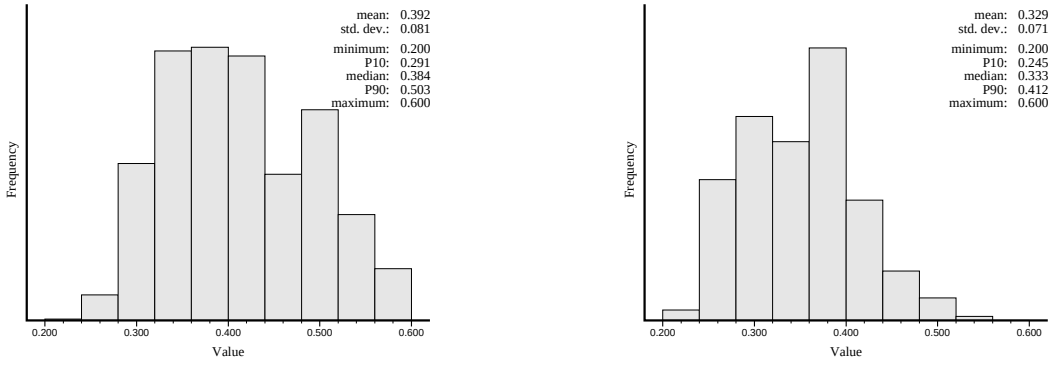

(a) Preferentially located wells

(b) Non-preferentially located wells

Figure 2.8: Posterior NTG distributions resulting from two different sets of initial wells.

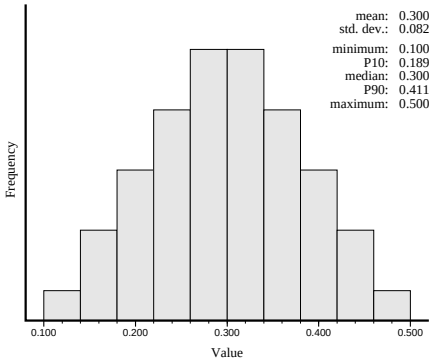

Figure 2.9: Second triangular prior NTG distribution used for Stanford VI.

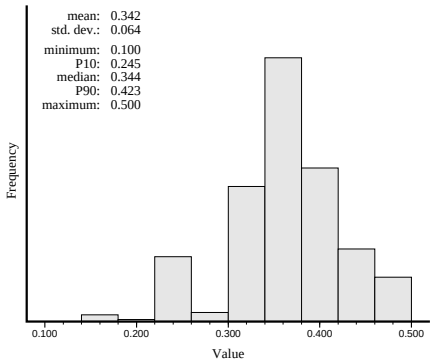

(a) With triangular (0.10,0.30,0.50)

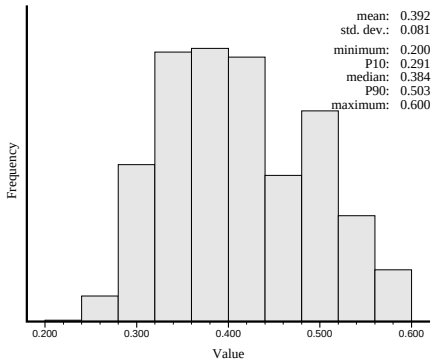

(b) With triangular (0.20,0.35,0.60)

Figure 2.10: Posterior NTG distributions resulting from two different prior NTG distributions with preferentially located wells (initial NTG estimate 0.49). True NTG is 0.27.

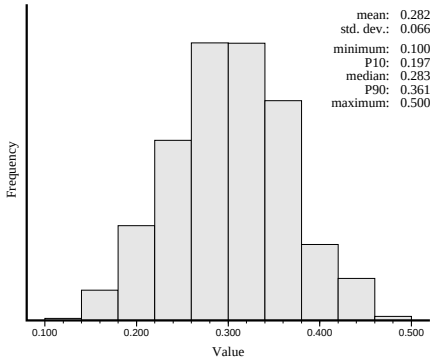

(a) With triangular (0.10,0.30,0.50)

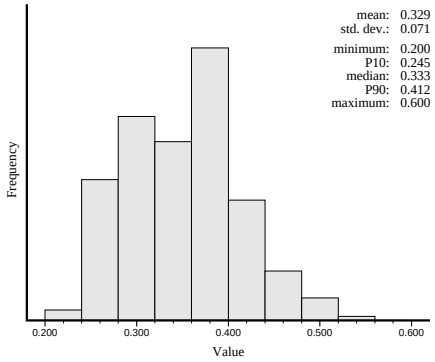

(b) With triangular (0.20,0.35,0.60)

Figure 2.11: Posterior NTG distributions resulting from two different prior NTG distributions with randomly located wells (initial NTG estimate 0.26). True NTG is 0.27.

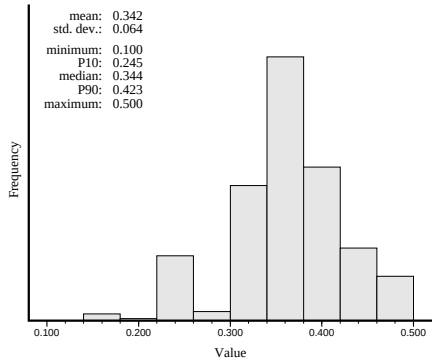

(a) Fixed well configuration

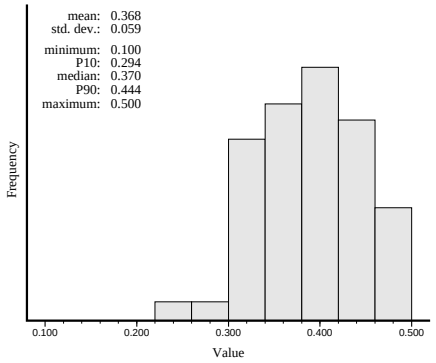

(b) Minimum interdistance (800m)

Figure 2.12: Posterior NTG distributions resulting from different re-sampling strategies. Initial NTG estimate in both cases is 0.49. True NTG is 0.27.

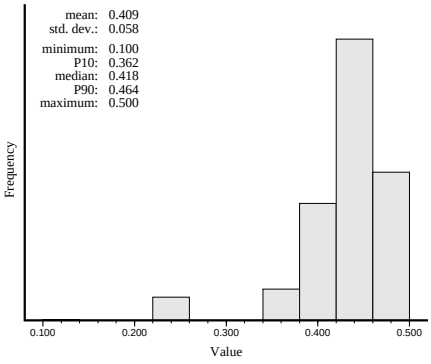

(a) Preferentially located wells

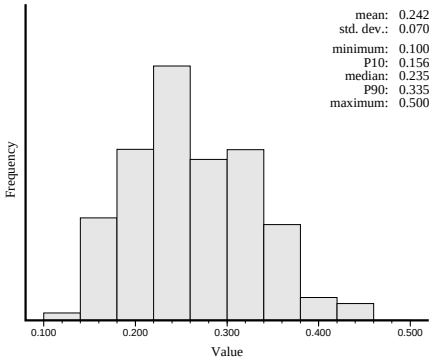

(b) Non-preferentially located wells

Figure 2.13: Posterior NTG distributions resulting from two different sets of initial wells without using seismic data. Triangular prior [0.10, 0.30, 0.50] is used in both cases.

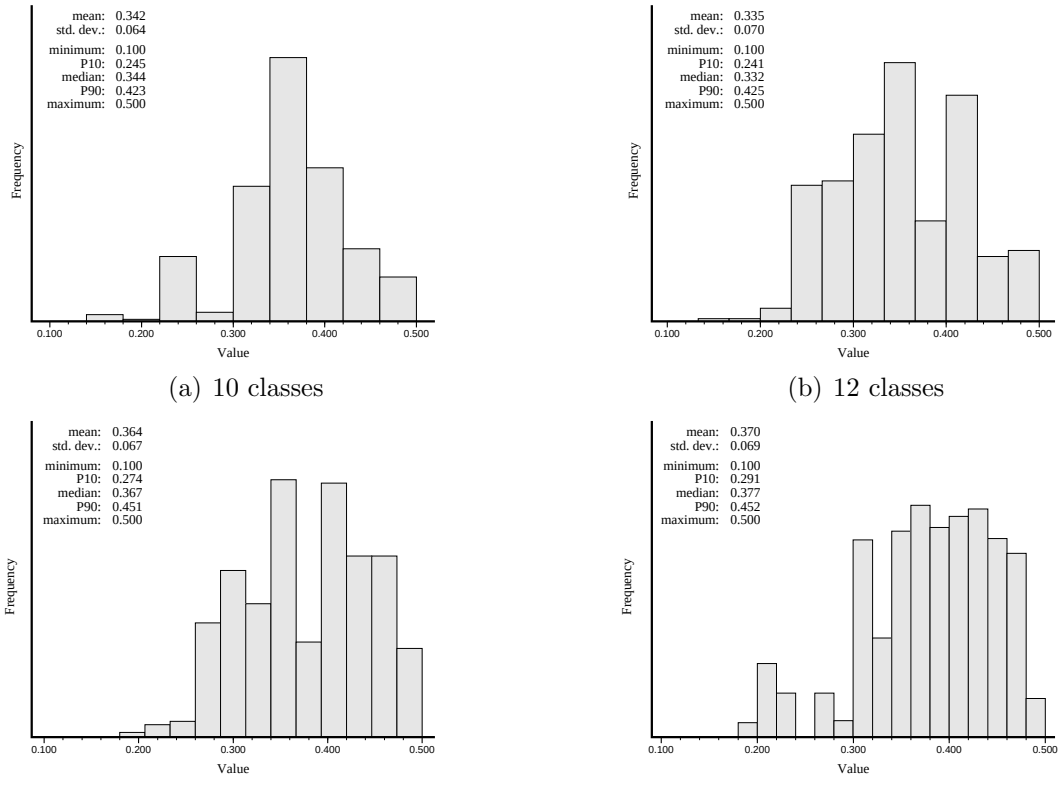

(a) 10 classes

(b) 12 classes

(c) 15 classes

(d) 20 classes

Figure 2.14: Posterior NTG distributions corresponding to different number of prior NTG classes. The initial NTG estimate in all cases is 0.49.

Chapter 3

Application to a turbidite reservoir

A large data set is available from a deep-water turbidite reservoir offshore West Coast of Africa. The objective of this chapter is to apply the proposed NTG uncertainty workflow to assess the uncertainty about the net-to-gross of this reservoir by mimicking appraisal stage conditions. Early stratigraphic interpretation is retained and different depositional facies scenarios are considered. The structural setting is well-known, hence the uncertainty about the geological scenario is related to types and distribution of facies. A prior NTG distribution is obtained from the company database of analog reservoirs. Four appraisal stage wells and acoustic impedance data from a 3D seismic survey are retained for the uncertainty study.

First, the information available at appraisal stage is described. Next, we demonstrate the importance of freezing sampling strategy in domains of both uniform and non-uniform thickness. Finally, the results of the NTG uncertainty workflow are presented. The impact of variable geological scenarios on the NTG uncertainty is demonstrated. The impact of additional data is investigated by conducting the study with one well and then repeating it each time a new well is added. With each additional well the posterior NTG distribution becomes narrower, which implies that additional data is reducing the uncertainty interval. The posterior NTG distribution with the actual twenty-eight wells available, which provide a good coverage of the reservoir, is compared with that from the four appraisal stage wells.

3.1 Information available at appraisal stage

3.1.1 Geological scenarios

At the appraisal stage the uncertainty about the geological setting depends on several factors. If the reservoir is located in a frontier basin the uncertainty tends to be much higher as opposed to a mature basin where the geological setting is known with greater confidence. In deep-water settings the quality of seismic data also plays a large role. Well-imaged seismic data can significantly reduce the uncertainty about the structural setting and, in exceptionally good cases, even the facies types and geometries can be deduced from the seismic amplitude slices. Conversely, poorly imaged seismic data can lead to higher uncertainty about, the reservoir boundaries and the facies types.

In the WCA reservoir the seismic data quality is sufficiently good to identify the structural setting with a high degree of confidence. It was determined to be a slope valley system from the very get-go. However, the actual internal complexity of this slope valley was increasingly understood as the seismic data was better interpreted. It was observed that the greater the number of mapped geobodies, the smaller the gross reservoir volume, and consequently the smaller the OOIP. For this study we retain the appraisal stage stratigraphic architecture shown in Figure 3.1. Figure 3.1(a) shows a schematic of the reservoir interpreted from the seismic data and Figure 3.1(b) shows the actual reservoir grid. The number of grid blocks in x, y, and z vary spatially. This reservoir volume is frozen (deemed known) and retained for this study.

The depositional facies filling the slope valley, however, cannot be easily inferred from the seismic data. Since the structural setting is assumed known, the uncertainty about geological setting boils down to the uncertainty about the type and distribution of the depositional facies. This facies uncertainty is expressed through different training images (Ti). A Ti is a necessary input to multiple-point simulation (mps) algorithms. It is a repository of types of structures deemed present in the reservoir. It must depict not only the shapes and dimensions of all facies, but also how these facies interact with one another. See Appendix A for details about the program used to generate the various training images for this case study.

Four depositional facies with varying NTG ratios are identified from core analysis.

The NTG ratio within these facies are given in Table 3.1. Facies 1, which has the lowest NTG, is the background shaly facies. Facies 4 is the main reservoir facies; it is interpreted as channels with massive sand fill. The Tis can be divided into two families depending on how facies 3 and 4 are characterized. In the first family of scenarios, facies 2 with 47.3 percent NTG is characterized as poor quality channels, and facies 3 with 63.0 percent NTG as intermediate quality channels (Figure 3.2). In the second set of scenarios, facies 2 and facies 3 have been interpreted as poor and intermediate quality debris flow deposits respectively (Figure 3.3). The within-family scenarios differ one from another with respect to channel widths, width-to-depth ratio, and channel sinuosity. To study the impact of geological scenario, one representative Ti is retained from each of these two families of Tis. Figure 3.4 shows these two scenarios. In scenario 1 the high NTG channels (red) erode the intermediate NTG channels (green), which in turn erode the low NTG channels (blue). Similarly, in scenario 2 the high NTG channels (red) erode the intermediate NTG lobes (green), which in turn erode the low NTG lobes (blue).

Note that these two Tis are only conceptual scenarios. During spatial bootstrap, synthetic data sets are not resampled from these Tis. Instead, they are obtained from stochastic reservoir models conditional to both well and seismic data and reflecting each of these two Tis. The geological scenario depicted by a Ti is only one of the parameters of the mps algorithm.

Facies number	1	2	3	4
NTG value (%)	3.8	47.3	63.0	90.7

Table 3.1: Within-facies NTG values for the four facies in the WCA reservoir

3.1.2 Prior probability distribution for global net-to-gross

A prior probability distribution of global NTG for the WCA reservoir is obtained from a database of analog reservoirs. This distribution is shown in Figure 3.5. The bounds of this distribution, [0.06, 0.61], specify the minimum and maximum NTG values expected to be found in a slope valley reservoir. In the Bayesian framework adopted

in this workflow the bounds of the posterior (final) distribution cannot be greater than those of the prior distribution, hence it is advisable to have a conservative (i.e. wide) prior distribution, as is the case in Figure 3.5.

Note that the prior distribution is defined independently of the actual data of the WCA reservoir. It is obtained by pooling together information from other reservoirs that are deemed geologically analogous to the WCA reservoir; hence it is truly a prior in the Bayesian sense. The goal of the workflow is to update this prior distribution given the actual quantitative data from the WCA reservoir. The analog database used to obtain this prior distribution classifies reservoirs at the system/structural scale, not at the depositional facies scale. For the WCA reservoir since its structural style is unambiguously determined to be slope valley, only one prior NTG distribution is available for the different facies scenarios. Ideally, each of the alternative geological scenarios retained should have a different prior NTG distribution.

Since the prior NTG distribution is independent from the local reservoir data, it does not change as new data becomes available. However, if the uncertainty about the geological scenario changes in light of new data, then a new prior distribution may have to be considered.

3.1.3 Well and seismic data

In reality, the WCA reservoir has been in production for a few years and 28 wells are available which provide a good coverage of the reservoir (Figure 3.6(a)). The wells are marked with the order they were drilled, which makes it possible to study the impact of additional data on NTG uncertainty. At the appraisal stage only four wells were available, which we retain for this study (Figure 3.6(b)). Four different facies are apparent from cores, but the interpretation of these facies varies from one geological scenario to the other (see section 3.1.1). Each facies has a constant NTG value, the same for all geological scenarios, see Table 3.1. Recall that NTG is proportion of sand.

Seismic amplitude and four derived seismic attributes are available for this study.

These attributes are acoustic impedance and Vshale values obtained from three different calibration techniques. To determine which attribute is the most informative in terms of discriminating between facies, we compute the likelihood of observing a particular seismic datum value given a facies value from colocated facies-seismic data pairs along the wells. The smaller the overlap between the likelihood histograms of different facies, the better the discrimination power. Amongst the seismic attributes provided, acoustic impedance proved to be the best discriminator of facies; hence, was retained for NTG estimation (Figure 3.7). Note that impedance discriminates reasonably facies 1 from the others. However, the discrimination amongst facies 2, 3 and 4 is poor. The Vshale attribute does not discriminate well the facies as seen from its seismic likelihoods (Figure 3.8).

3.2 NTG estimation

At reservoir appraisal stage wells are few and they tend to be preferentially located in high pay zones. The four appraisal wells in the WCA reservoir are indeed preferentially located in the Eastern part of the incised valley (Figure 3.6(b)), hence the NTG estimate retained from these four clustered wells might not be representative of the global NTG of the reservoir. Seismic data, on the other hand, informs the entire area. If seismic is informative and properly calibrated with the reservoir facies, then an integrated well-seismic NTG estimate would provide a better (less biased) estimate of to the global NTG value. Bayes inversion, as described in Section 1.3.1, is retained to calibrate acoustic impedance with facies for this case study. The corresponding impedance likelihood histograms are given in Figure 3.7.

If the calibration is properly done and the seismic data are informative, we expect that these updated proportions would be more representative of the actual global facies proportions in the reservoir than the well facies proportions. Table 3.2 gives the original proportions of the four facies from wells and the updated proportions after integrating acoustic impedance with the well facies data.

Notice that the proportion of facies 4, which is has highest NTG ratio has gone down, while that of facies 1, which is the low NTG background facies has gone up.

Facies number	1	2	3	4
Well propotions	0.63	0.10	0.06	0.21
Updated proportions	0.66	0.09	0.06	0.18

Table 3.2: Facies proportions observed along the wells and after integrating well data with acoustic impedance data.

This implies that the initial wells were preferentially located in higher pay zone. Without the correction induced by seismic data the reservoir NTG might be over estimated from the sole well data. Equation 3.1 is used to compute the reservoir NTG by combining the updated facies proportions p_i and the within-facies NTG values n_i given in Table 3.1 under the constraint that the proportions sum to one.

$$a^\star = \sum_i (p_i \times n_i) \quad ; \quad with \ \sum_i p_i = 1 \tag{3.1}$$

The well NTG estimate and the updated NTG estimate after integrating acoustic impedance (AI) data are given in Table 3.3.

Data	NTG estimate
4 wells	0.484
4 wells + AI	0.436

Table 3.3: NTG estimate from wells and estimate after integrating well and acoustic impedance (AI) data.

Consider the reverse situation when the global NTG value (i.e. the average sand proportion) and the within-facies NTG values n_i are fixed and we need to compute the proportion of each facies. This computation is needed for the part of the workflow in which facies realizations honoring a global target are to be simulated. The simulation algorithm needs to know the average proportions of each facies separately. Recall that the prior global NTG distribution only gives the average proportion of sand in the reservoir, not the average proportion of each facies.

In a two facies case Equation 3.1 is sufficient to compute the facies proportions because we have two unknowns (facies proportions) and two constraints (Equation

3.1 and $\sum_i p_i = 1$). For more than two facies, however, we have more unknowns than constraints. It is not possible to compute facies proportions unless additional constraints are introduced to match the number of unknowns. In the WCA reservoir there are four facies; hence, two additional constraints are necessary to solve for the four unknown facies proportions.

We propose to freeze the ratio of facies proportions to get these additional constraints. This is a reasonable constraint in many depositional environments. Consider the example of four common facies in a fluvial reservoir, namely channels, levees, crevasse and floodbasin. By freezing the ratio of channel to levee and that of channel to crevasse, we can eliminate two unknowns proportions (levee and crevasse), and then solve for channel and floodbasin proportions using Equation 3.1. Once the proportion of channel is known, the proportions of levee and crevasse can be obtained from the ratios. These facies proportions ratio are uncertain parameters; they can be read from a training image, analog outcrops and reservoirs or can be provided by an expert geologist. This approach works best when facies proportions are tightly related as in a fluvial case. In case of the WCA, we froze the ratio of proportions of facies 2 to facies 4 and that of facies 3 to facies 4. These ratios for each scenario were taken from the corresponding Ti. The proportion of the four facies in the two scenarios are very similar, see Table 3.4.

Facies #	1	2	3	4
Ti1	0.51	0.10	0.09	0.30
Ti2	0.50	0.11	0.09	0.30

Table 3.4: Global facies proportions of Ti1 and Ti2.

3.3 Sampling in uniformly thick domain

Spatial bootstrap is a technique of resampling synthetic data sets from conditional stochastic realizations. It asks the question: what would be the NTG estimate if the wells were drilled elsewhere in the reservoir. Since one does not have the luxury of

drilling new wells from the actual reservoir due to economic constraints, synthetic wells are sampled from virtual representations of the reservoir. Spatial bootstrap is more suitable to earth sciences data sets than classical bootstrap because data along a well and between wells are spatially correlated. When resampling from a virtual field, this correlation must be honored. This can be achieved by preserving the original drilling strategy, which includes the original well pattern (for instance drill pairs of wells in low impedance zones). As discussed in Section 1.3.4, the original well pattern can be honored in two ways: 1) by freezing the exact inter-well geometry of the original well configuration and displacing this configuration when sampling, or 2) by maintaining a minimum distance between the synthetic wells so that no two wells are closer than the prescribed distance.

Three sampling strategies for spatial bootstrap histogram are considered here: 1) fixed configuration, 2) minimum interdistance, and 3) random (i.e. no constraints between wells).

In the fixed configuration bootstrap the inter-well geometry is fixed. That well geometry is computed as follows: first, the (x,y) locations of all actual wells are noted. For deviated wells all data (x,y,z) coordinates must be noted. A centroid of the well configuration is calculated. Then, the relative distance of all other wells from that centroid is stored in a well geometry vector. When sampling a new data set, fixed configuration bootstrap proceeds as follows:

- Pick a vertical centroid location at random using the random number seed
- Drill all wells relative to the centroid using the well geometry vector

Any other sampling constraints such as specific region, specific well deviations, vertical cut-off, etc, can be honored. If all specified constraints are not satisfied, then a well will not be drilled at that location. If a synthetic data set contains fewer wells than the original set, it is rejected.

The minimum interdistance constraint is less restrictive than the fixed configuration constraint. When sampling, we only need to ensure that the minimum distance between any two resampled wells is greater than or equal to the specified distance.

This constraint may be more appropriate than the fixed configuration constraint when the actual wells are not heavily clustered or their number is large. Minimum interdistance constraint approaches random sampling when the minimum distance between wells becomes very small.

Random sampling is devoid of any constraints, all well locations are permissible. It may be used when no drilling strategy is apparent from the actual wells.

The importance of freezing well configuration was briefly demonstrated in Section 2.2.3. In this section we investigate further how different sampling strategies impact the spatial bootstrap histograms. Re-sampling is allowed over the entire grid; there are no restrictions due to region, vertical cutoffs, etc. Because the domain is of constant thickness, all synthetic data sets with the same number of wells have the same number of data points. Seismic data is not used in the present exercise. The following parameters are varied: 1) geological scenario, and 2) original well configuration.

3.3.1 Different geological scenarios

The three geological scenarios considered are shown in Figure 3.9. These scenarios were obtained as conditional stochastic realizations generated from the multiple-point simulation (mps) algorithm *snesim*. For each scenario, we compare the spatial bootstrap histograms obtained using the three different re-sampling techniques. Number of re-samplings is fixed at 500 and the initial random number seed in all cases is 37591.

The reference field contains 78 x 59 x 116 grid blocks; block dimensions are 75 x 75 meter in X and Y directions and 2.5 meter in Z. Each scenario contains four facies with different within-facies net-to-gross (NTG) values, see Table 3.5. In every scenario, the red facies (4) has the highest NTG, followed by the green (3) and blue (2) facies. The white facies (1) is the low NTG, dominantly mud facies. In scenario 1 (Figure 3.9(a)) all the facies are channelized. In scenario 2 (Figure 3.9(b)), the high NTG facies is channelized, and the intermediate NTG facies are lobes. In scenario 3 (Figure 3.9(c)), all facies are in form of lobes.

The three reference well locations are shown in Figure 3.10. The net-to-gross

Facies #	1	2	3	4
NTG value (%)	3.8	47.3	63.0	90.7
Scenario 1	0.51	0.10	0.09	0.30
Scenario 2	0.49	0.10	0.08	0.33
Scenario 3	0.51	0.10	0.08	0.31

Table 3.5: True global facies proportions of different scenarios used for the study.

estimate from these wells for the three scenarios and the corresponding reference global NTG values are given in Table 3.6. Note that the well NTG estimates are close to the global NTG values. For the fixed configuration spatial bootstrap, the inter-well geometry is computed from these three wells. For the minimum interdistance spatial bootstrap, a minimum distance of 500 meter is maintained between the wells. As for random sampling, it is free of all constraints.

Scenario #	1	2	3
3 Well NTG	0.39	0.39	0.41
True Global NTG	0.40	0.42	0.40

Table 3.6: Net-to-gross estimates and global NTG for three different geological scenarios.

Results for Scenario 1

The spatial bootstrap histograms for the three sampling techniques for scenario 1 are shown in Figure 3.11. Selected summary statistics are presented in Table 3.7.

The three histograms are very similar because the channel geometry does not coincide with the triangular well geometry. The mean and median of all three histograms identify the true global NTG value (0.40). The three $[p_{10}, p_{90}]$ intervals are all centered on the mean.

Results for Scenario 2

The spatial bootstrap histograms for the three sampling techniques for scenario 2 are shown in Figure 3.12. Selected summary statistics are given in Table 3.8.

Constraint	FC	MD	CR
mean	0.40	0.40	0.40
median	0.40	0.40	0.40
p_{10}	0.35	0.36	0.35
p_{90}	0.44	0.44	0.44
$p_{90} - p_{10}$	0.09	0.08	0.09

Table 3.7: Summary statistics of the spatial bootstrap histograms for different sampling techniques for scenario 1 (True NTG = 0.40). FC = fixed configuration; MD = minimum interdistance; CR = completely random.

Constraint	FC	MD	CR
mean	0.41	0.41	0.41
median	0.41	0.41	0.41
p_{10}	0.37	0.36	0.37
p_{90}	0.45	0.46	0.46
$p_{90} - p_{10}$	0.08	0.10	0.09

Table 3.8: Summary statistics of the spatial bootstrap histograms for different sampling techniques for scenario 2 (True NTG = 0.42). FC = fixed configuration; MD = minimum interdistance; CR = completely random.

The three histograms are again very similar because the high NTG facies in this scenario are also channelized. The mean and median of all three histograms are close to the true global NTG value of scenario 2 (0.42). The three $[p_{10}, p_{90}]$ intervals are centered on the mean.

Results for Scenario 3

The spatial bootstrap histograms for the three sampling techniques for scenario 3 are shown in Figure 3.13. The summary statistics are given in Table 3.9.

The three histograms are no longer similar. The $[p_{10}, p_{90}]$ interval corresponding to the fixed configuration strategy is significantly wider than the intervals of the minimum interdistance and random sampling techniques. The minimum interdistance and random sampling strategies produce similar uncertainty intervals. All histograms are symmetric and centered on their respective means. The histogram means are

Constraint	FC	MD	CR
mean	0.40	0.39	0.39
median	0.40	0.39	0.39
p_{10}	0.29	0.32	0.32
p_{90}	0.51	0.46	0.46
$p_{90} - p_{10}$	0.22	0.14	0.14

Table 3.9: Summary statistics of the spatial bootstrap histograms for different sampling techniques for scenario 3 (True NTG = 0.40). FC = fixed configuration; MD = minimum interdistance; CR = completely random.

reasonably close to the true global NTG of scenario 3 (0.40).

Discussion of impact of geological scenario

These experiments demonstrate that sampling strategy does impact the spatial bootstrap histograms, but the magnitude of the impact is case-specific. For scenarios 1 and 2 (Figures 3.9(a) and 3.9(b)), the different sampling strategies produced similar results because this particular three well configuration was not designed to detect channelized features in these two scenarios. However, the sampling strategy proved to be very important for the lobe scenario 3. Minimum interdistance and random sampling provided narrower uncertainty intervals, see Table 3.9. The wider range of estimates obtained with the fixed configuration sampling in scenario 3 is explained as follows: the average size of the high NTG lobes is such that the likelihood of all three wells either hitting or missing these lobes is high.

For all three scenarios we observe that the histograms resulting from minimum interdistance and random sampling strategies are very similar. This is because the minimum interdistance of 500 m, which corresponds to about seven grid blocks, is so small (lax) that it is equivalent to random sampling. Instead, when wells are tightly clustered, we should have considered a maximum interdistance constraint to honor the high spatial correlation between the original wells. This fact is clearly demonstrated in scenario 3, where freezing the original well configuration resulted in a much wider uncertainty interval.

Scenario 2 is a hybrid of scenarios 1 (all channels) and 3 (all lobes), because it contains both channels and lobes. However, in terms of NTG estimation uncertainty scenario 2 is closer to scenario 1 because of the common high NTG facies which controls the global estimate. The intermediate quality facies in scenario 2 are lobes, but these lobes are small and in small relative proportion compared to the channels; hence they do not contribute much to the global NTG. Figure 3.14 shows the Q-Q plots of histograms corresponding to scenario 1 and 2 for the three different sampling techniques. Contrast these Q-Q plots with the ones corresponding to scenario 1 and 3 (Figure 3.15). The Q-Q plots of scenario 2 versus scenario 3 (not given) are similar to those given in Figure 3.15.

3.3.2 Different well configurations

In case of the lobe scenario 3 we saw that freezing the well configuration has a large impact on the spatial bootstrap histogram because the average size of the high NTG lobes was wide enough to contain or exclude all three wells arranged in a triangular configuration (Figure 3.10). To study the impact of different well configuration, we compare the spatial bootstrap histograms resulting from the triangular three well configuration of Figure 3.10 to those resulting from the linear three well configuration of Figure 3.16. The three linear wells are actual appraisal stage wells from Kuito. Only the lobe scenario 3 (Figure 3.9(c)) is retained for this experiment as it is the most revealing. The number of re-samplings is fixed at 500 and the initial random number seed is set to 37591. We compare the spatial bootstrap histograms resulting from these two different well configurations for the fixed configuration and minimum interdistance re-sampling strategies.

Results for fixed configuration bootstrap

Figure 3.17 shows the spatial bootstrap histograms corresponding to the triangular and linear three well configurations. Table 3.10 gives selected summary statistics.

The $[p_{10}, p_{90}]$ interval of the histogram corresponding to the triangular well configuration is slightly wider than that of the linear configuration. The wider range is

Configuration	Triangular	Linear
mean	0.40	0.40
median	0.40	0.40
p_{10}	0.29	0.30
p_{90}	0.51	0.49
$p_{90} - p_{10}$	0.22	0.19

Table 3.10: Summary statistics of the fixed configuration spatial bootstrap histograms for triangular vs linear 3 well configuration in scenario 3 (Figure 3.9(c)).

explained by the fact that the likelihood that all three wells hit or miss a high NTG lobe is higher in the triangular case because the well configuration is tighter. Both histograms have similar mean and median values.

Results for minimum interdistance

Figure 3.18 shows the spatial bootstrap histograms corresponding to the two different well configurations for the minimum interdistance constraint. The minimum distance between any two wells in the triangular configuration is 500 meters. In the linear configuration, the minimum distance is only 200 meters. Figure 3.18 shows the spatial bootstrap histograms corresponding to the two different well configurations. Table 3.11 gives selected summary statistics.

	Triangular (500 m)	Linear (200 m)
mean	0.39	0.39
median	0.39	0.39
p_{10}	0.32	0.32
p_{90}	0.46	0.47
$p_{90} - p_{10}$	0.14	0.15

Table 3.11: Summary statistics of the minimum interdistance spatial bootstrap histograms for triangular vs linear 3 well configuration in scenario 3 (Figure 3.9(c)).

The two histograms have similar mean and median values. The $[p_{10}, p_{90}]$ interval of the histogram corresponding to the linear 3 wells configuration is comparable to that of the triangular configuration. Even though the minimum interdistance in the

triangular case (500 m) is greater than in the linear configuration case (200 m), that difference carries little consequence.

Fixed configuration vs. minimum interdistance

Consider a new triangular 3-well configuration similar to the one shown in Figure 3.10, but now the minimum interdistance between any two wells is only 200 meters. The minimum interdistance between the wells in the linear case remains at 200 meters. Since this minimum interdistance between the wells is the same for both configurations, the resulting spatial bootstrap histograms are identical. However, the bootstrap histogram for the fixed configuration case is very different (Figure 3.19), since the two well configurations are very different - one is a triangular 3-well configuration with narrowly spaced wells, the other is a linear configuration. Table 3.12 gives the summary statistics of the histograms in the fixed configuration case. It is not surprising that the histogram in the narrowly spaced triangular configuration is the widest, followed by the wider 3-well triangular configuration and the linear 3-well configuration.

	Triangular (200 m)	Triangular (500 m)	Linear (200 m)
mean	0.40	0.40	0.40
median	0.40	0.40	0.40
p_{10}	0.27	0.29	0.30
p_{90}	0.52	0.51	0.49
$p_{90} - p_{10}$	0.25	0.22	0.19

Table 3.12: Summary statistics of the fixed configuration spatial bootstrap histograms for the new triangular vs linear 3 well configuration in the lobe scenario 3 (Figure 3.9(c)).

Discussion of impact of initial well configuration

In this section we compared the spatial bootstrap histograms resulting from using different well configurations. These tests were performed for the lobe scenario, with

the average size of the high NTG lobes coinciding with some of the well interdistances. The results demonstrate that a minimum interdistance constraint is not sufficient to differentiate between such different well configurations (Figure 3.20(b)). For instance, when the interdistance between wells was similar, the bootstrap histograms for the triangular vs. linear configurations were identical. A maximum interdistance imposed to the resampled wells should be considered. In the fixed configuration resampling case, the impact of well configuration depends on the well geometry and the facies geometries. But it is safe to advise freezing the original well configuration in presence of sparse and clustered well geometry.

3.4 Sampling in non-uniformly thick domain

The importance of freezing any tightly clustered well configuration was demonstrated for a uniformly thick domain. Deep-water reservoirs like the WCA reservoir tend to have complex stratigraphic architecture with non-uniformly thick domains. When re-sampling vertical wells in such non-uniformly thick domains, problems arise because of the resulting unequal number of samples. Some locations in the domain may not be suitable for sampling, and in thinner zones the original number of data points may not be available. Figure 3.21 depicts the average thickness map of the two vertically overlapping slope valleys shown in Figure 3.1. Valley AB, which is bigger and stratigraphically younger, is thickest in the East and thins out going West. Both valleys also thin as they pinch out along the edges parallel to their long axes. The appraisal stage four wells are located in the thicker Eastern part of valley AB, these wells have a total of 274 data points. Wells located in the thinner parts of the valley will yield fewer data points. NTG estimates from wells with fewer samples would artifically widens the spatial bootstrap histograms. This is especially true in the fixed configuration case because all four wells are closely clustered. To ensure reliable statistical inference, we reject any re-sampled data set with fewer than 75% of the original points. Such 75% tolerance is imposed because a strict 100% requirement would be too restrictive and would not yield enough re-sampled data sets for proper inference. Re-sampled data sets with fewer wells than original number of wells are

also rejected.

Spatial bootstrap with the fixed configuration is performed in the slope valley region using the four appraisal stage wells. Since these wells are deviated, they were approximated using vertical wells that pass through the center of each deviated wells (Figure 3.22). After 1000 iterations only 142 acceptable locations were found. Figure 3.23 shows the locations of the centroids of these 142 data sets. Recall that in fixed configuration re-sampling the synthetic wells are drilled relative to the centroid location. The centroids of Figure 3.23 show the area of the slope valley which is actually re-sampled. Notice how all these synthetic data sets are all located in a limited region of valley. Other areas of the valley were too thin to yield enough data points when drilled with the well geometry shown in Figure 3.22. Compare the sampled valley region in Figure 3.23 to that of Figure 3.24, which corresponds to the minimum interdistance case. Indeed, the minimum interdistance constraint does not force the wells to be tightly clustered, hence, more locations are acceptable.

To increase the possible number of drillable locations when re-sampling with fixed well configuration, we allow the well configuration to be rotated about its centroid by a random angle between [-30, 30] degrees. This increases the number of acceptable locations for this well configuration (Figure 3.25), but the valley is still not evenly sampled. When the well configuration is allowed to rotate from [0, 180] degrees (full rotation), the sampled area of the valley increases (Figure 3.26). Such rotation may not be appropriate in an anisotropic field because the spatial correlation hence redundancy between the re-sampled wells will be different, but it is acceptable in an isotropic case. When rotation is not an option, other approximations of the original well configuration should be considered.

Notice how the centroids in Figure 3.26 are closely clustered. Since the sampling domain and its discretization are limited, drilling 200 sets of four synthetic wells would cause some locations to be sampled multiple times. Thus, instead of sampling all 200 sets from a single realization, we generate two conditional realizations using the same training image and jointly consider them as scenario 3. Then, we sample 100 sets of four wells from each realization and pool together their NTG estimates to generate the spatial bootstrap distributions. Two such realizations are shown in

Figure (Figure 3.27); the global NTG of these two realizations pulled together is 0.42.

Constraint	FC	MD
mean	0.44	0.42
median	0.43	0.42
p_{10}	0.35	0.36
p_{90}	0.52	0.49
$p_{90} - p_{10}$	0.17	0.13

Table 3.13: Summary statistics of the spatial bootstrap histograms for different sampling techniques for scenario 3 (NTG = 0.42) in the slope valley region. FC = fixed configuration; MD = minimum interdistance.

Figure 3.28 gives the spatial bootstrap histograms for the fixed configuration with full rotation and the minimum interdistance sampling. Figure 3.29 shows the sampled region of valley corresponding to the two sampling strategies. Table 3.13 gives the summary statistics of these histograms. The means of the two histograms are comparable, however, the $[p_{10}, p_{90}]$ interval of the fixed configuration histogram is wider than that of the minimum interdistance histogram. These results are consistent with the ones obtained from sampling in a uniformly thick domain. The two $[p_{10}, p_{90}]$ intervals of Table 3.13 are different, but not as different as in the uniformly thick domain case. We attribute this to the various approximations that must be made when sampling in non-uniform domains.

3.5 Posterior NTG distributions for the actual WCA reservoir

In the previous sections we demonstrated the importance of freezing the original well configuration for spatial bootstrap histograms in domains of both uniform and non-uniform thickness. We also saw the impact of different geological scenarios on the spatial bootstrap histograms. Understanding the impact of these parameters on the spatial bootstrap distributions is key to understanding the results of the workflow.

In this section we first document the impact of sampling strategy on the posterior NTG distribution. Then we present the impact of geological scenario, of the prior probability distribution of global NTG, of additional wells, and of seismic data. Finally, for verification we compare the posterior probability distributions of global NTG obtained from using all 28 wells to that obtained using only the 4 appraisal stage wells. All these runs are performed in the slope valley region (non-uniformly thick domain).

3.5.1 Impact of sampling strategy

To show the impact of fixed configuration vs. the minimum interdistance sampling strategies on the posterior NTG distribution, we retain the lobe scenario 3 and the three closely clustered well configuration (Figure 3.30). The minimum interdistance between wells is 500 m. All parameters, except the sampling strategy, are the same for the two runs. The NTG estimate from the three original wells is 0.43. The posterior NTG distributions corresponding to the two sampling strategies are given in Figure 3.31. Table 3.14 gives selected summary statistics of the distributions.

Constraint	FC	MD
mean	0.35	0.37
median	0.34	0.36
p_{10}	0.24	0.30
p_{90}	0.45	0.45
$p_{90} - p_{10}$	0.21	0.15

Table 3.14: Summary statistics of posterior NTG distributions resulting from using different sampling techniques for scenario 3 in the slope valley region. FC = fixed configuration; MD = minimum interdistance.

The posterior $[p_{10}, p_{90}]$ interval corresponding to the fixed configuration (FC) sampling is significantly wider than the one corresponding to minimum interdistance (MD) sampling. Specifically, the p_{10} in the FC case is much smaller than in the MD case. Indeed, when the clustered 3-well configuration is fixed, the probability of all three wells hitting or missing a high NTG lobe is higher than in the MD case

where the wells are not necessarily clustered. This result is consistent with the trend seen in the spatial bootstrap histograms of Section 3.4. The actual impact of well configuration on the posterior NTG distribution depends on the type of patterns in the geological scenario and the well spacing. Since the actual four appraisal stage wells of the WCA reservoir are preferentially clustered, only the fixed configuration constraint will be used for re-sampling in all subsequent workflow runs.

3.5.2 Impact of geological scenario

The goal of this section is to understand how the geological scenario affects the posterior NTG distribution. In the case of the WCA reservoir the main source of geological uncertainty is related to the type of depositional facies. As discussed in section 3.1.1 we retain the two scenarios shown in Figure 3.4 as representative of two families of scenarios. In addition, we retain a third hypothetical lobes scenario. Using the same four appraisal stage wells, the NTG uncertainty workflow is carried out three times, once for each scenario. All other parameters of the workflow were frozen; see Table 3.15 for details. The NTG values within each facies (Table 3.1) are held constant throughout the study.

Wells	4	Well NTG	0.48
Seismic data	Impedance	Nb impedance classes	15
Prior NTG distribution	from database	Nb NTG classes	10
Nb facies realizations per class	2	Nb of resamplings per realization	150

Table 3.15: Key parameters of the NTG uncertainty workflow used to study the impact of geological scenario uncertainty on posterior NTG distribution.

The prior probability distribution of global NTG (Figure 3.5) is discretized into 10 classes. For each such class of global NTG, the individual proportions of the four WCA facies are computed using the methodology described in section 3.2. Table 3.16 gives the facies proportions found for the three Tis. For a more reliable likelihood computation, we generate two realizations conditional to well and seismic data for each class of global NTG. From each realization, approximately 150 sets of four

synthetic wells are re-sampled. The soft probability cubes for conditioning facies realizations are derived from acoustic impedance as described in section 3.2. A different set of probability cubes is generated for each class of global NTG so that the average of these probability cubes is close to the global NTG value imposed to the simulated realization.

Facies #	1	2	3	4
Channel scenario (Ti1)	0.51	0.10	0.09	0.30
Channel + lobe (Ti2)	0.50	0.11	0.09	0.30
Lobe scenario (Ti3)	0.51	0.13	0.09	0.27

Table 3.16: Global facies proportions of Ti1, Ti2 and Ti3.

Construction of geological scenarios for different global NTG classes

As seen from previous sections, spatial bootstrap histograms depend heavily on the geological scenarios from which re-sampling is done. Thus, it is important to be able to reproduce, as faithfully as possible, the structures contained in the scenario. Different simulation algorithms have different capabilities and limitations for generating facies realizations; hence, it is important to carefully choose the simulation algorithm. For example, Sequential Indicator Simulation (SIS) is a variogram-based algorithm, which means it can only account for two-point statistics. It has excellent data conditioning capabilities for both hard and soft data. However, curvilinear features like channels cannot be simulated using SIS because such features require more than two-point statistics.

For this study, we decided to use the multiple-point simulation (mps) algorithm *snesim* (Strebelle, 2002; Remy et al., 2008), which is a well-known and a widely available program for simulating categorical variables. Unlike SIS the *snesim* algorithm utilizes multiple-point statistics expressed through a training image (Ti).

The different facies deemed present in the WCA reservoir are conveniently expressed as Tis. However, no open source software was available for generating these Tis. Hence, a new program called *TiGenerator* was written specifically for this purpose. *TiGenerator* is a program for creating unconditional Boolean simulations. It is

available as a plug-in for the open source geostatistical software SGeMS (Remy et al., 2008). The algorithm and a description of its parameters are presented in Appendix A.

The virtual reservoirs from which synthetic wells are sampled are not the Tis, but the snesim conditional realizations generated using that Ti. Thus, the mps simulation algorithm, the parameters of that algorithm (which includes the Ti), and the conditioning data jointly define the geological scenario underlying the simulated realizations used for resampling.

The range of prior NTG distribution for WCA is quite large (0.06 to 0.61) (Figure 3.5). Using a single Ti with intermediate proportions (say 0.40) to generate facies realizations for all prior global NTG classes would result in poor pattern reproduction. When the proportion of facies in the Ti is very different from the target proportion to be simulated, that inconsistency leads to poor pattern reproduction. In the *snesim* algorithm, the larger the proportion(s) difference, the poorer the reproduction of Ti patterns.

To reduce the amount of servosystem correction for target proportion correction, we generate a different Ti for each class of global NTG using *TiGenerator*. Each Ti contains the same geometric patterns that characterize a scenario, but the global NTG of these Tis vary from one class to another. Figures 3.32, 3.35 and 3.38 show Tis for scenarios 1 to 3 for selected global NTG classes.

A common misconception is that a Ti is the structural model for mps. In reality, Ti is just one of the input parameters to the mps exercise. The actual structural model used by *snesim* depends on the size and shape of template which is used for scanning the Ti. The only way to check this input structural model is to generate unconditional realizations. Figures 3.33, 3.36, and 3.39 show the unconditional realizations corresponding to the three geological scenarios, for selected global NTG classes. Table 3.17 gives the key *snesim* parameters used for generating these realizations.

As seen from Figure 3.36, scenario 2 Ti is by far the poorest reproduced by the non-conditional realizations, because of the additional complexity brought by the interaction of channel and lobe patterns. These two features exhibit very different shapes and spatial continuity. A hierarchical simulation approach (Maharaja, 2005)

Parameter	Value
Max template nodes	81
Template anisotropy	2:2:1
Min nb replicates	1
Nb multi-grids	4

Table 3.17: Key parameters of the *snesim* algorithm used for generating the three geological scenarios.

in which facies are simulated sequentially instead of jointly would have improved channel connectivity in such case. For example, first simulate the two lobe facies, then simulate channels that erode both these lobes. In this study, for lack of time we performed joint simulation of the four facies.

Figures 3.34, 3.37, and 3.40 give *snesim* conditional realizations for the corresponding global NTG for the two scenarios. These realizations are conditional to the four appraisal stage wells and the facies probability cubes derived from acoustic impedance data. As seen from the realizations in Figures 3.34 and 3.37, the channels are not well reproduced, especially for the low NTG classes. Even though the Ti facies proportions are close to the target simulation proportions, it is difficult to simulate thin continuous channels. Unlike in object-based simulations, these images are built one pixel at a time. This enables easy conditioning to different types of data, but the connectivity of thin, curvilinear channels is not well reproduced. Notice that the channels are already fragmented in the unconditional simulations of scenarios 1 and 2. The patterns present in these unconditional simulations are representative of how the *snesim* algorithm performs for a given set of parameters, not of what is depicted by the Ti.

Tables 3.18 and 3.19 present the individual facies proportions corresponding to the 10 global NTG classes for the WCA reservoir. These proportions were obtained using the methodology described in section 3.2. The facies proportions for scenarios 1 and 2 are similar (Table 3.18), since the fixed ratios of proportions of facies in these two scenarios are the same. The individual facies proportions for scenario 3 are slightly different (Table 3.19).

Global NTG	1	2	3	4
0.09	0.93	0.02	0.01	0.04
0.14	0.86	0.03	0.02	0.09
0.20	0.78	0.05	0.04	0.13
0.25	0.70	0.07	0.05	0.18
0.31	0.63	0.08	0.07	0.22
0.36	0.55	0.10	0.08	0.27
0.42	0.47	0.12	0.09	0.32
0.47	0.40	0.13	0.11	0.36
0.53	0.32	0.15	0.12	0.41
0.58	0.25	0.17	0.13	0.45

Table 3.18: Individual facies proportions for different global NTG values for scenarios 1 and 2.

Global NTG	1	2	3	4
0.09	0.93	0.02	0.01	0.04
0.14	0.85	0.04	0.03	0.08
0.20	0.77	0.06	0.04	0.13
0.25	0.70	0.08	0.06	0.16
0.31	0.62	0.10	0.07	0.21
0.36	0.53	0.12	0.08	0.26
0.42	0.46	0.14	0.10	0.30
0.47	0.39	0.16	0.11	0.34
0.53	0.30	0.19	0.13	0.38
0.58	0.22	0.21	0.14	0.43

Table 3.19: Individual facies proportions for different global NTG values for scenario 3.

Posterior NTG distributions for different scenarios

The four appraisal stage wells are retained for all three scenarios. An integrated well and seismic NTG estimate of 0.436 is obtained using the estimation procedure described in section 3.2. The posterior distributions conditional to this estimate are given in Figure 3.41. The mean, median and $[p_{90}, p_{10}]$ intervals of these three posteriors are summarized in Table 3.20.

The mean and median of the three posteriors are comparable. However, the

Scenario	1	2	3
mean	0.38	0.37	0.37
median	0.38	0.36	0.38
p_{10}	0.32	0.27	0.26
p_{90}	0.44	0.45	0.46
$p_{90} - p_{10}$	0.12	0.18	0.20

Table 3.20: Summary statistics of the posterior NTG distributions obtained using scenarios 1, 2 and 3.

width of the $[p_{90}, p_{10}]$ interval changes with the scenario. This confirms the fact that geological scenario matters. Hence, if a geological scenario is uncertain, which is likely at appraisal stage, alternate scenarios that fit the data should be considered. The $[p_{90}, p_{10}]$ interval corresponding to scenario 1 (all channels) is the narrowest. The p_{10} of both scenario 2 (channels and lobes) and scenario 3 (all lobes) is lower than that of scenario 1. Lobes, as opposed to channels, increase the likelihood that the four wells are either all contained inside or outside the lobes. In scenario 2 the high NTG channel facies are thicker than in scenario 1 and the channels tend to be more clustered. Moreover, the two intermediate NTG facies in scenario 2 are lobate. Scenario 2 is a hybrid between scenarios 1 and 3, so it is reassuring that its posterior statistics fall between those of the two more extreme scenarios.

Recall from Section 3.1.1 that originally there were four scenarios (Tis) in which all reservoir facies are channelized (Figure 3.2). The channels in these channels, however, have different widths and sinuosity. Ti1 (Figure 3.2(b)) was retained as a representative scenario out of these four Tis to study geological scenario uncertainty. Figure 3.42 gives the posterior NTG distributions corresponding to the three other channelized scenarios (Figures 3.2(b) to 3.2(d)); Table 3.21 gives the corresponding posterior statistics. These posterior NTG distributions are more or less similar, which implies that NTG uncertainty is governed by the major differences between scenarios, for example, lobes vs. channels, not so much by subtle differences, such as small variations in channel width and sinuosity from one scenario to another

mean	0.37	0.38	0.39
median	0.38	0.38	0.39
p_{10}	0.29	0.32	0.32
p_{90}	0.44	0.44	0.46
$p_{90} - p_{10}$	0.15	0.12	0.14

Table 3.21: Summary statistics of the posterior NTG distributions corresponding to different channelized scenarios shown in Figures 3.2(b) to 3.2(d).

3.5.3 Impact of prior NTG distribution

As mentioned in section 3.1.2, unfortunately only one prior probability distribution for global NTG is available for the different facies scenarios because, in the analog database system used for this study, the reservoirs are classified at the system scale and not based on the depositional facies. Ideally, each geological scenario should have a different prior distribution associated with it. Since, we do not have different prior NTG distributions for the WCA reservoir, we retain for the lobe scenario 3 a triangular probability distribution between [0.25, 0.65] with a mode 0.50. The distribution is discretized into 10 classes (Figure 3.43). Notice that this distribution is much narrower than the distribution obtained from the analog database (Figure 3.5). Only scenario 3 is used for this run. Summary statistics of the two prior NTG distributions and the corresponding posterior NTG distributions are give in Table 3.22.

Distribution	Prior from analogs	Posterior from analog prior	Triangular prior	Posterior from triangular prior
mean	0.34	0.37	0.47	0.41
median	0.32	0.38	0.47	0.41
p_{10}	0.18	0.26	0.35	0.34
p_{90}	0.52	0.46	0.57	0.49
$p_{90} - p_{10}$	0.34	0.20	0.22	0.15

Table 3.22: Summary statistics of two prior NTG distributions and their corresponding posterior NTG distributions for scenario 3.

Figure 3.44 and Table 3.22 compare the posteriors resulting from using the two

different prior distributions. Note that the initial NTG estimate, 0.44, is the same in both cases because the same set of four initial wells and acoustic impedance data are retained. The mean of the posterior distribution resulting from the Triangular prior is higher than that resulting from the analog prior, which is a consequence of the difference observed in the two prior NTG distributions. In both cases, the posterior $[p_{10}, p_{90}]$ intervals are smaller than the prior intervals, as expected. But, the posterior $[p_{10}, p_{90}]$ interval corresponding to the Triangular prior is smaller than that of the posterior resulting from the analog prior. This is also consistent with the $[p_{10}, p_{90}]$ interval difference of the two prior distributions.

Consider now a uniform probability distribution over [0.25, 0.65] as a prior global NTG distribution. This is an extreme distribution because it implies that each class of NTG between its bounds is equally likely. The posterior NTG distribution corresponding to this uniform prior NTG distribution is given in Figure 3.45(b). Compare it with the posterior resulting from the triangular distribution with the same bounds (Figure 3.43). Table 3.23 summarizes the statistics of the uniform prior distribution and the corresponding posterior distribution. The statistics of the triangular prior distribution and its posterior are also given for comparison.

Distribution	Uniform prior	Posterior from uniform prior	Triangular prior	Posterior from triangular prior
mean	0.45	0.38	0.47	0.41
median	0.45	0.39	0.47	0.41
p_{10}	0.29	0.31	0.35	0.34
p_{90}	0.61	0.47	0.57	0.49
$p_{90} - p_{10}$	0.32	0.16	0.22	0.15

Table 3.23: Summary statistics of uniform and triangular prior NTG distributions and their corresponding posterior NTG distributions for scenario 3.

Both runs are done using exactly the same parameters and both prior distributions have the same 10 global NTG classes ($A = a_m; m = 1, \ldots, 10$). Hence, the likelihood of observing a NTG estimate $a_0^\star = 0.44$ in any global NTG class given scenario g_3, $P(A^\star = 0.44|A = a_m, G = g_3)$, is the same in both cases. Thus, the difference in the posterior probability of a given class of global NTG $P(A = a_m|A^\star = 0.44, G = g_3)$

comes entirely from the prior probability of that class $P(A = a_m)$ (Equation 1.5). Indeed, the prior probability for the first three global NTG classes from the uniform prior is significantly higher than that from the triangular prior distribution. Hence, the posterior probability of these classes is also higher for the posterior corresponding to the uniform prior. The prior and posterior probabilities of each global NTG class for the two cases are presented in Table 3.24.

$A = a_m$	Likelihood $P(a_0^\star \mid a_m)$	Uniform $P(a_m)$	Uniform $P(a_m \mid a_0^\star)$	Triangular $P(a_m)$	Triangular $P(a_m \mid a_0^\star)$
0.27	0.061	0.1	0.039	0.004	0.0028
0.31	0.047	0.1	0.061	0.032	0.018
0.35	0.13	0.1	0.16	0.064	0.094
0.39	0.18	0.1	0.23	0.096	0.20
0.43	0.19	0.1	0.24	0.128	0.29
0.47	0.12	0.1	0.15	0.16	0.22
0.51	0.062	0.1	0.08	0.18	0.14
0.55	0.017	0.1	0.02	0.16	0.031
0.59	0.0	0.1	0.0	0.10	0.0
0.63	0.0	0.1	0.0	0.053	0.0

Table 3.24: Prior and posterior probabilities corresponding to different global NTG values for uniform and triangular NTG distributions using scenario 3. Here $a_0^\star = 0.44$.

These experiments demonstrate the impact of the range and shape of the prior NTG distribution on the posterior NTG distribution. The range of the posterior distribution is always smaller than that of the prior distribution. The shape of the prior distribution impacts the posterior probability $P(A = a_m | A^\star = a_0^\star, G = g_k)$ through Equation 1.5.

3.5.4 Impact of additional data

The impact of additional data on the posterior NTG distribution is studied using the channel scenario 1. The goal is to see how the posterior NTG distribution changes as additional well data become available. We repeat the entire workflow four times, first using only well 1, then adding well 2, then well 3 and finally with all four

appraisal stage wells. The only parameters that change from one run to another are the number of wells and the corresponding initial NTG estimates. The same seismic data is used in all four runs. Table 3.25 summarizes the well NTG and the updated NTG estimates after integration of acoustic impedance data. The resulting posterior NTG distributions are shown in Figure 3.46; summary statistics are given in Table 3.25.

Nb wells	Well NTG	Updated NTG	Posterior mean	Posterior $[p_{10}, p_{90}]$
1	0.36	0.35	0.33	[0.23, 0.44]
1,2	0.47	0.45	0.43	[0.36, 0.50]
1,2,3	0.47	0.43	0.38	[0.32, 0.45]
1,2,3,4	0.48	0.44	0.38	[0.32, 0.44]

Table 3.25: Well NTG and the corresponding updated NTG estimates for wells 1 to 4. The updated estimates are retained for the study.

The $[p_{10}, p_{90}]$ interval of the posterior distribution with the first well (Figure 3.46(a)) is much narrower than that of the prior NTG distribution $[0.18, 0.52]$ (Figure 3.5). The posterior distribution mean and the $[p_{10}, p_{90}]$ interval shifts to the right when well 2 is introduced (Figure 3.46(b)) because the combined NTG estimate of wells 1 and 2 is much higher than that of well 1. Also, the $[p_{10}, p_{90}]$ interval of the posterior with two wells is narrower than that with well 1 only. This trend is also observed when wells 3 and 4 are introduced. In all four cases the $[p_{10}, p_{90}]$ interval is roughly centered over the corresponding posterior mean as expected. The initial NTG estimates (Table 3.25) are included in all posterior $[p_{10}, p_{90}]$ intervals. The mean and the $[p_{10}, p_{90}]$ intervals of the posterior distributions are strongly impacted by the initial NTG estimate as demonstrated by this study. Hence, when estimating NTG it is critical to carefully choose the estimation algorithm and consider all available data and account for errors in data, data uncertainty and the redundancy between different data.

3.5.5 Impact of seismic data

The four initial wells are used to study the impact of seismic data on the posterior NTG distribution. The workflow is run twice, once using acoustic impedance and once without using it. Scenario 1 and the analog prior NTG distribution shown in Figure 3.5 are used for both runs. Table 3.26 gives the initial NTG estimate and the posterior statistics resulting from the two runs. The resulting posterior distributions are shown in Figure 3.47.

	with seismic (AI)	without seismic
Well NTG	0.48	0.48
Initial estimate	0.44	0.48
Posterior mean	0.38	0.44
Posterior $[p_{10}, p_{90}]$	[0.32, 0.44]	[0.38, 0.49]

Table 3.26: Posterior NTG distribution statistics for scenario 1 with and without using acoustic impedance (AI) data.

When seismic data is not used the initial estimate is the same as the well estimate. Integrating seismic data lowers the estimate which indicates that the four appraisal stage wells are preferentially located. Comparing the posterior distribution in Figure 3.47(a) with that in Figure 3.47(b) we observe that the posterior $[p_{10}, p_{90}]$ interval widths are comparable in the two cases, however, the $[p_{10}, p_{90}]$ without seismic is shifted to the right as the initial NTG estimate without seismic data is higher. Note that in both cases the initial estimate is included in the posterior $[p_{10}, p_{90}]$ and this interval is roughly centered around the posterior mean.

3.5.6 Comparison with dense well data

In real life we do not have the luxury of knowing the true global NTG of a reservoir. In the case of the WCA reservoir, however, we do have at later times dense well data that provides a good coverage of the WCA reservoir, see Figure 3.6(a) for the location of all 28 wells. The NTG estimate from these 28 wells and the integrated 28 well and seismic NTG estimate are given in Table 3.27 along with the estimates from

the four initial wells. Note that the acoustic impedance distribution was discretized into 30 classes (instead of 15) for the 28 wells because we have more calibration data than with only 4 wells. We notice that after integrating seismic data the 28 well NTG estimate is only slightly lowered. This suggests that these 28 wells sample the reservoir NTG reasonably well. Also, notice that the NTG estimate from the initial, clustered, four wells (0.48) is not too far from the estimate using all 28 wells (0.43).

When sampling with 28 wells, it is impractical and unnecessary to fix the well configuration when re-sampling since the wells are scattered all over the valley. Hence, for re-sampling only a minimum interdistance of 100 meter was maintained between the wells. Any re-sampled data set with fewer than 28 wells is rejected. However, the rejection criterion based on the total number of re-sampled data points was relaxed from 75% to 70% of original data points, because with 28 wells it was difficult to obtain enough re-sampled data sets with the stricter 75% criterion. The channel scenario 1 and the analog prior NTG distribution are retained for both runs.

	4 initial wells	All 28 wells
Only well estimate	0.48	0.43
Well + AI estimate	0.44	0.41
Posterior mean	0.38	0.39
Posterior $[p_{10}, p_{90}]$	[0.32, 0.44]	[0.36, 0.41]

Table 3.27: Comparison of posterior NTG distribution statistics resulting from using the 4 appraisal-stage wells vs. all 28 wells from the WCA reservoir.

Figure 3.48 and Table 3.27 compare the posterior distributions resulting from using only the four initial wells and then using all 28 wells. The means of the two posterior are similar. However, the posterior $[p_{10}, p_{90}]$ interval corresponding to the 28 wells case is significantly narrower compared to that with four initial wells. This is consistent with the results in section 3.5.4 that additional data reduces the uncertainty about NTG distribution. Indeed, with 28 wells, the global NTG is closely estimated; the mean of the spatial bootstrap histogram for each class of global NTG is close to the global NTG with small uncertainty (narrow $[p_{10}, p_{90}]$ intervals). Figure 3.49 shows the spatial bootstrap histograms corresponding to three global NTG classes

- 0.36, 0.42, 0.47. Compare these three distributions to the ones corresponding to the 4 appraisal stage wells (Figure 3.50). Because all the bootstrap distributions are narrow in the 28 well case, the likelihood of observing an estimate of 0.41 is zero for all global NTG classes, except the ones closest to 0.41. Consequently, the posterior probability distribution in the 28 well case is also very narrow.

3.6 Chapter Summary

In this chapter, we presented different posterior NTG distributions resulting from different decisions, such as, which geological scenarios should be retained, what are the prior NTG distributions, which sampling strategy should be used, how to handle re-sampling in a non-uniformly thick domain, whether or not to use seismic data, etc. Each posterior distribution is a model of uncertainty for the global NTG of the WCA reservoir. Each such model would be incomplete without a clear statement of all the modeling decisions that went into the model building. The learnings from this case study are summarized below.

- The impact of the geological scenario on the posterior NTG distribution is larger when the facies geometries are very different. Generating a different Ti for different global NTG values is better for pattern reproduction than using a single Ti. In certain cases, a hierarchical simulation of facies may be better than joint simulation of all Ti facies.

- The geological uncertainty is related to a specific well configuration; it is important to freeze well pattern when re-sampling, especially when the wells are sparse and clustered. Ignoring spatial correlation between wells can lead to inaccurate models of NTG uncertainty.

- In the Bayesian framework adopted in this workflow, the range of the posterior distribution cannot be larger than that of the prior distribution; hence, the prior distribution should be chosen carefully. The shape of the prior distribution impacts the posterior probability. Ideally, different prior NTG distributions should be used with different geological scenarios.

- In the WCA case study, as more wells were used the posterior uncertainty intervals became narrower. This is because more wells provide a more precise estimate of the global NTG. However, more wells does not necessarily always means less uncertainty. If the additional well drastically changes the NTG estimate or the geological scenario, then the posterior interval may be wider than before.

- As more wells become available, the number of geological scenarios g_k and their prior probability $P(G = g_k)$ may change. Some scenarios may become more or less likely, and some may be eliminated altogether. Reassessment of the geological scenarios and their prior probability of occurence was not addressed in this case study.

- The mean of the posterior distribution is heavily influenced by the initial NTG estimate, hence care should be taken to remove any suspected bias from that initial estimate. Integrating seismic data helps correct for any bias due to preferential location of the appraisal-stage wells.

- In the multiple facies case, additional constraints are required to estimate individual facies proportions corresponding to a global NTG value. We proposed to freeze the ratio of proportions of facies, which can be taken from a Ti or provided by an expert geologist.

- When re-sampling from a domain of varying thickness, various approximations have to be made to ensure enough replicates of the original data are available for reliable statistics computation. In case of the WCA reservoir, we rotated the original well configuration, re-sampled wells from multiple realizations, and accepted synthetic data sets that had atleast 75% of the original data points.

Figures

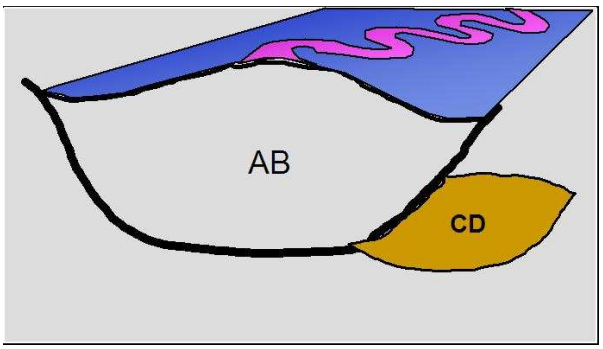

(a) Conceptual model

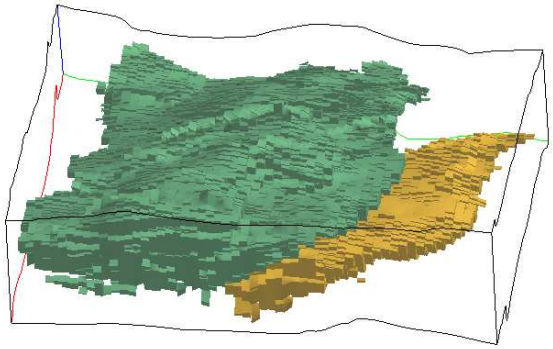

(b) Stratigraphic model

Figure 3.1: Appraisal stage stratigraphic interpretation of WCA reservoir (vertical exaggeration $\times 5$).

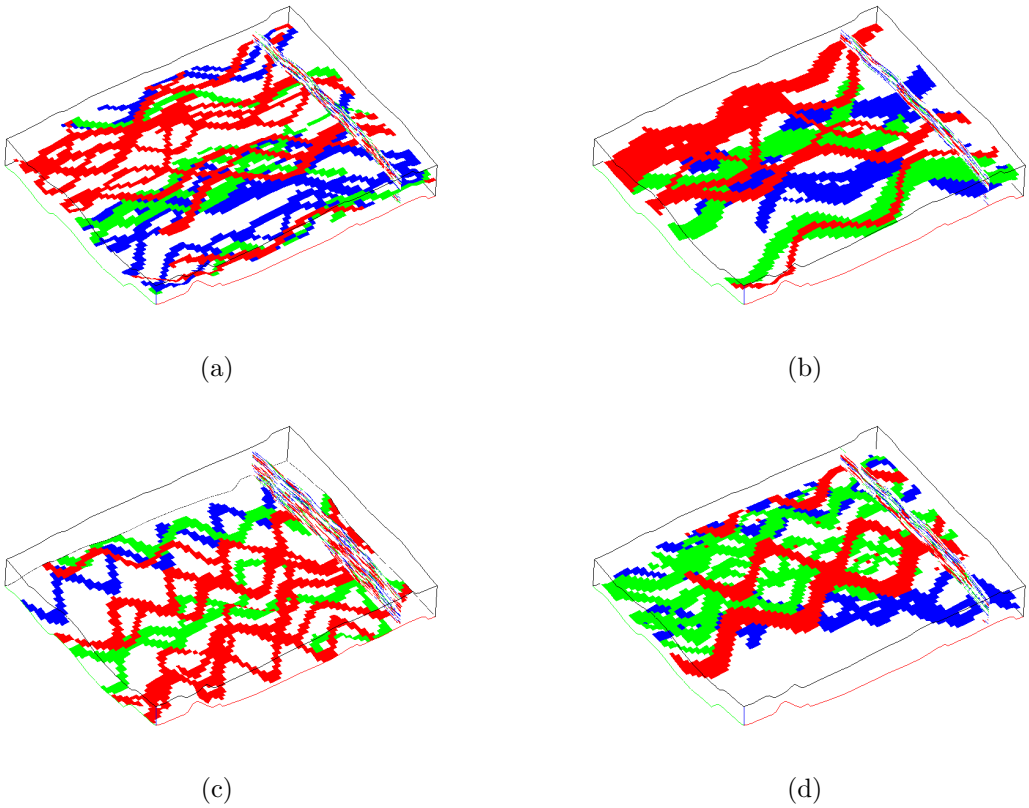

(a) (b)

(c) (d)

Figure 3.2: Training images from the first family of interpretations. Note the different channel widths and sinuosity.

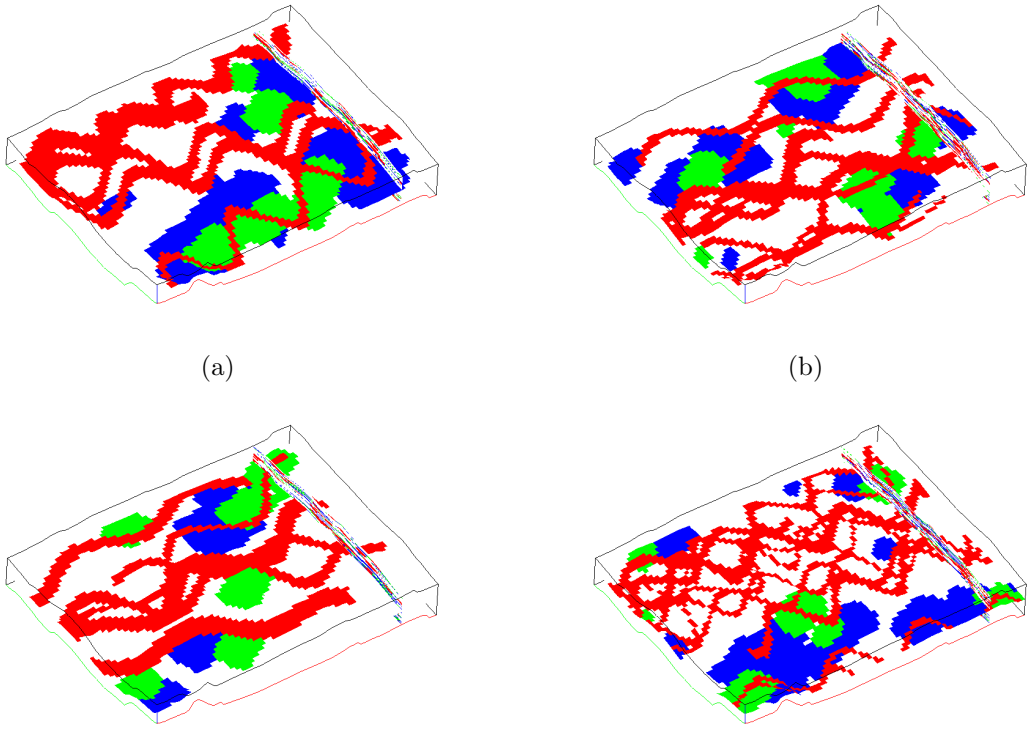

(a) (b)

(c) (d)

Figure 3.3: Training images from the second family of interpretations. Note the different channel widths and sinuosity.

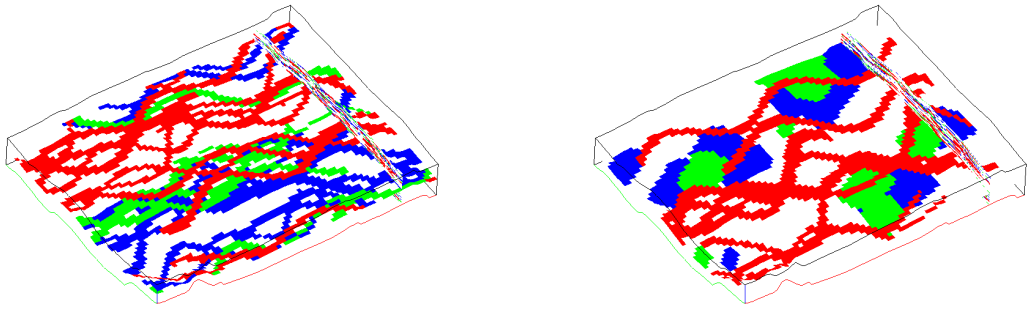

(a) Ti1 (b) Ti2

Figure 3.4: Two representative geological interpretations retained to study the impact of geological scenario.

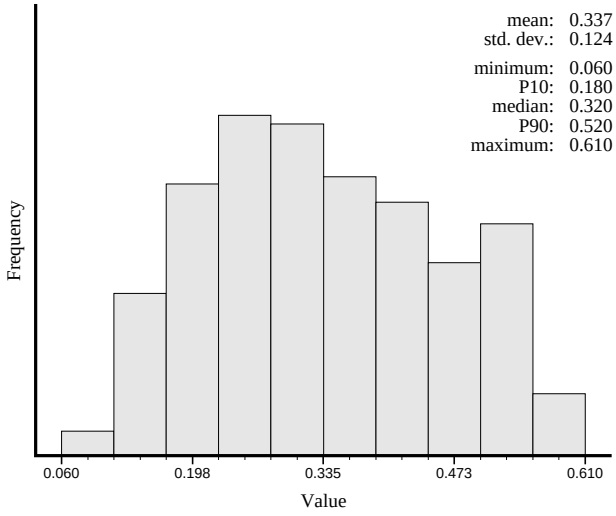

Figure 3.5: Prior global net-to-gross probability distribution for the WCA reservoir obtained from a database of analog reservoirs.

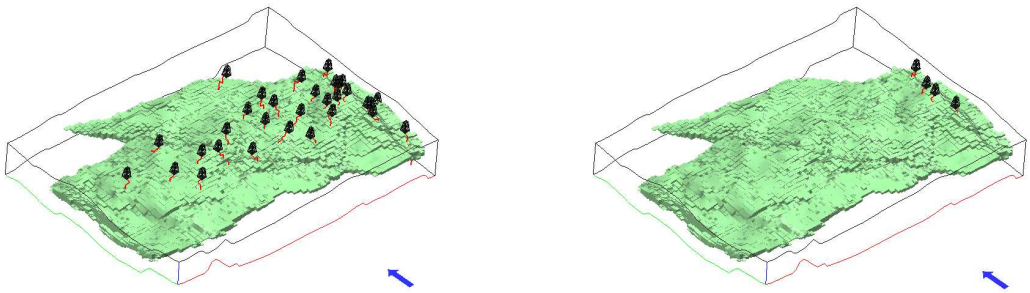

(a) All available wells

(b) First four wells

Figure 3.6: Figure showing the location of all available wells and the four wells available at appraisal stage in the Slope Valley region (vertical exaggeration $\times 3$).

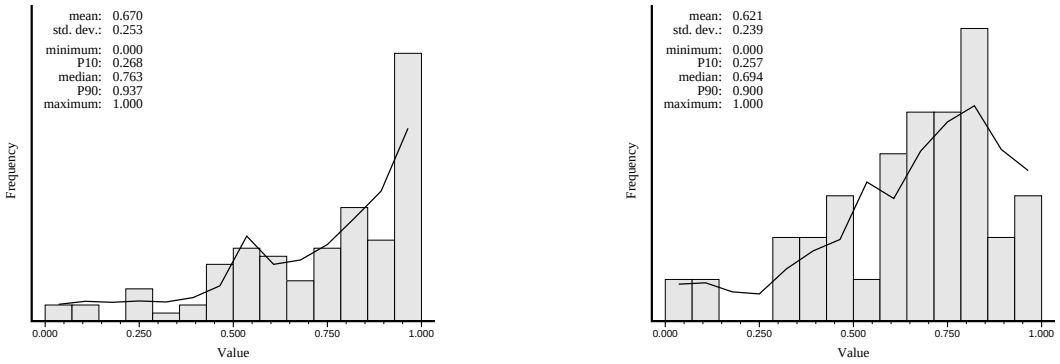

(a) facies 1

(b) facies 2

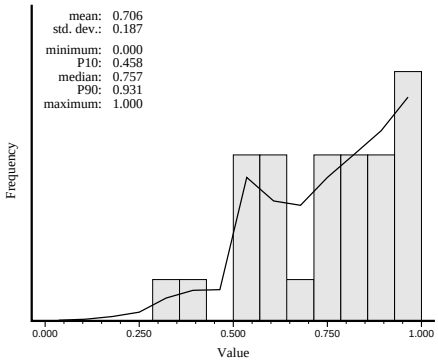

(c) facies 3

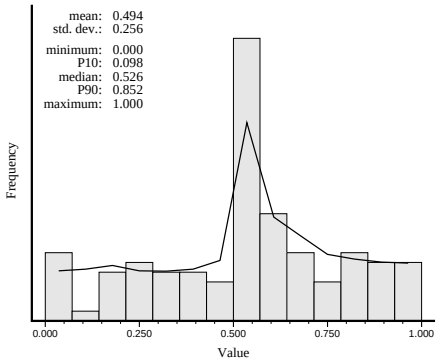

(d) facies 4

Figure 3.7: Likelihood of observing impedance value (x axis) given a particular facies, as obtained using Bayes inversion in the Slope Valley region. Impedance values have been normalized between 0 and 1. Y axis gives the likelihood probability.

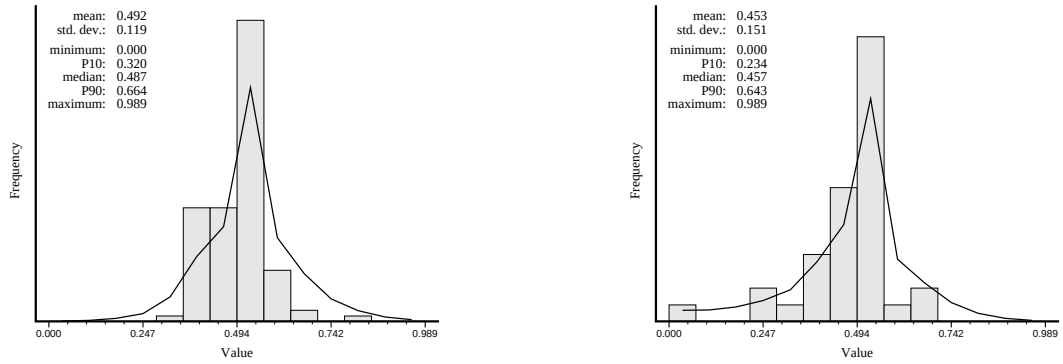

(a) facies 1

(b) facies 2

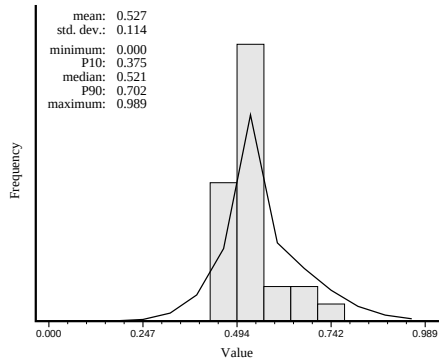

(c) facies 3

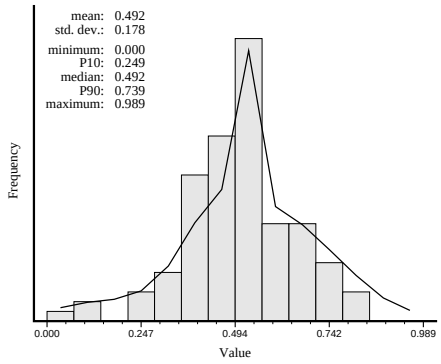

(d) facies 4

Figure 3.8: Likelihood of observing VShale value (x axis) given a particular facies, as obtained using Bayes inversion in the Slope Valley region.

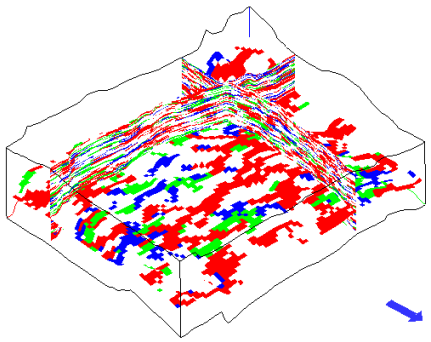

(a) Scenario 1

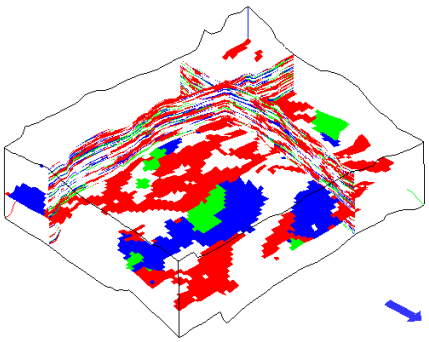

(b) Scenario 2

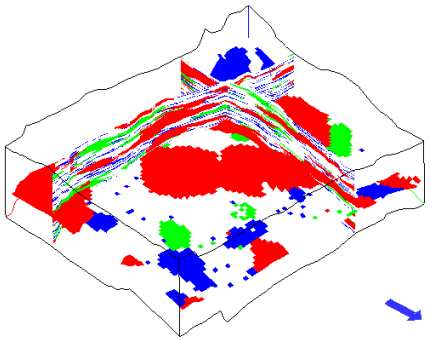

(c) Scenario 3

Figure 3.9: Reference geological scenarios used for sensitivity analysis (vertical exaggeration $\times 5$).

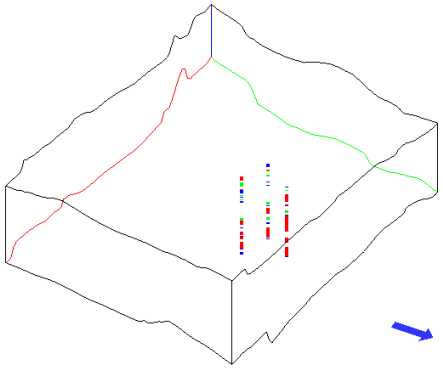

Figure 3.10: Locations of three initial wells (vertical exaggeration $\times 5$). Relative well configuration vector is [(0,0), (-3,-7), (4,-9)].

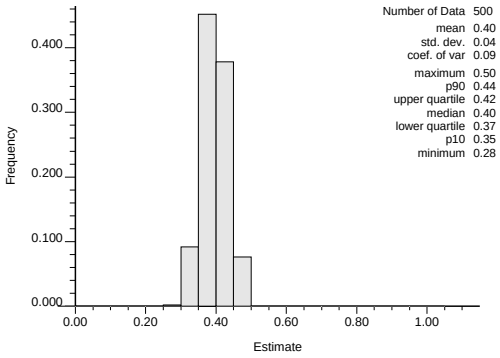

(a) Fixed configuration

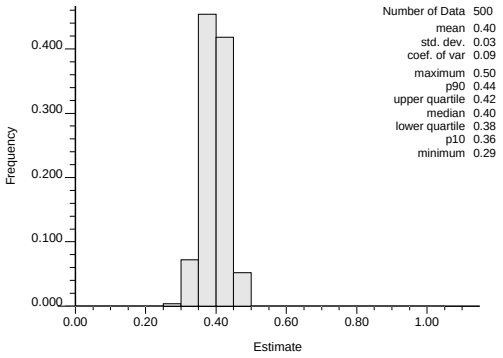

(b) Minimum interdistance

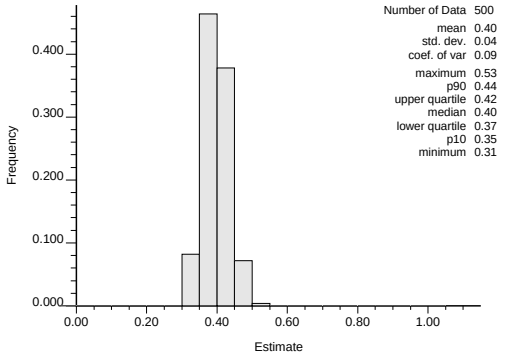

(c) Random sampling

Figure 3.11: Spatial bootstrap histograms corresponding to the different sampling strategies for the channels scenario 1.

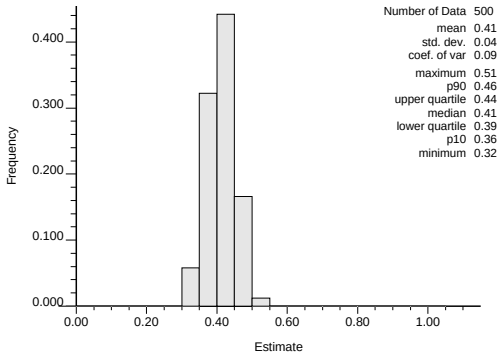

(a) Fixed configuration

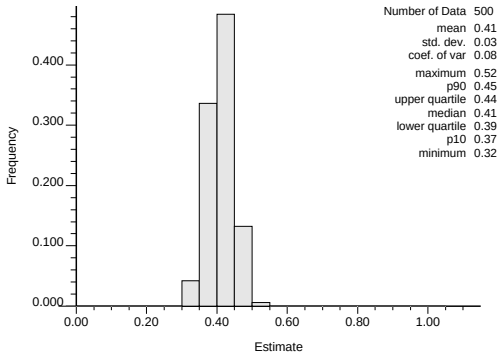

(b) Minimum interdistance

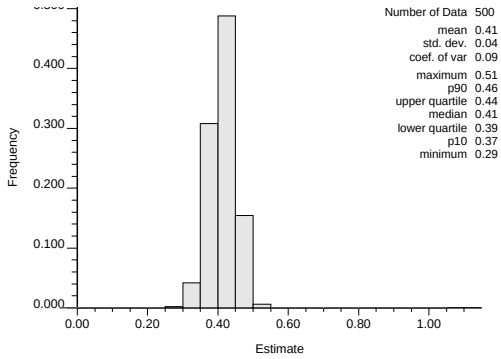

(c) Random sampling

Figure 3.12: Spatial bootstrap histograms corresponding to the different sampling strategies for channel and lobes scenario 2.

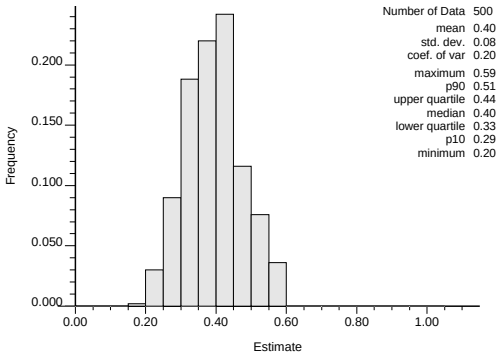

(a) Fixed configuration

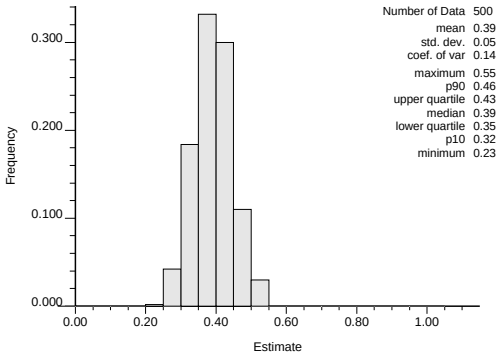

(b) Minimum interdistance

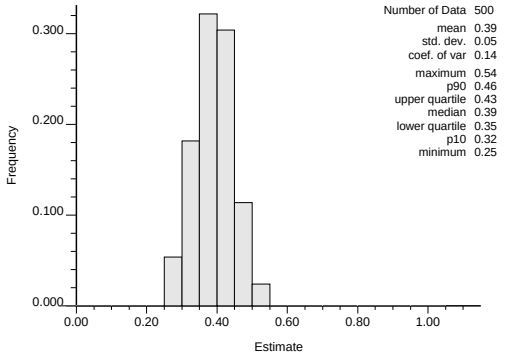

(c) Random sampling

Figure 3.13: Spatial bootstrap histograms corresponding to the different sampling strategies for the lobes scenario 3.

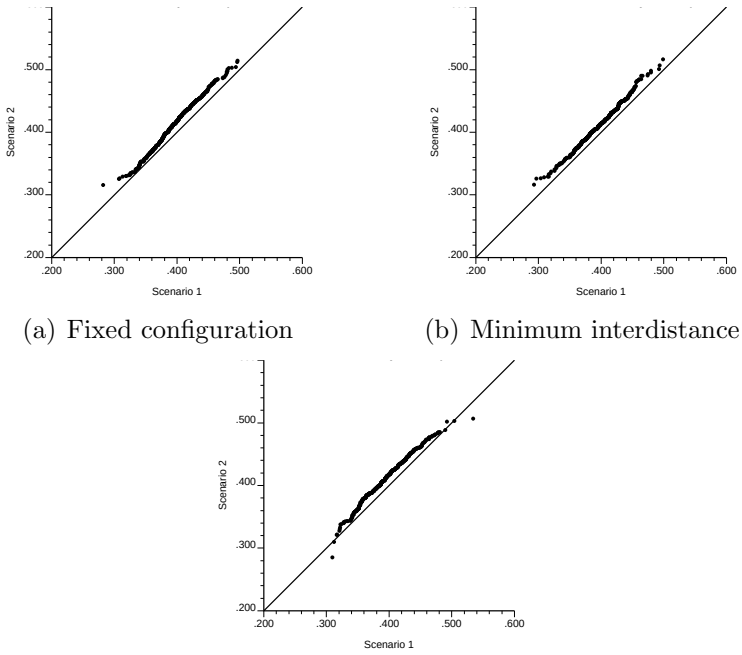

(a) Fixed configuration

(b) Minimum interdistance

(c) Random sampling

Figure 3.14: Q-Q plots of spatial bootstrap histograms of scenario 1 versus scenario 2 for different sampling strategies.

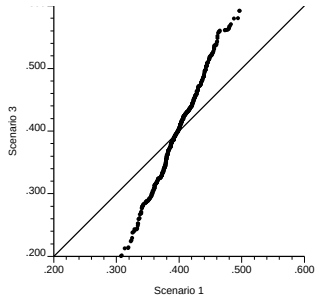

(a) Fixed configuration

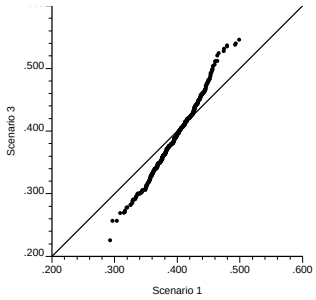

(b) Minimum interdistance

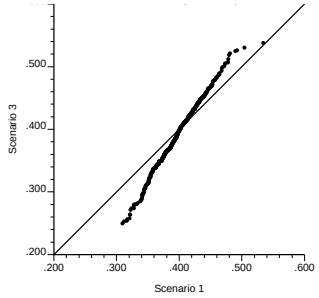

(c) Random sampling

Figure 3.15: Q-Q plots of spatial bootstrap histograms of scenario 1 versus scenario 3 for different sampling strategies.

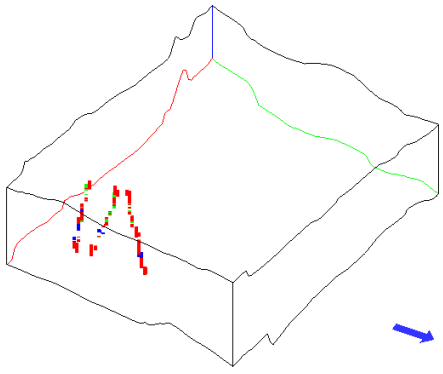

Figure 3.16: Linear three well configuration (vertical exaggeration $\times 5$)

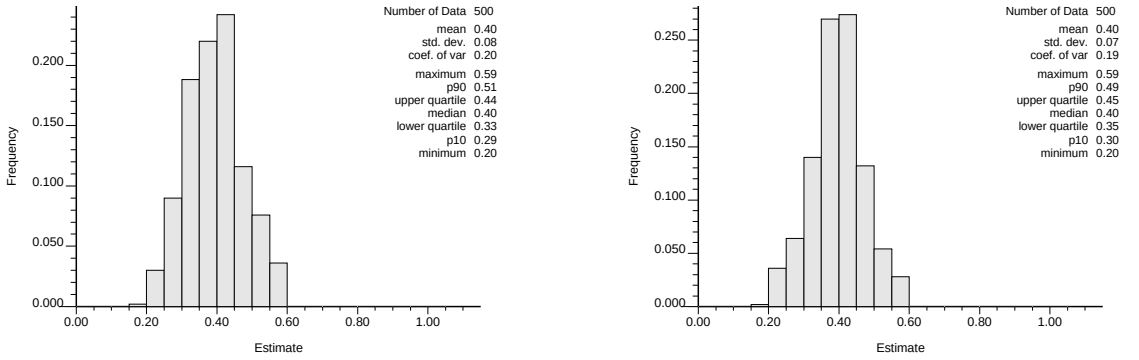

(a) Triangular configuration (b) Linear configuration

Figure 3.17: Fixed configuration spatial bootstrap histograms corresponding to different initial well configurations for the lobe scenario 3.

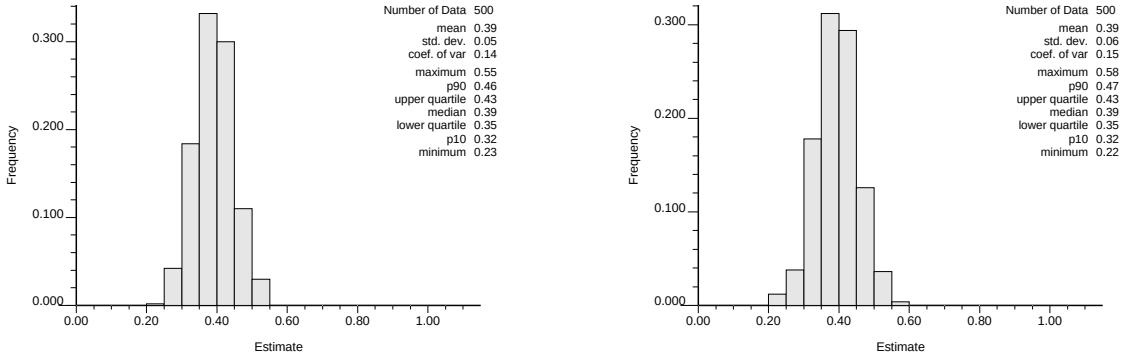

(a) Triangular configuration (b) Linear configuration

Figure 3.18: Minimum interdistance spatial bootstrap histograms corresponding to different initial well configurations for the lobe scenario 3.

- recent

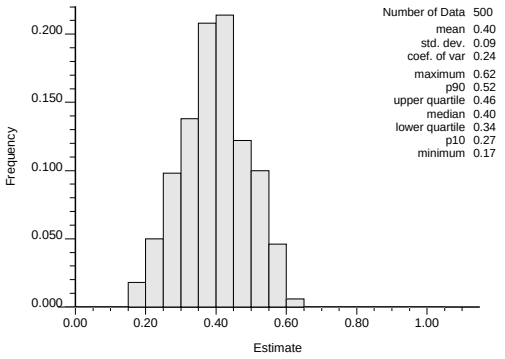

(a) Triangular configuration (200 m)

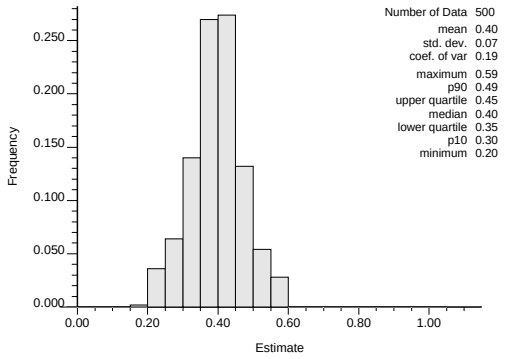

(b) Linear configuration (200 m)

Figure 3.19: Fixed configuration spatial bootstrap histograms corresponding to the new triangular configuration and the linear configurations.

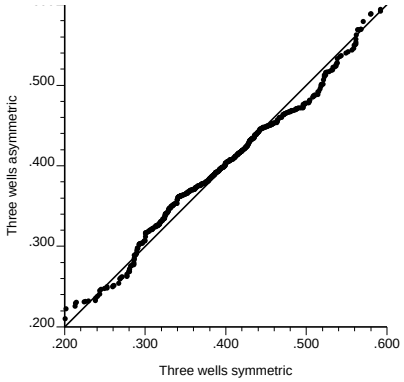

(a) Fixed configuration

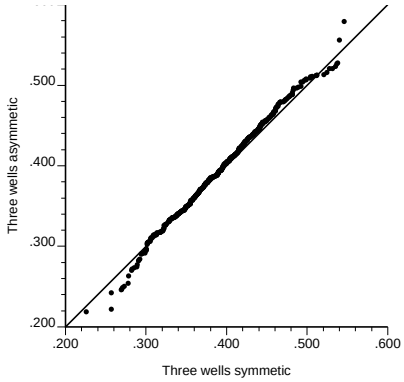

(b) Minimum interdistance

Figure 3.20: Q-Q plots of triangular versus linear 3-well configuration spatial bootstrap histograms for the lobe scenario 3.

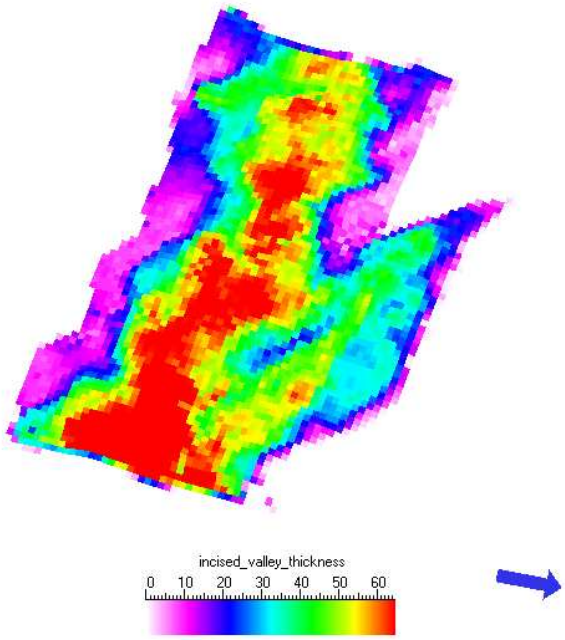

Figure 3.21: Map showing variable thickness of the slope valley region

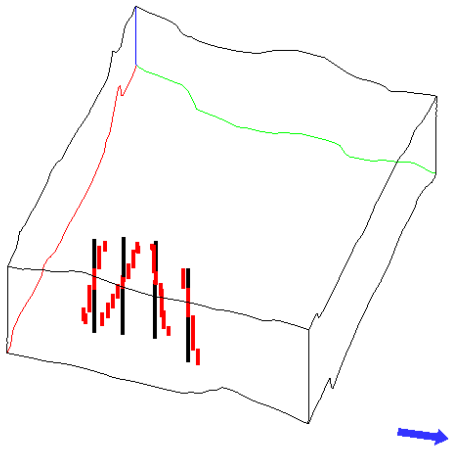

Figure 3.22: Four deviated appraisal stage wells (red) and their vertical approximations (black). Vertical exaggeration $\times 5$.

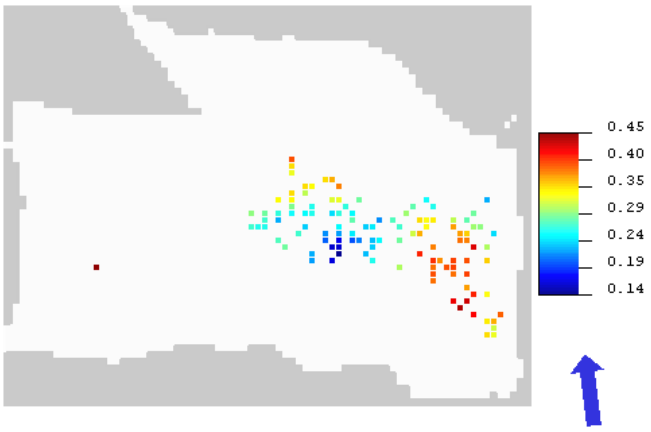

Figure 3.23: Locations of centroids of 142 sets of synthetic wells drilled in the slope valley region using fixed well configuration without rotation.

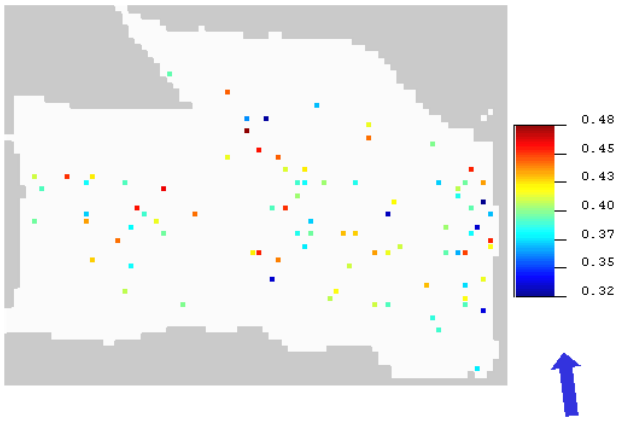

Figure 3.24: Map showing the area of slope valley sampled using minimum interdistance constraint.

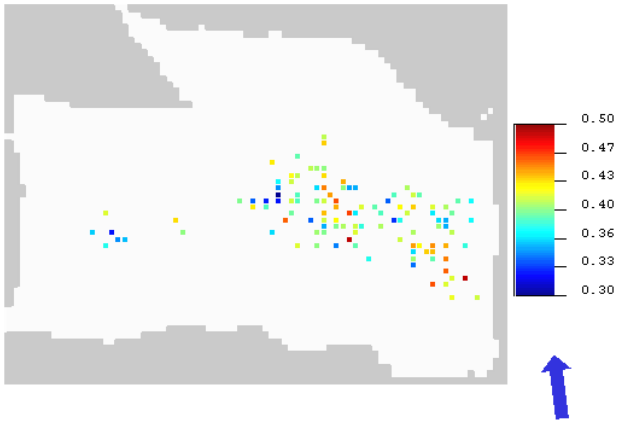

Figure 3.25: Locations of centroids of 100 sets of synthetic wells drilled in the slope valley region using fixed well configuration with limited rotation flexibility.

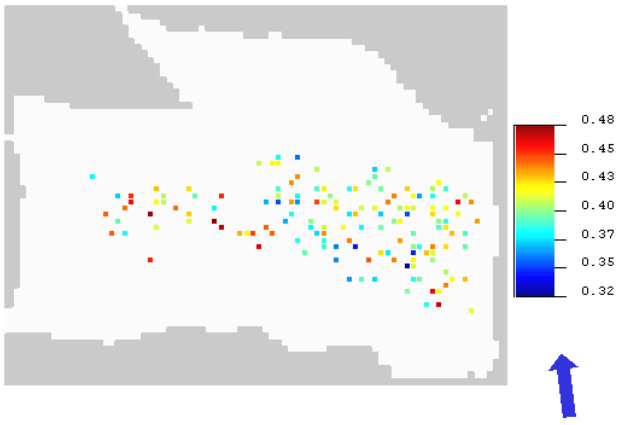

Figure 3.26: Locations of centroids of 100 sets of synthetic wells drilled in the slope valley region using fixed well configuration with full rotation flexibility.

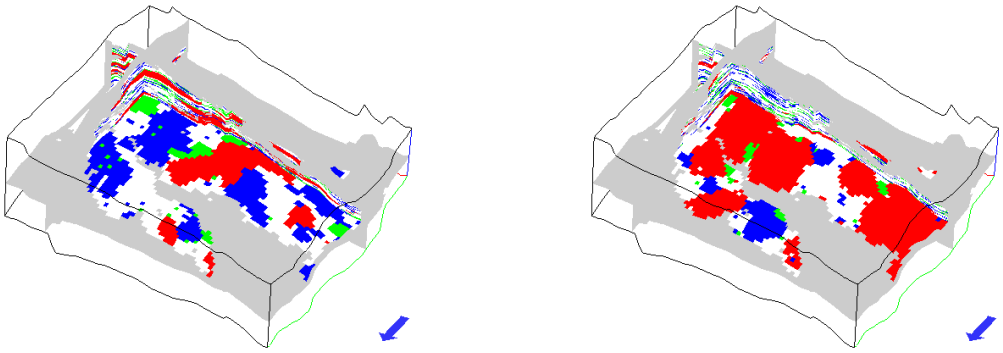

(a) Realization 1 (b) Realization 2

Figure 3.27: Two realizations of scenario 3 used for sampling synthetic data sets (vertical exaggeration $\times 5$).

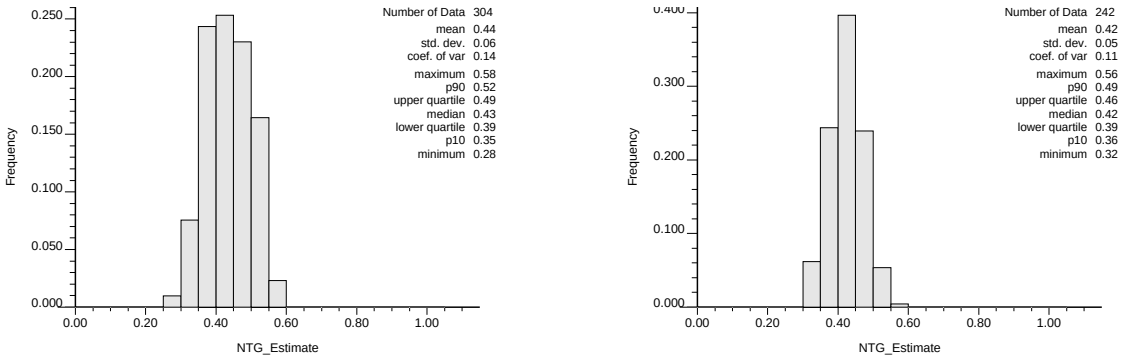

(a) Fixed configuration (b) Minimum interdistance

Figure 3.28: Spatial bootstrap histograms corresponding to the different sampling strategies for scenario 3.

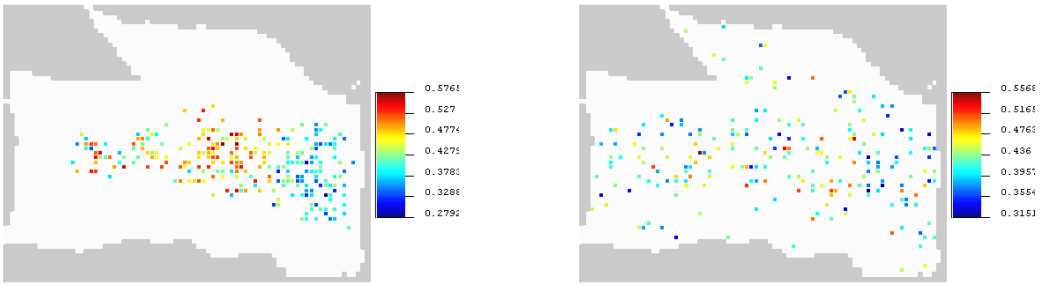

(a) Fixed configuration (b) Minimum interdistance

Figure 3.29: Location maps of synthetic wells drilled in the slope valley region for different sampling strategies.

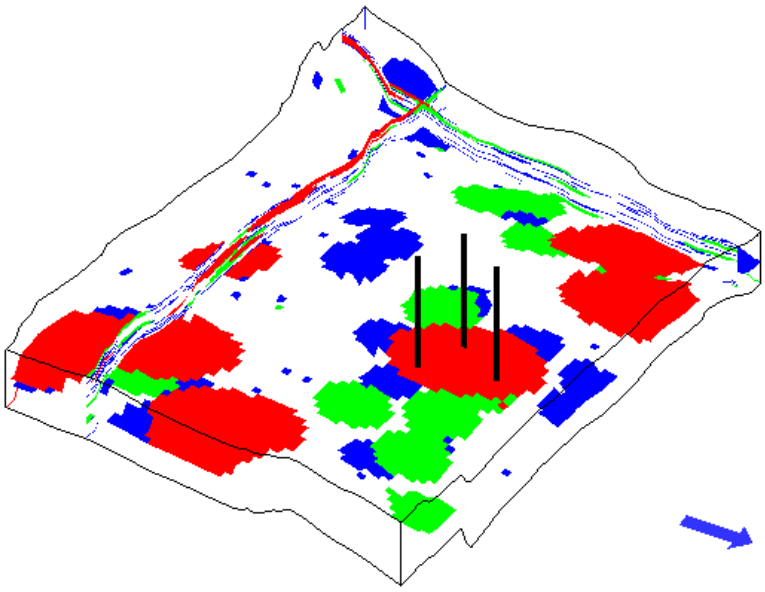

Figure 3.30: Training image for scenario 3 with three tightly clustered wells (vertical exaggeration $\times 5$).

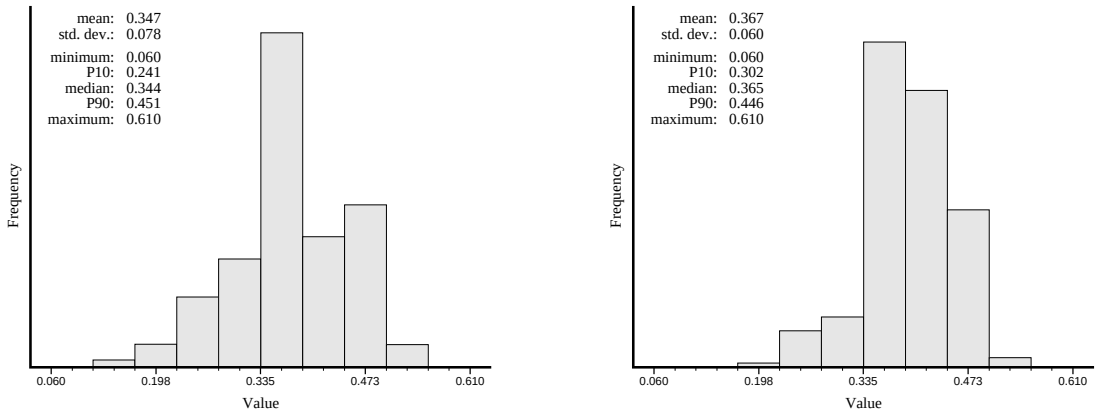

(a) Fixed configuration

(b) Minimum interdistance

Figure 3.31: Posterior NTG distributions corresponding to two different re-sampling strategies for lobe scenario 3.

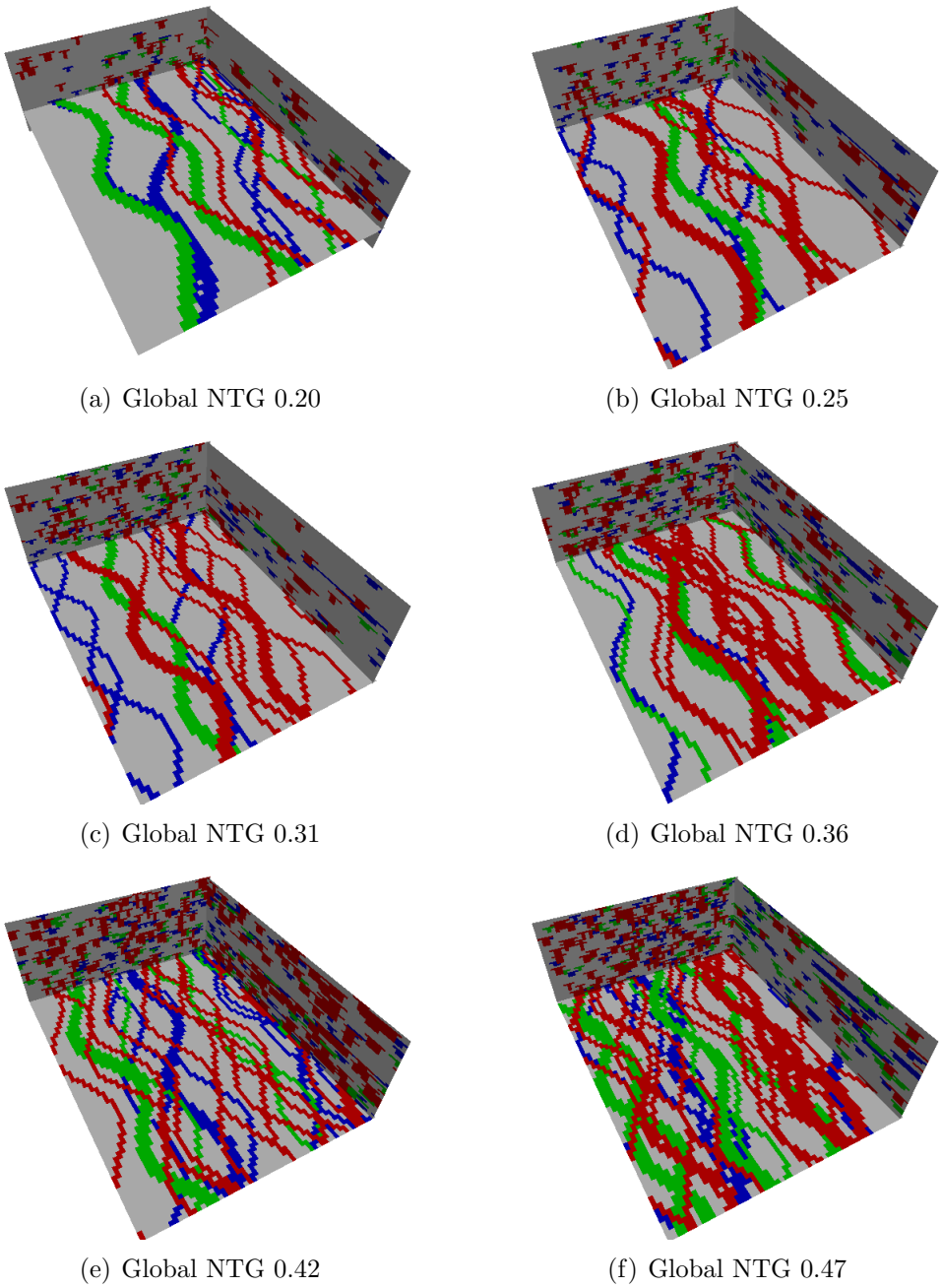

(a) Global NTG 0.20

(b) Global NTG 0.25

(c) Global NTG 0.31

(d) Global NTG 0.36

(e) Global NTG 0.42

(f) Global NTG 0.47

Figure 3.32: Training images generated using *TiGenerator* for scenario 1 for different global NTG values.

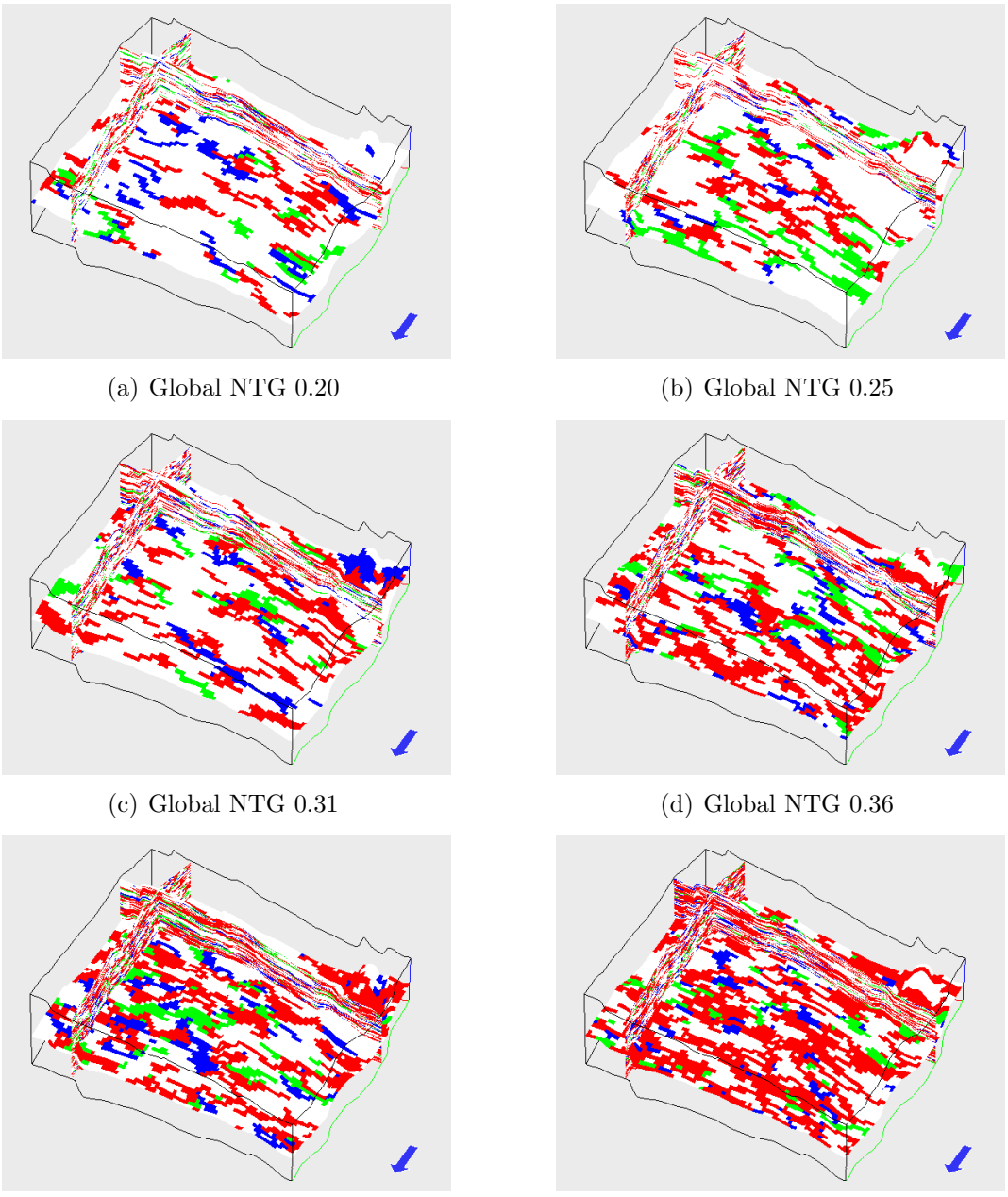

(a) Global NTG 0.20

(b) Global NTG 0.25

(c) Global NTG 0.31

(d) Global NTG 0.36

(e) Global NTG 0.42

(f) Global NTG 0.47

Figure 3.33: Scenario 1 unconditional realizations generated using *snesim* for different global NTG values (vertical exaggeration $\times 5$).

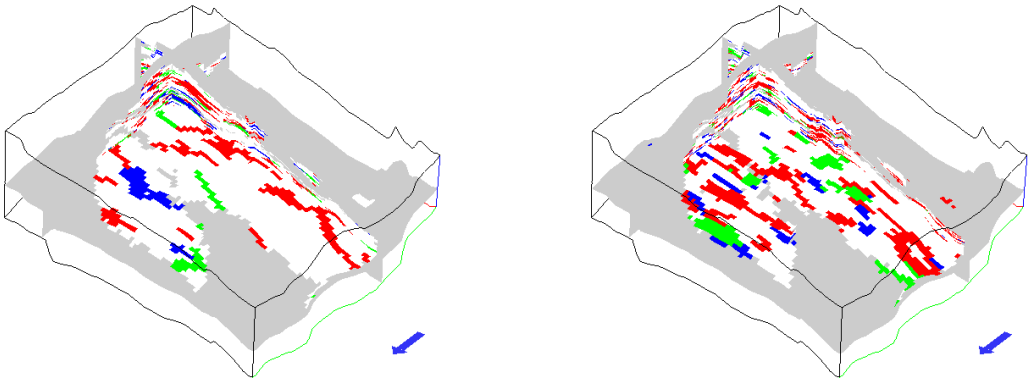

(a) Global NTG 0.20

(b) Global NTG 0.25

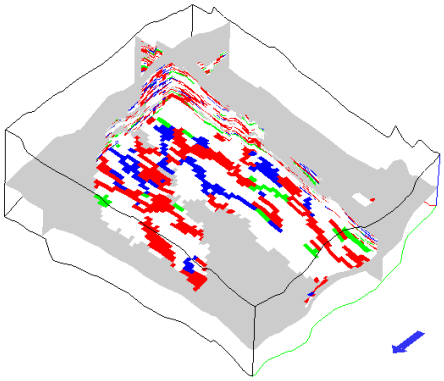

(c) Global NTG 0.31

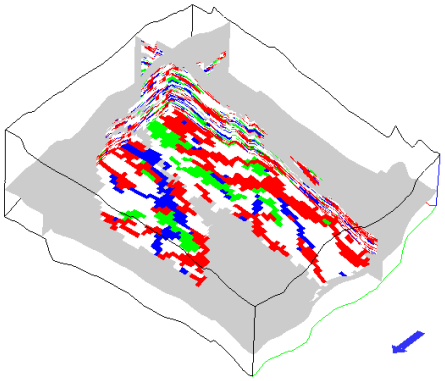

(d) Global NTG 0.36

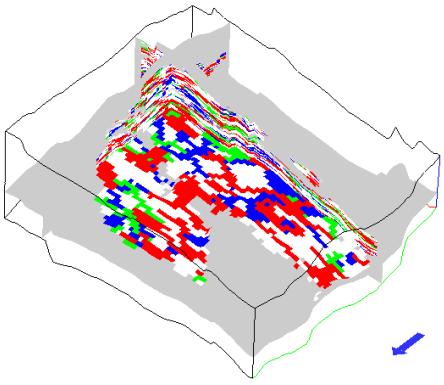

(e) Global NTG 0.42

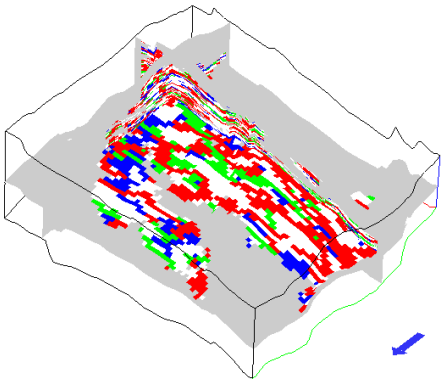

(f) Global NTG 0.47

Figure 3.34: Scenario 1 conditional realizations generated using *snesim* for different global NTG values (vertical exaggeration ×5).

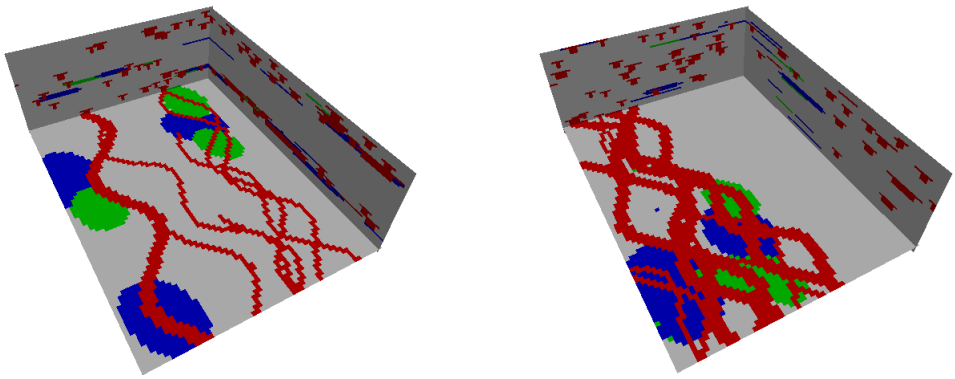

(a) Global NTG 0.20

(b) Global NTG 0.25

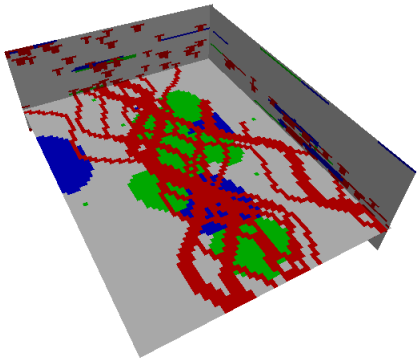

(c) Global NTG 0.31

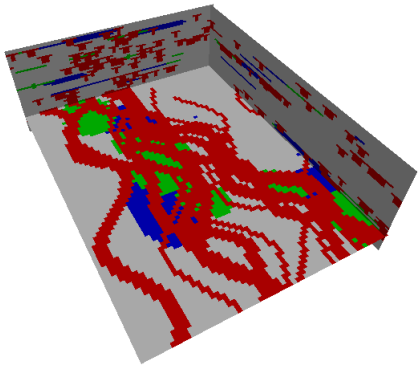

(d) Global NTG 0.36

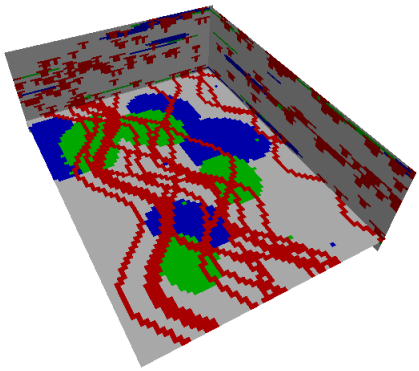

(e) Global NTG 0.42

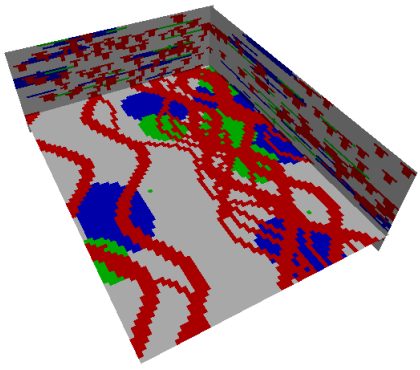

(f) Global NTG 0.47

Figure 3.35: Training images generated using *TiGenerator* for scenario 2 for different global NTG values.

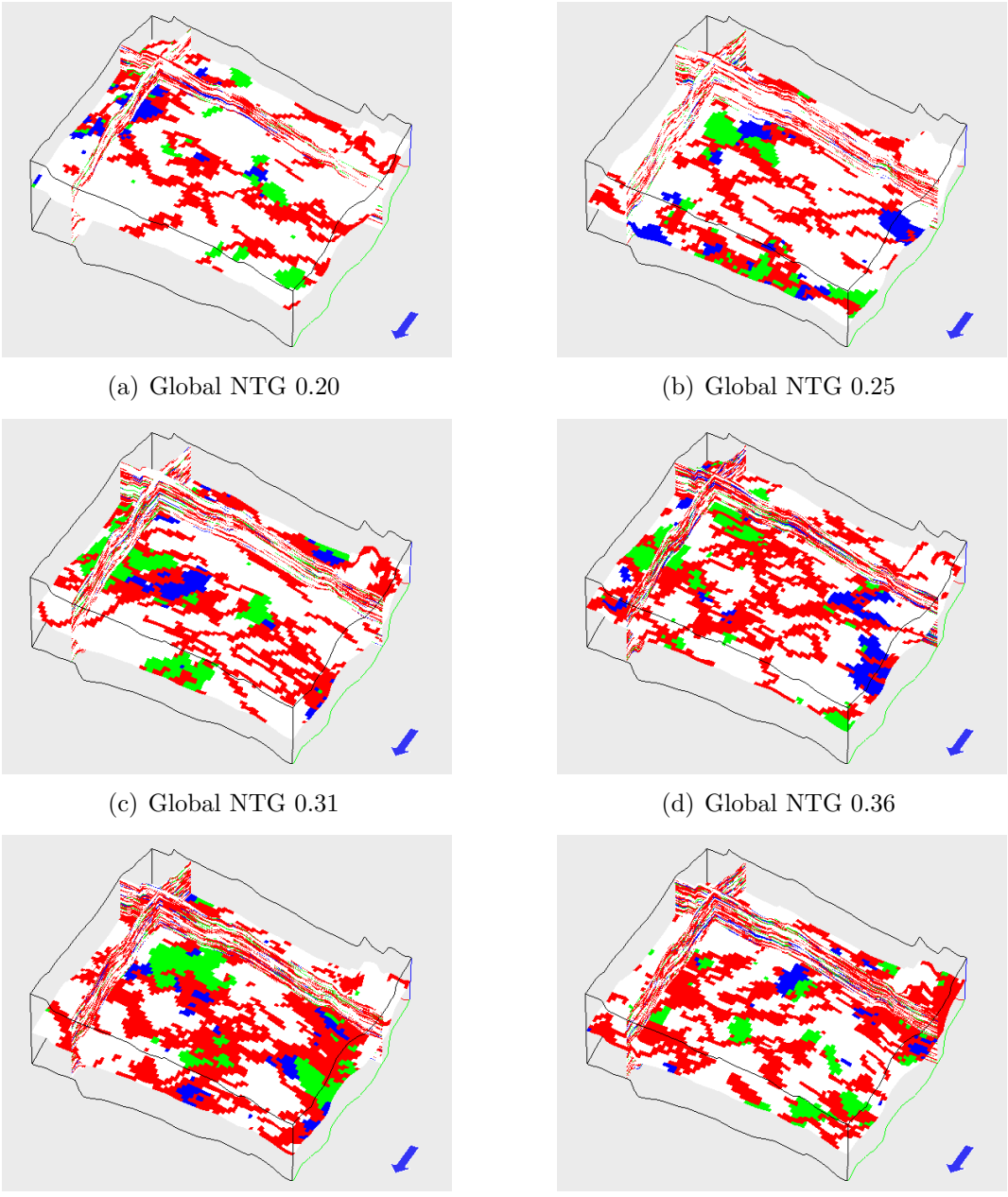

(a) Global NTG 0.20

(b) Global NTG 0.25

(c) Global NTG 0.31

(d) Global NTG 0.36

(e) Global NTG 0.42

(f) Global NTG 0.47

Figure 3.36: Scenario 2 unconditional realizations generated using *snesim* for different global NTG values (vertical exaggeration ×5).

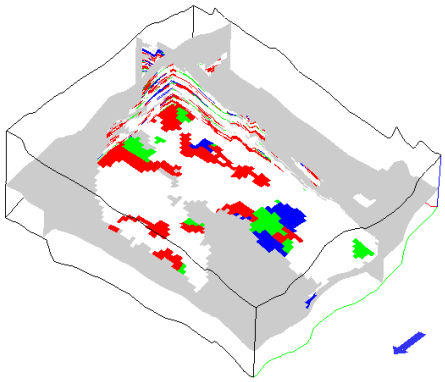

(a) Global NTG 0.20

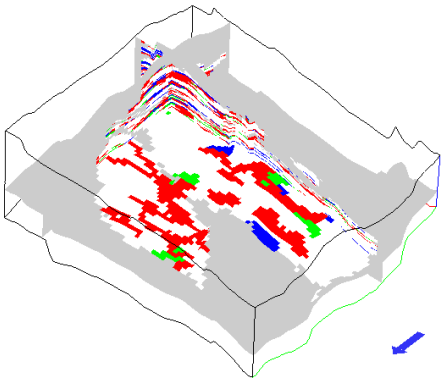

(b) Global NTG 0.25

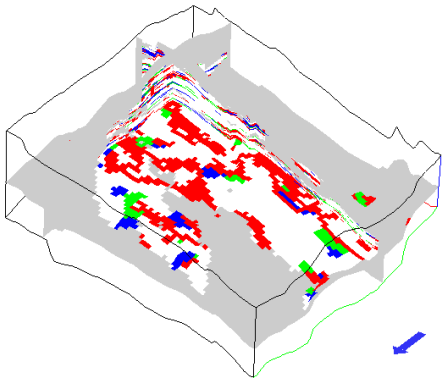

(c) Global NTG 0.31

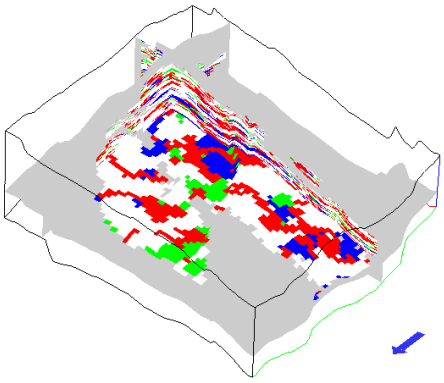

(d) Global NTG 0.36

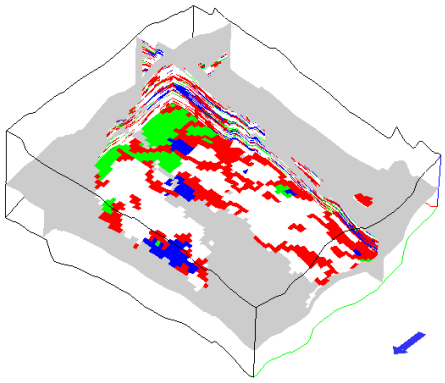

(e) Global NTG 0.42

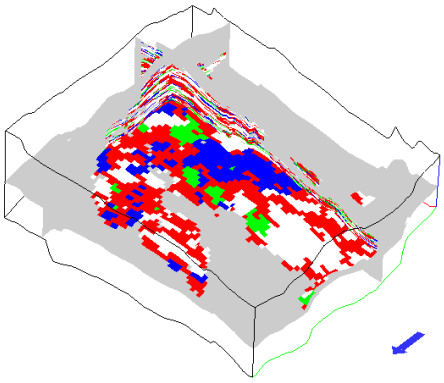

(f) Global NTG 0.47

Figure 3.37: Scenario 2 conditional realizations generated using *snesim* for different global NTG values (vertical exaggeration $\times 5$).

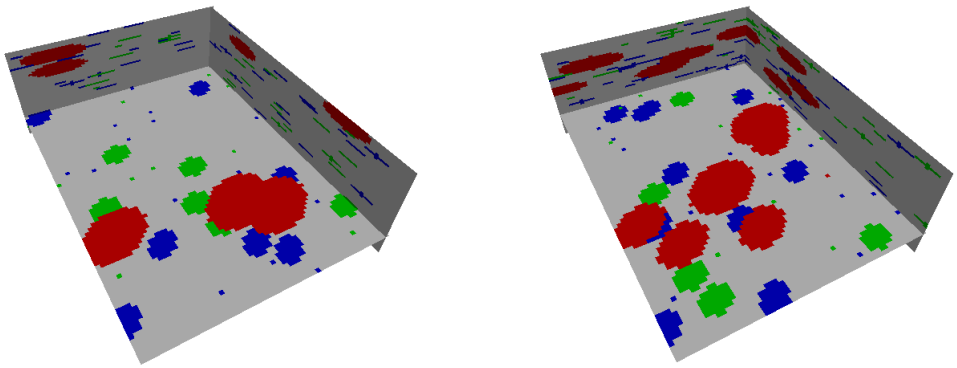

(a) Global NTG 0.20

(b) Global NTG 0.25

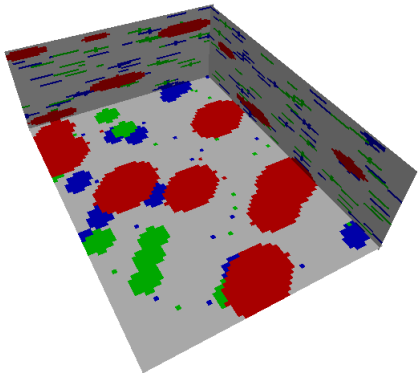

(c) Global NTG 0.31

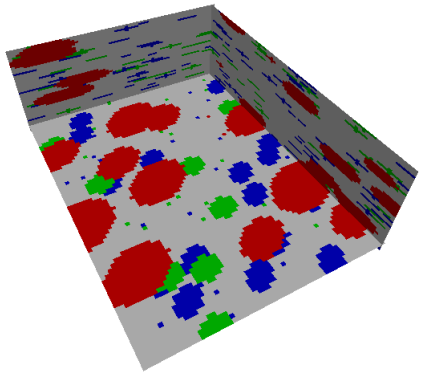

(d) Global NTG 0.36

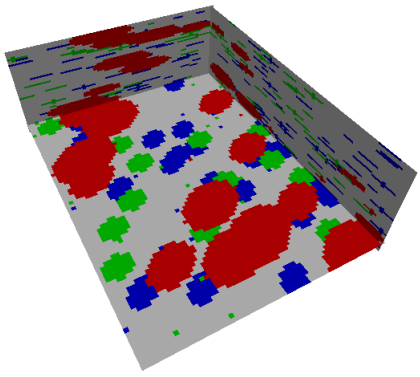

(e) Global NTG 0.42

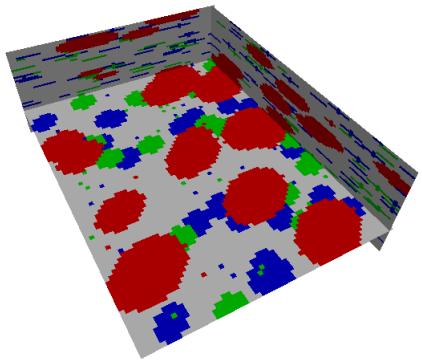

(f) Global NTG 0.47

Figure 3.38: Training images generated using *TiGenerator* for scenario 3 for different global NTG values.

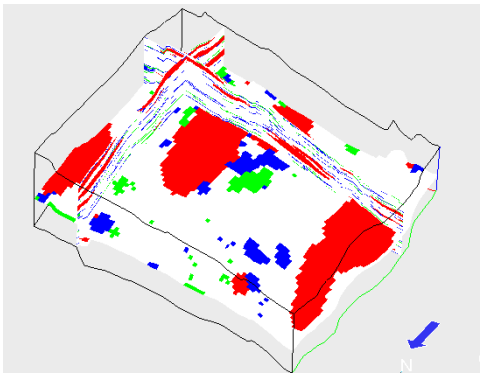

(a) Global NTG 0.20

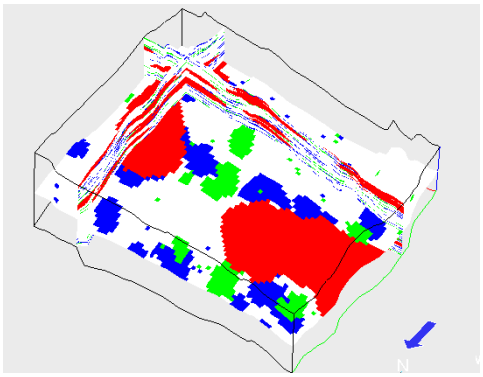

(b) Global NTG 0.25

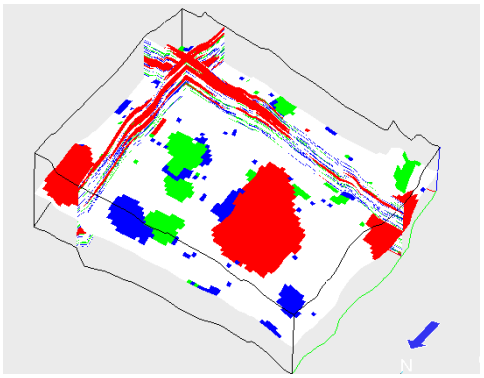

(c) Global NTG 0.31

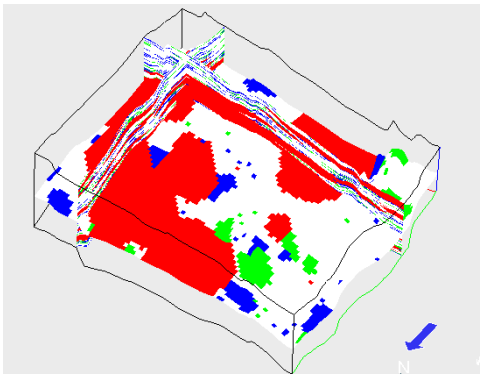

(d) Global NTG 0.36

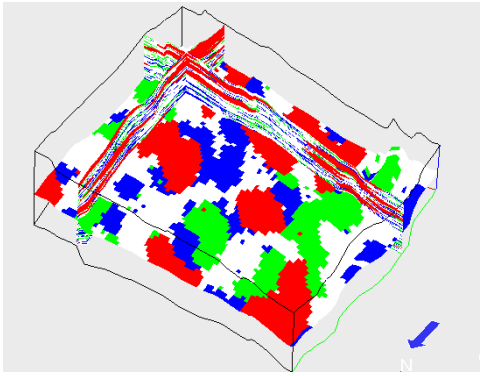

(e) Global NTG 0.42

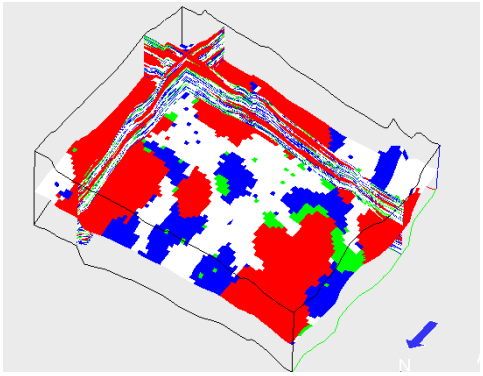

(f) Global NTG 0.47

Figure 3.39: Scenario 3 unconditional realizations generated using *snesim* for different global NTG values (vertical exaggeration $\times 5$).

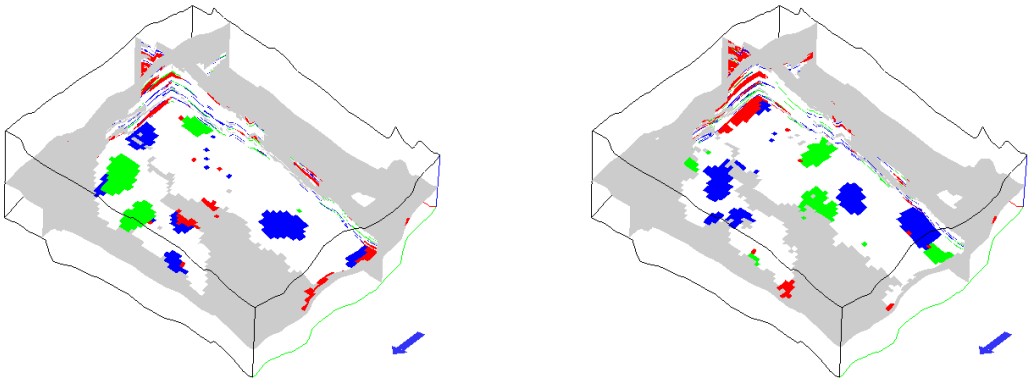

(a) Global NTG 0.20

(b) Global NTG 0.25

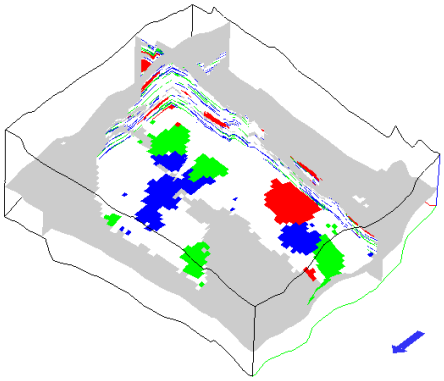

(c) Global NTG 0.31

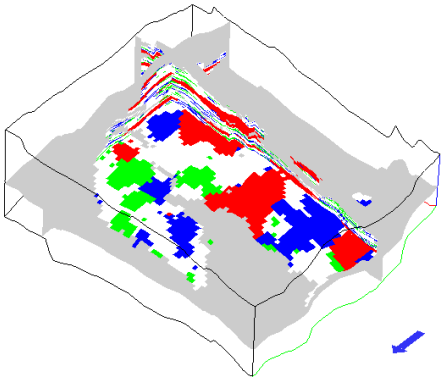

(d) Global NTG 0.36

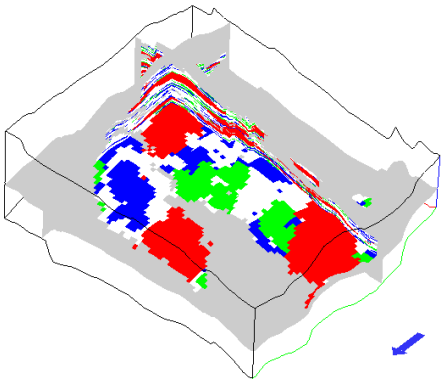

(e) Global NTG 0.42

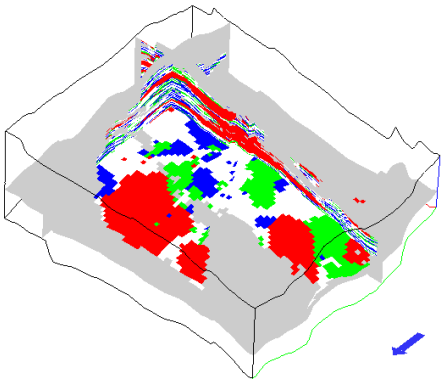

(f) Global NTG 0.47

Figure 3.40: Scenario 3 conditional realizations generated using *snesim* for different global NTG values (vertical exaggeration ×5).

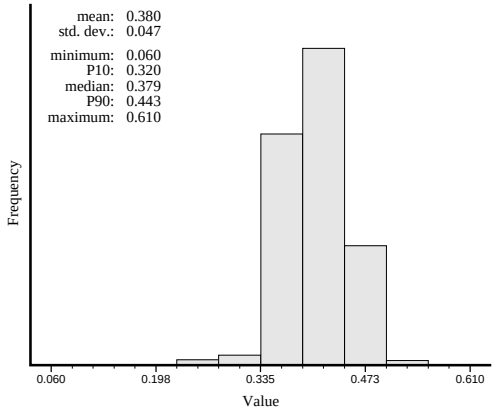

(a) All channels scenario

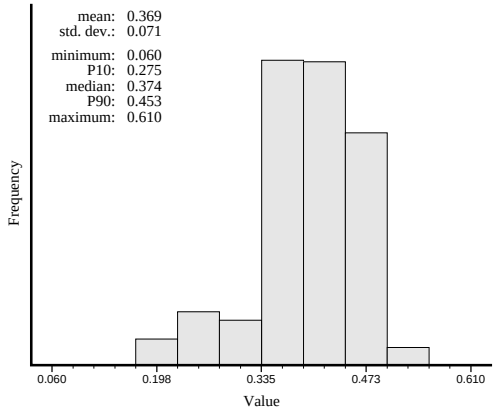

(b) Channel and lobes scenario

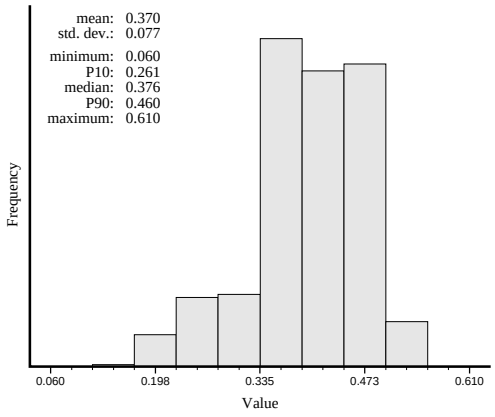

(c) All lobes scenario

Figure 3.41: Posterior NTG distributions obtained using scenarios 1, 2 and 3 given a NTG estimate of 0.436.

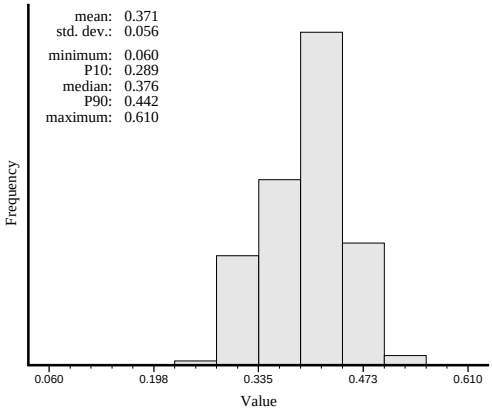

(a) Channel scenario 2

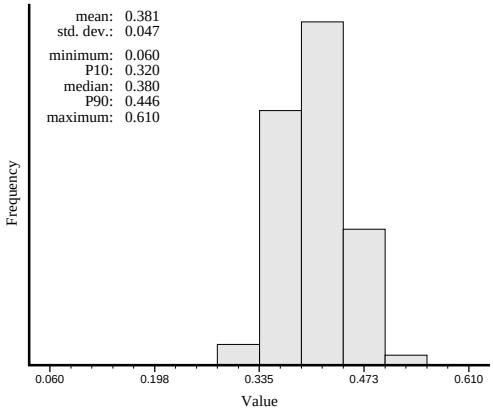

(b) Channel scenario 3

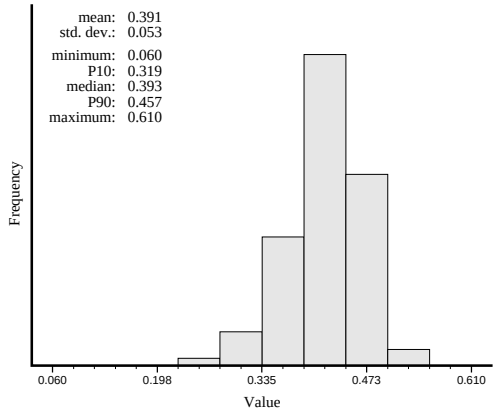

(c) Channel scenario 4

Figure 3.42: Posterior NTG distributions resulting from the three different channelized scenarios shown in Figures 3.2(b) to 3.2(d).

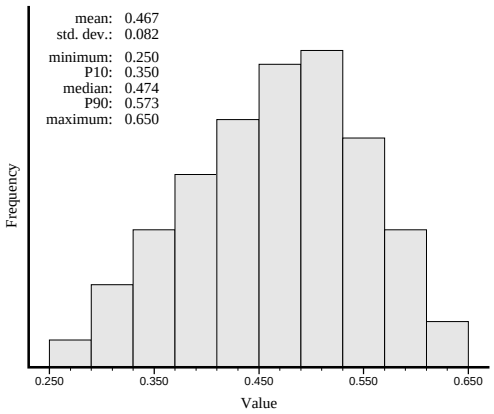

Figure 3.43: Triangular prior probability distribution for global NTG.

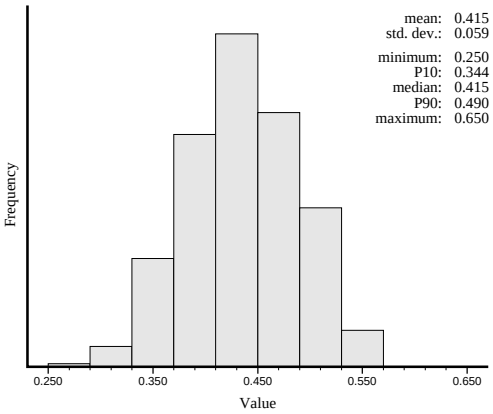

(a) with triangular prior NTG distribution

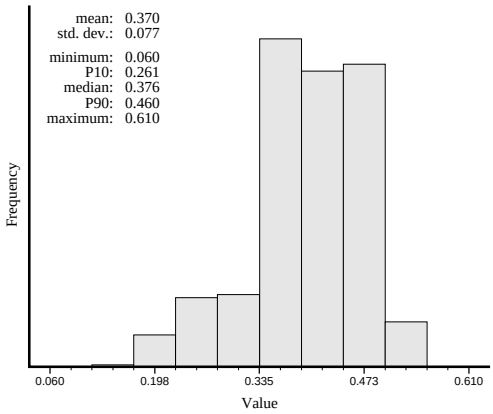

(b) with analog prior NTG distribution

Figure 3.44: Posteriors for scenario 3 resulting from two different prior distributions.

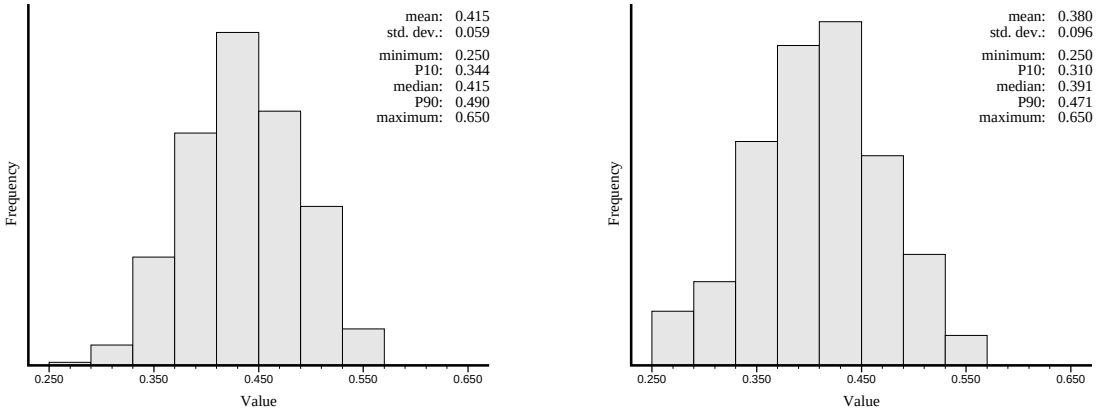

(a) with triangular prior NTG distribution

(b) with uniform prior NTG distribution

Figure 3.45: Posteriors for scenario 3 resulting from triangular and uniform prior distributions.

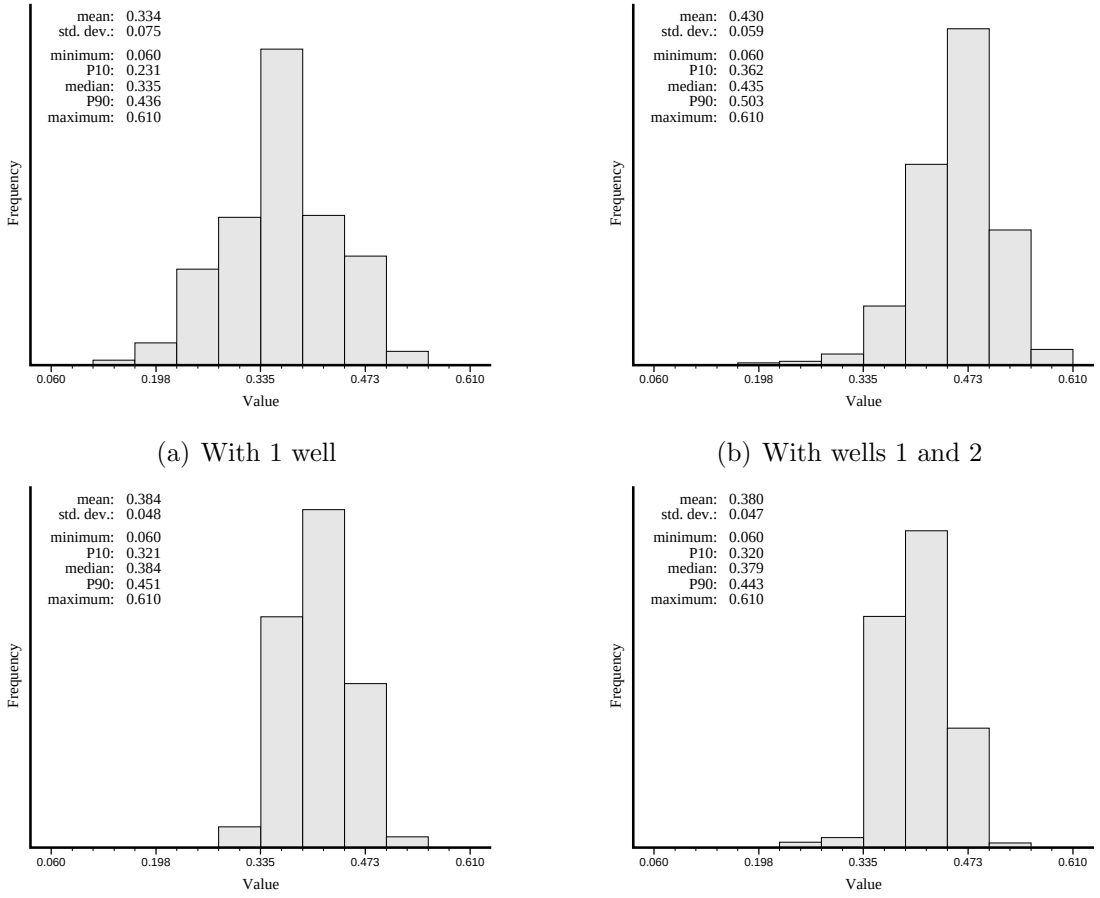

(a) With 1 well

(b) With wells 1 and 2

(c) With wells 1,2 and 3

(d) With wells 1 to 4

Figure 3.46: Impact of additional well data on posterior NTG distributions for scenario 1.

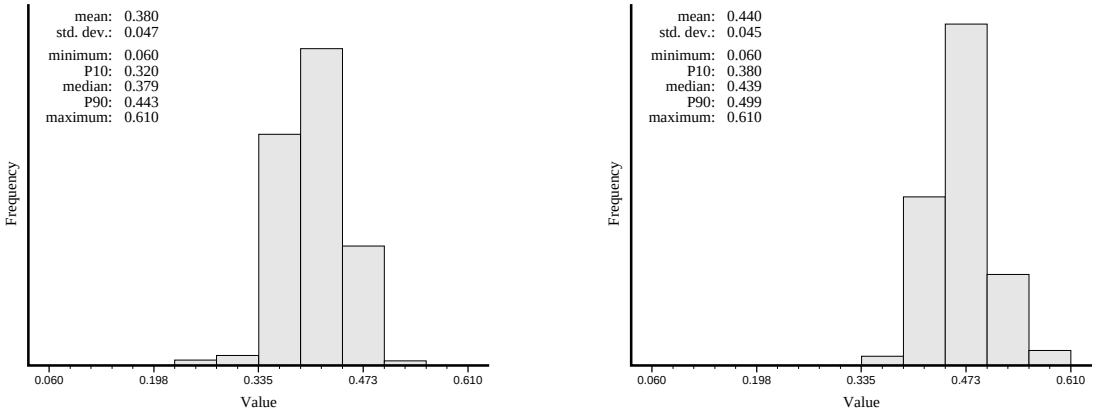

(a) with seismic (AI) (b) without seismic

Figure 3.47: Impact of seismic data on posterior NTG distributions for scenario 1.

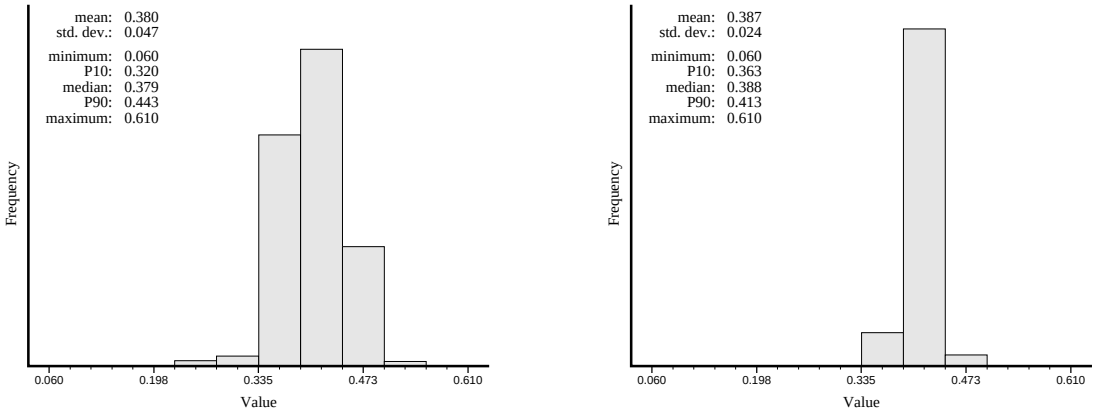

(a) with four initial wells (b) with 28 wells

Figure 3.48: Posterior NTG distributions resulting from using only four appraisal stage wells and all 28 wells from the WCA reservoir.

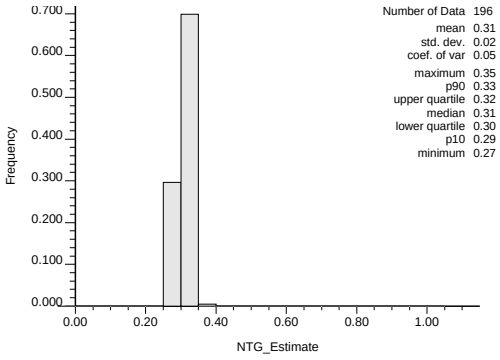

(a) Global NTG = 0.31

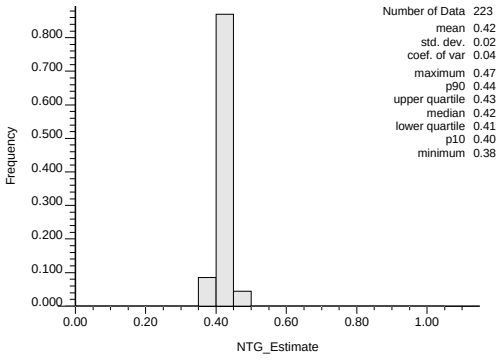

(b) Global NTG = 0.42

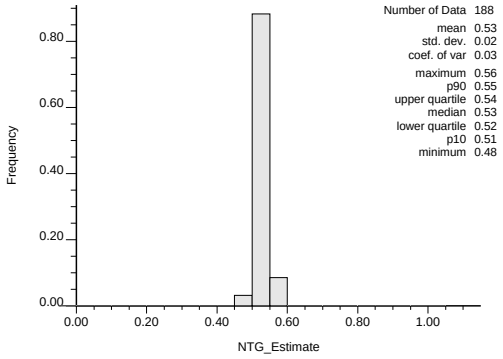

(c) Global NTG = 0.53

Figure 3.49: Spatial bootstrap histograms corresponding to different global NTG values when using all 28 wells from the WCA reservoir.

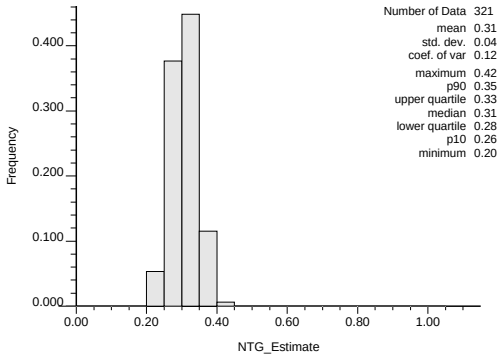

(a) Global NTG = 0.31

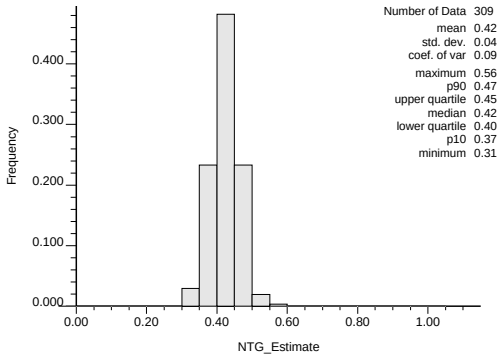

(b) Global NTG = 0.42

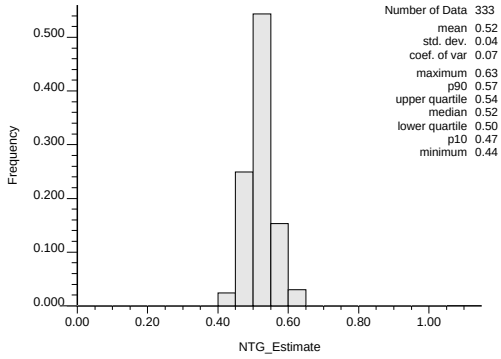

(c) Global NTG = 0.53

Figure 3.50: Spatial bootstrap histograms corresponding to different global NTG values when using the 4 appraisal-stage wells from the WCA reservoir.

Chapter 4

Conclusions and Future Work

A general framework for global NTG uncertainty assessment has been proposed. It accounts for three major sources of uncertainty, namely the geological scenario, the prior global NTG, and the data. The methodology has been tested on a synthetic data set then applied to an actual deep-water turbidite reservoir. In this final chapter, the advantages and limitations of the workflow are considered. Next, the various decisions required during the different stages of the workflow are discussed. Finally, avenues for future work are presented.

4.1 Advantages and limitations of the workflow

The workflow proposed here for uncertainty assessment is demanding because it requires more decisions and modeling effort than any of the previous approaches. Classical bootstrap does not call for any facies modeling, hence does not require any prior decision about the geological scenario or facies proportions. The Dirichlet approach requires that the prior probability of facies occurence takes the form of uniform or Dirichlet distributions, and it does not call for geostatistical simulations of facies. Spatial bootstrap requires geostatistical simulation, which calls for prior knowledge of the geological scenario and corresponding facies proportions. It also requires decision of which sampling strategy to retain for bootstrap.

Classical bootstrap does not call for geological scenarios because it is not meant

to be used for spatially correlated attributes. The Dirichlet model proposed by Haas and Formery (2002) is an elegant analytical formulation but it does not hold well in case of spatially correlated attributes, because the observed proportions do not follow a multinomial distribution if the data are spatially correlated.

Instead of a single geological scenario like in spatial bootstrap, the workflow proposed calls for multiple geological scenarios and the probability of occurence of each scenario. Additionally, for each scenario, it requires a prior probability distribution of global NTG values which is unlikely to be uniform or Dirichlet. Coming up with multiple geological scenarios may seem like a difficult requisite at appraisal stage where time is of essence. There is hardly enough time to interpret the data once, let alone multiple times by multiple disagreeing experts. These interpretations and the resulting geological models are required by the workflow, however, they do not have to be very detailed. As seen in the WCA case study, NTG uncertainty is governed by the major differences between scenarios, for example, lobes vs. channels, not by subtle differences, such as variation in channel sinuosity from one scenario to another. The advantage of using multiple scenarios is a better NTG uncertainty model that spans a wider space of uncertainty than the one corresponding to multiple stochastic realizations resulting from a single structural model like in spatial bootstrap.

The workflow incorporates past experience and company expertise through the prior probability distribution for global NTG. Unlike the Dirichlet approach, this prior probability model need not be a uniform or Dirichlet distribution. A prior NTG distribution obtained by pooling together data from previously discovered reservoirs allows a company to capitalize on historical information and prevents overly optimistic NTG uncertainty intervals. The synthetic Stanford VI exercise showed that by using a less optimistic prior distribution, a more relevant NTG uncertainty model was obtained in spite of severe initial over-estimation. In practice, such over-estimation is likely due to preferential location appraisal stage wells.

Amongst the methods available for global uncertainty assessment, the proposed workflow is the most time-consuming and effort-intensive. In return what it provides are more informed models of uncertainty, which reflect a company's geological expertise and historical information. This is valuable information, especially at appraisal

stage when well data is sparse and the stakes are high. Through the case studies, we have shown how to incorporate these diverse sources of information into final models of uncertainty that can be used for financial risk analysis and decision-making.

4.2 Decisions involved in modeling uncertainty

Modeling uncertainty about an attribute requires decisions regarding 1) what are the uncertain parameters 2) which of these uncertain parameters should be randomized and 3) how can they be randomized.

Step one requires determining the main sources of uncertainty related to the attribute under study. In the case of global NTG we identified three major sources of uncertainty: the data, the geological scenario and the prior NTG of that scenario. The data, or the NTG estimate obtained from the data, is the first source of uncertainty. The various hard and soft data are themselves uncertain. For example, cores and well logs are prone to interpretation and measurement uncertainty. Seismic amplitude and derived attributes (for example acoustic impedance) are uncertain because of underlying uncertain velocity models. A NTG estimate obtained from these data is a summary (potentially non-linear) of the data. Hence, it is sensitive to both the data and the estimation algorithm retained. The estimation algorithm consists of a calibration method to obtain facies probability from seismic attributes. Examples of calibration algorithm are Bayes inversion, logistic regression, PCA-based techniques, neural network based techniques, etc. As seen from the Stanford VI and WCA reservoir case studies, the initial NTG estimate has a large impact on the posterior NTG distribution, hence it is very important to account for the uncertainty about this estimate. As required by step 1, we have identified the uncertain parameters involved in NTG estimation. Next, we need to determine which of these parameters should be randomized (i.e. considered uncertain), and finally how can they be randomized.

Figure 4.1 summarizes the workflow used for the WCA reservoir case study. The top part shows that the initial estimate depends on the well data $\mathbf{d}$, the seismic attribute α, and the estimation algorithm Φ. In the case of the WCA resevoir, four wells with facies data, one seismic attribute - acoustic impedance, and one estimation

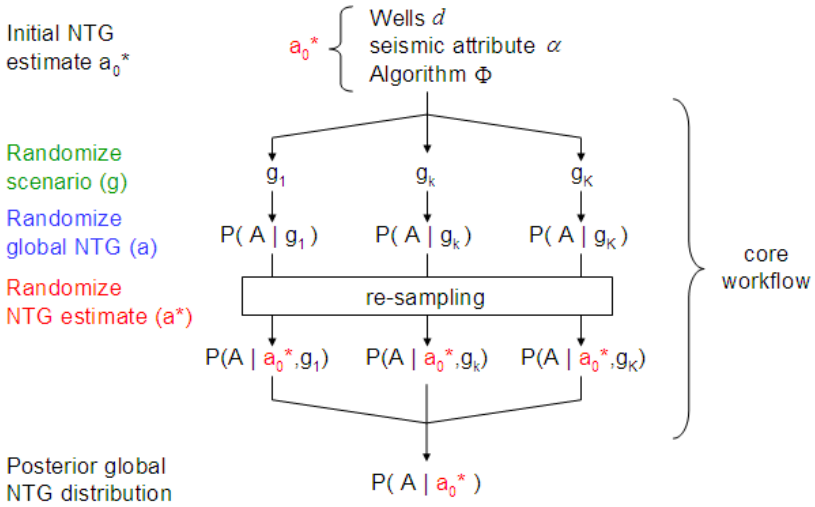

Figure 4.1: Current workflow

algorithm - Bayes inversion, were used to obtain a single initial estimate $a_0^\star$. The geological scenario G was randomized. For each scenario g_k the global NTG A was randomized. The prior probability distribution $P(A|g_k)$ is discretized, and for each class of global NTG a facies realization is simulated to re-sample synthetic wells. This re-sampling is done to assess the uncertainty about the initial estimate by randomizing the well locations. But well location is only one aspect of NTG estimate uncertainty. Suppose that we want to assess the uncertainty about the seismic attribute. Say we have two acoustic impedance data sets α_1 and α_2 obtained from two different velocity models. Figure 4.2 shows how this additional randomization can be incorporated into the proposed workflow.

Instead of one initial estimate $a_0^\star$, we now have two initial estimates $a_{01}^\star$ and $a_{02}^\star$ corresponding to the seismic attributes α_1 and α_2 respectively. The workflow must be carried-out twice, once using $a_{01}^\star$ and then using $a_{02}^\star$. The resulting posterior NTG distributions are denoted $P(A|a_{01}^\star)$ and $P(A|a_{02}^\star)$. Recall that these two estimates use the same well data d and estimation function Φ, but different impedance data sets. Hence, these posterior distributions can also be denoted as $P(A|d, \Phi, \alpha_1)$ and $P(A|d, \Phi, \alpha_2)$. To combine these two posterior distributions into a single posterior

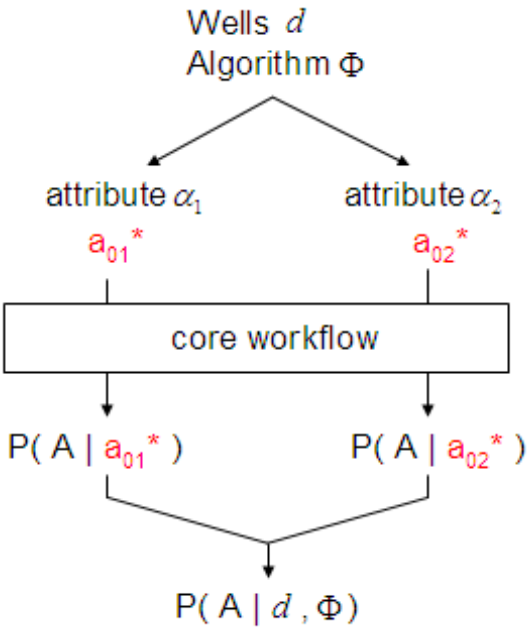

Figure 4.2: Randomize seismic attribute α

distribution given the well data and estimation algorithm $P(A|d,\Phi)$, we need the prior probability of the two impedance data sets, $P(\alpha_1)$ and $P(\alpha_2)$:

$$P(A|d,\Phi) = P(A|d,\Phi,\alpha_1) \times P(\alpha_1) + P(A|d,\Phi,\alpha_2) \times P(\alpha_2) \tag{4.1}$$

This can easily be generalized to multiple acoustic impedance data set case:

$$P(A|d,\Phi) = \sum_i P(A|d,\Phi,\alpha_i) \times P(\alpha_i) \quad ; \quad i = 1,\ldots,n \tag{4.2}$$

Assigning a prior probability to an impedance data data is not a straightforward task. One solution is to assign a probability based upon the confidence on the velocity model. Another alternative is to assume the different impedance data sets to be equally likely.

Now, suppose we want to randomize both the seismic attribute and the estimation function. Assume that we have two seismic attributes α_1 and α_2 and two different

estimation algorithms Φ_1 and Φ_2. Figure 4.3 shows the workflow corresponding to this case. We now have four initial estimates, $a^{\star}_{011}$, $a^{\star}_{012}$, $a^{\star}_{021}$, and $a^{\star}_{022}$. The subscript 0 indicates that it is the estimate from the actual data. The first subscript after zero corresponds to the seismic attribute; the second one corresponds to the estimation algorithm, which reflects the sequence of randomization shown in Figure 4.3. The sequence, however, is not important. The estimation algorithm can be randomized first, followed by the seismic attribute. The workflow must be carried out 4 times for the 4 initial estimates, resulting in 4 corresponding posterior NTG distributions.

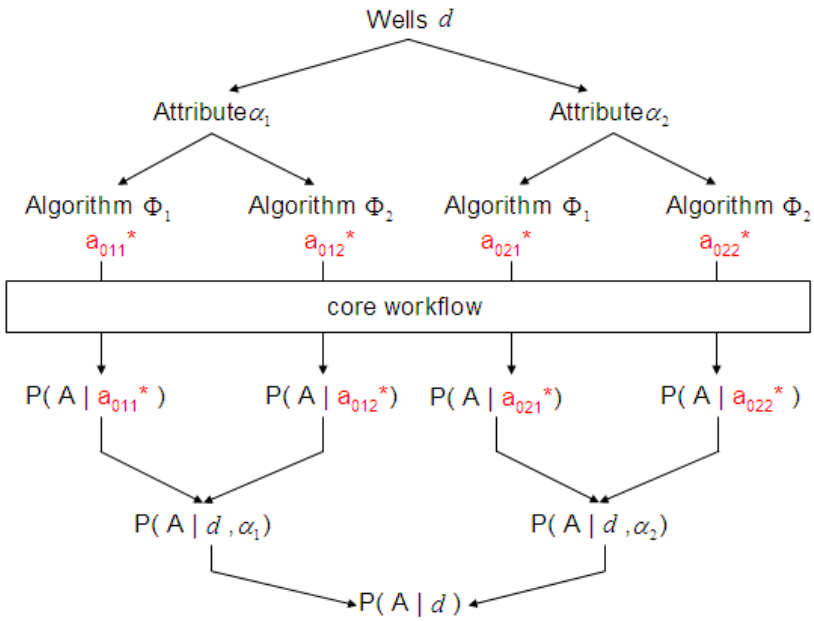

Figure 4.3: Randomize seismic attribute α and estimation algorithm Φ

If the estimation algorithm is randomized first, as in Figure 4.3, then the posterior NTG distributions resulting from estimates $a^{\star}_{011}$ and $a^{\star}_{012}$ are combined into a single posterior given the well data and the first seismic attribute as follows:

$$P(A|d,\alpha_1) = P(A|d,\alpha_1,\Phi_1) \times P(\Phi_1) + P(A|d,\alpha_1,\Phi_2) \times P(\Phi_2) \qquad (4.3)$$

Equation 4.3 calls for the prior probability of estimation algorithms Φ_1 and Φ_2.

It is not obvious how to assign a prior probability to an algorithm. Possible solutions are to treat each algorithm as equally likely or to subjectively assign a probability based on prior experience about the robustness of the algorithm under sparse data conditions. Thus, in this case the probability represents our prior confidence on the algorithm based on prior experience. Similarly, the posterior probability distribution $P(A|d, \alpha_2)$ can be obtained by combining the posterior distributions $P(A|a^{\star}_{021})$ and $P(A|a^{\star}_{022})$. The two posterior distributions corresponding to the two different seismic attributes can be combined into a single posterior distribution given well data through Equation 4.1.

The geological scenario is another major source of uncertainty as seen from the WCA reservoir case study. When randomizing geological scenarios one has to decide 1) how many scenarios should be retained, 2) what level of detail should be contained in the scenarios, 3) which simulation algorithm should be used. The answers to the above questions will naturally vary from one case to another. But, we can draw some lessons from the WCA case study. Originally, we had 8 different training images (Tis) describing the facies variability in the WCA reservoir (Figures 3.2 and 3.3). However, these 8 Tis could be grouped into two categories, one where all facies were channelized and the other in which some facies were channelized and others were in form of lobes. We retained one Ti from the above two categories to study the impact of the scenario on posterior NTG distribution (Figure 3.4). The results showed that the difference between the two posterior distributions was larger when the two scenarios were very different, such as channel vs. lobes, rather than high sinuosity vs. low sinuosity channels. Thus, for WCA reservoir geological uncertainty, it was enough to retain just 2 scenarios out of the 8 originally presented. Thus, the general advise is to group scenarios that are similar and retain the ones that are very different for NTG uncertainty assessment.

As for the level of details, the scenarios should only contain as much detail as is relevant for NTG uncertainty assessment. A sensitivity study should be performed to filter out details that do not have a large impact on NTG estimate and the corresponding uncertainty distributions.

Questions 2 and 3 are linked. The level of detail required would determine which

simulation algorithm should be used. We retained the multiple-point simulation (mps) algorithm *snesim* for the WCA case study because the facies heterogeneity could be conveniently expressed in form of training images. Whatever simulation algorithm is retained, it should be able to condition to all available data (wells and seismic).

If we randomize everything at once, it will be very difficult to keep track of and to interpret the results. Hence, one needs to decide which parameters should be randomized and which can be frozen (fixed). A decision to randomize or fix a parameter, whether it is due lack of time or means, should be justified and carefully documented to aid proper interpretation of the results. Given that so many decisions go into building these uncertainty models, we can safely claim that there is not such thing as an objective model of uncertainty.

4.3 Recommendations for Future Work

The proposed NTG uncertainty workflow is a significant improvement over the previously used methods for global uncertainty assessment. Whether or not a new method is widely used depends on several things:

1. Is the method easy to understand?
2. Is it easy to use?
3. How much time and effort does it require?
4. Does it provide a significant advantage over existing methods?

The pros and cons of the workflow were discussed in Section 4.1. Its main advantages are also its disadvantages. It is both time consuming and effort intensive, but in return it allows more informed decision-making based on uncertainty models that capitalize on a company's geological expertise and historical information. Whether or not this workflow provides a significant advantage over other global uncertainty assessment methods would require a few successful applications.

This thesis has been devoted to understanding, testing, and broadening this workflow. It has been taken apart piece-by-piece and the impact of its various parameters

on the resulting NTG uncertainty models has been documented. The case studies have hopefully explained how to apply it. Additionally, we have provided guidelines about selecting and building geological scenarios, obtaining prior NTG distribution, etc. We have suggested how to randomize certain parameters that were not randomized in the case studies. Suggestions for future work to improve global NTG uncertainty assessment are discussed below.

- Jointly randomize reservoir volume and facies

  Any NTG uncertainty model obtained using this workflow is tied to the sampling domain. The reservoir volume, however, was frozen throughout the NTG uncertainty study. A joint randomization of volume and NTG uncertainty is a top consideration for future work. As discussed in Chapter 1, reservoir volume uncertainty is linked to uncertainty about seismic data processing and interpretation. Time-to-depth conversion is one of the largest sources of uncertainty about the seismic data because of the poorly understood velocity models required for this conversion. In spite of such uncertainty involved, seismic data processing has been largely deterministic. Recently, (Clapp, 2001, 2003) has stochatically generated multiple seismic images by considering alternate velocity models. To account for reservoir volume uncertainty in NTG uncertainty assessment, we can retain different seismic images resulting from widely different velocity models. The reservoir volumes interpreted from these different seismic images would provide top-level randomization for the workflow, since the reservoir volume impacts all aspects of NTG computation and uncertainty assessment.

- Randomize initial NTG estimate

  As seen from the synthetic Stanford VI reservoir and the WCA reservoir case studies, initial NTG estimate has a large impact on the posterior NTG distribution. Instead of retaining a single initial NTG estimate from the appraisal stage data, it might be better to retain multiple NTG estimates resulting from using different seismic attributes and estimation algorithms. See Section 4.2 for

a discussion about how to randomize the NTG estimate and how to incorporate this uncertainty into the posterior NTG distributions.

- Randomize hard data

  Cores and well logs are often treated as "hard" data, but these data are nonetheless uncertain (Akamine and Caers, 2007). Well log uncertainty can be incorporated into the NTG estimation by applying different cut-offs or different interpretations on the initial well logs. This results in different facies interpretations, which in turn yields different initial NTG estimates and possibly different geological scenarios. Running the workflow with the different initial estimates would yield different posterior NTG distributions, which reflect the well log interpretation uncertainty.

- Volume approximations

  Real reservoirs are not uniform boxes; they have pinch-outs, and layers with unequal thickness. Geostatistical simulation of facies and petrophysical properties requires the stratigraphic grid to be transformed into a regular, cartesian grid, where all cells are of equal size (Mallet, 2004). Currently, the impact of this transformation on volumetric computation is ignored. Ways to deal with this change of support from cartesian to stratigraphic grid should be investigated.

- Prior probability for geological scenarios

  To combine posterior NTG distributions resulting from the different geological scenarios, we need a prior probability for each scenario. This can be assigned based on knowledge of geological setting of nearby reservoirs, but still it is a subjective, expert task. If no prior information is available, each scenario can be assumed to be equally likely; this is not an unreasonable assumption at appraisal stage. Geological scenarios are inherently linked to the reservoir data from which they are interpreted, hence uncertainty about a scenario is also linked to the observed data. Computing likelihood of a geological scenario based on observed data by process-based (Sun et al., 2002) or process-mimicking (Pyrcz et al., 2005) models is an exciting avenue of research.

- Utilize other types of data

  In the WCA case study, we used well (cores and well logs) and seismic (acoustic impedance) data for NTG estimation. Production and pressure data, if available at appraisal stage, can provide additional information about the connected volume of reservoir-quality rocks and help improve NTG estimation.

- Resampling with structural constraints

  Appraisal stage wells may be drilled with different objectives, for instance, to evaluate the extent of the reservoir, depth of the water-oil contact (WOC), etc. The proposed workflow cannot be used to assess the uncertainty about reservoir extent or depth of WOC contact. However, if the original drilling strategy consists of drilling in structurally high zones of the reservoir, then resampling can be restricted to those zones by flagging the nodes in the reservoir that are above a certain depth, for instance. In case of multiple constraints, the subset of flagged nodes that honor all constraints are retained. Care should be exercised when imposing constraints; with too many constraints enough replicates may not be available.

- Resample deviated wells

  The four appraisal stage wells in the WCA reservoir were slightly deviated, yet we used vertical wells when re-sampling from facies realizations. Honoring a deviated well geometry when re-sampling is critical in cases when such deviation is strategically done to hit important reservoir zones/features.

- Better reproduction of geological scenarios

  The WCA reservoir case study has shown that geological scenario has a large impact on posterior NTG uncertainty distributions. Multiple-point simulation (mps) algorithms allow a more explicit definition of the structural model in form of Tis; hence were used in the case studies. However, as seen from the realizations of scenario 2 (channel and lobes) in the WCA reservoir, the pattern reproduction can certainly be improved.

- Computing multiple facies proportions from a global NTG value

  In the multiple facies case, additional constraints are required to compute individual facies proportions from a single global NTG value. We proposed to freeze relative facies proportions taken from a training image, prior experience or expert decision, to provide additional constraints. These proportions are uncertain, hence they should be randomized. For cases when it is not appropriate to freeze relative facies proportions, other methods for estimating facies proportions need to be found.

Appendix A

TiGenerator: Object-based image generator

A.1 Introduction

The two presently available multiple-point simulation (mps) algorithms *snesim* (Strebelle, 2002) and *filtersim* (Zhang, 2006) require, as input structural model, a training image (Ti) that is a numerical description of the perceived geological heterogeneity. This training image, is a conceptual representation of the type of structures deemed present in the field/reservoir. A lack of open source, flexible, and easy-to-use programs for generating Tis has been a major stumbling block for the users of mp geostats. For instance, users of the open-source software SGeMS (Remy et al., 2008) use its mp-simulation algorithms *snesim* and *filtersim*, but find the lack of software to generate training images frustrating.

TiGenerator provides a single program to generate different parametric shapes using non-iterative, unconditional Boolean simulation. In addition, any non-parametric shape can be simulated by specifying a rasterized template of that shape. *TiGenerator* is fast because it is unconditional, it is flexible because the pattern distribution of a variety of depositional environments can be modeled using the available shapes and constraints. The various object geometry parameters and orientation can be kept constant or made to follow pre-defined probability distributions. Interaction between

objects can be modeled by specifying erosion and overlap rules.

A.1.1 Review of some commonly used programs

A first requisite to using mp-simulation algorithm is a training image. Information about facies geometry is descriptive and is typically available as 1D sedimentary columns, 2D outcrop sketches in map and cross-sectional view, or 3D block diagram pictures. Creating a 3D image by extrapolating from these 1D and 2D sections is not a trivial task (Caers, 2006). Drawing 3D sedimentary bodies is difficult and time-consuming because it can only be done on one 2D section at a time, leaving open the issue of 3D interpolation. Therefore, sedimentological deposits are generally interpreted in terms of generation processes and/or descriptions of geological bodies. The training images can then be obtained by runs of process-based forward simulations (Tetzlaff and Harbaugh, 1989; Mackey and Bridge, 1992; Bowman and Vail, 1999; Sun et al., 2002; Cojan et al., 2004; Pyrcz et al., 2005); or unconditional object-based simulations (Haldorsen and Chang, 1986; Damsleth et al., 1990; Jones and Larue, 1997; Shmaryan and Deutsch, 1999; Deutsch and Tran, 2002). The problem is that many of these programs are limited to a specific depositional system, can be very complex to use, and are proprietary or commercial (e.g. SBED software[1]). Process-based techniques produce more geologically realistic images than the object-based algorithms, sometimes with lamina-scale details. However, many such details cannot be accounted by mps and are sometimes irrelevant because they do not matter for flow simulation.

Whenever major petrophysical heterogeneity is controlled by geobodies, it is desirable to use object-based simulation to generate Ti because, typically, such simulation is easier to parametrize and implement than process-based models. For example, in a fluvial system, the major petrophysical heterogeneity is related to the geometry of channels, levees, crevasse splays and floodbasin. The program *fluvsim* (Deutsch and Tran, 2002) is a hierarchical, object-based FORTRAN code for modeling such fluvial systems. Being an object-based approach it is difficult to condition to

[1]

dense well data and 3D seismic-based trend data. However, unconditional realizations of *fluvsim* can be used for generating fluvial Tis, while the task of conditioning to data is left to the mp-simulation algorithms.

The program *ellipsim* (Deutsch and Journel, 1998) is a FORTRAN code to generate families of ellipsoids, each with a fixed geometry. It has limited utility because few geological structures can be modeled using only ellipsoids. More importantly, because these programs are separate, modeling interaction between the channel objects of *fluvsim* and ellipsoid objects of *ellipsim* is limited to simple overlap of the images generated.

TiGenerator provides an open source program that is general enough so that different geological systems can be modeled. It utilizes the visualization capabilities of SGeMS , and the resulting training images are in a format compatible with the existing mp-simulation programs in SGeMS. It is written such that new shapes and interaction rules can be easily added to expand its existing scope.

A.1.2 Role of training image in mp simulation

The role of a training image in mp simulation (mps) is often misunderstood, hence, deserves clarification. A training image is a conceptual depiction of patterns and structures that are deemed present in the field/reservoir being simulated. It is not an analogue of the field or phenomenon being modeled. The following points highlight the characteristics of a training image:

- It should be stationary, i.e. it should not depict patterns or pattern clusters that are specific to any sub-area. Indeed in mps, the Ti patterns are pooled together and classified in bins or search trees, hence, their actual location in the Ti is lost.

- It should not have any local accuracy. The patterns taken from the Ti can be reproduced anywhere over the simulation field as long as they honor the local data.

- It should not include any pattern deemed not relevant for mps.

Note: A Ti is not the final structural model actually used by mps. Different mps algorithms process the same Ti differently, hence, the only way to ascertain your input structural model is to generate unconditional realizations using that Ti taken along with a specific mps algorithm. These unconditional simulations represent the implicit structural model that will be used by the data conditioning algorithm.

A.2 Training image generator in SGeMS

The structure of the program is outlined in Algorithm 1.

Algorithm 1 Training image generator

```
1: Initialize a list of geobodies and their input proportions
2: for Each geobody i in the list do
3:    Define a random path visiting each node of the grid
4:    for Each node u along the path do
5:       Draw geobody i
6:       Update the proportion of geobody i
7:       if Simulated proportion ≥ target proportion of geobody i then
8:          Break out of loop
9:       end if
10:   end for
11: end for
12: Repeat for another realization
```

Currently, four parametric shapes (objects) are available: sinusoid, ellipsoid, half-ellipsoid and cuboid. The number of parametric shapes and mechanisms available to model interaction is still limited. However, by varying the dimensions, orientation and sinuosity of these objects and by specifying different interaction rules, many different types of geological scenarios can be modeled. In addition, any non-parametric shape can be input through a text file as a rasterized template. This last feature lends great flexibility to the types of images that can be generated. The four parametric shapes are described below:

Sinusoid In the horizontal plane a sinusoid is parametrized by an amplitude and a wavelength (Figure A.1(a)). Its vertical cross-section is a lower half-ellipse,

which is described by a width and a thickness (Figure A.1(b)). The sinusoid object can be rotated only in the horizontal plane.

Ellipsoid The ellipsoid object is parameterized by a maximum, medium and minimum axis (Figure A.2(a)). It can be rotated only in the horizontal plane.

Half-ellipsoid The vertical upper or lower section of a full ellipsoid. It can be rotated only in the horizontal plane.

Cuboid A rectangular parallelepiped characterized by its X,Y, and Z dimensions (Figure A.2(b)). It can be rotated in both the horizontal and vertical planes.

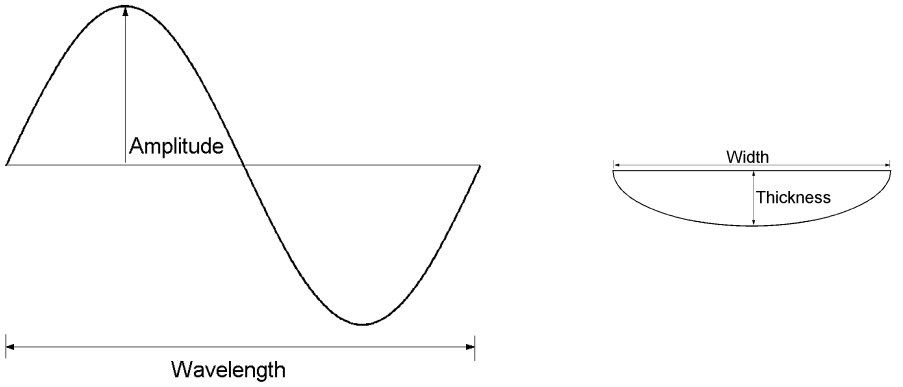

(a) Horizontal view (b) Vertical cross-section

Figure A.1: Horizontal and vertical views of a sinusoid.

Each object geometry and orientation parameter can be made to independently follow three types of distributions: Dirac, uniform or triangular. The user interface for these distributions is shown in Figure A.3.

Constant value or Dirac distribution Completely defined by the single parameter [`Mean`]; it is used to input constant parameters (Figure A.3(a)).

Uniform distribution A uniform distribution is parameterized with [`Min`] and [`Max`], the lower and the upper bounds of the distribution (Figure A.3(b)).

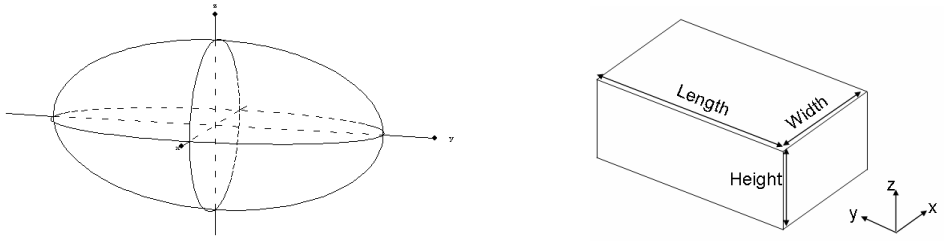

(a) Ellipsoid (b) Cuboid

Figure A.2: Ellipsoid and Cuboid objects.

Triangular distribution A triangular distribution is parameterized with [`Min`], [`Mode`] and [`Max`], the lower bound, the mode and the upper bound of the distribution (Figure A.3(c)).

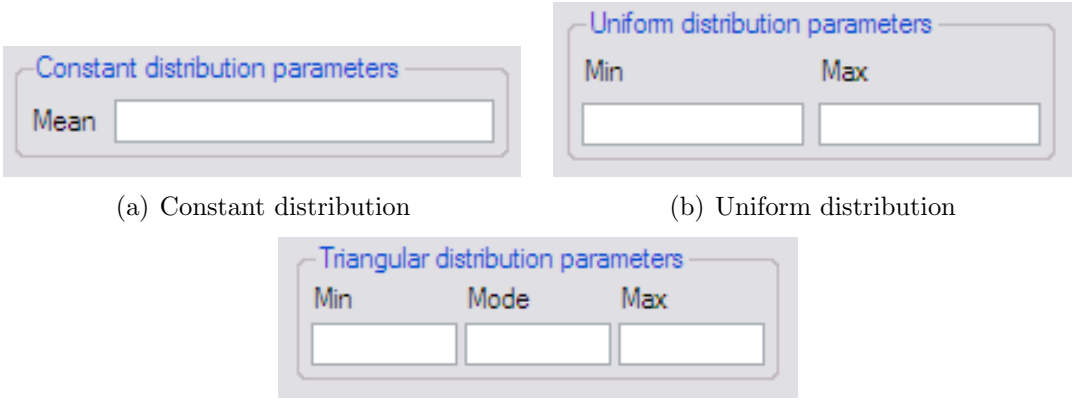

(a) Constant distribution (b) Uniform distribution

(c) Triangular distribution

Figure A.3: User interface to specify the distribution of object geometry and orientation.

A.2.1 Object interaction

A training image must depict not only each object, but also how these objects spatially relate with each other. Geological events cause objects to overlap and erode one

another. In *TiGenerator* these spatial relationships between objects are modeled by user-specified erosion and overlap rules.

Erosion rules: Erosion rules must be specified between a geobody and all geobodies that are simulated prior to it. A geobody can either erode (code 1) or be eroded by (code 0) the previously simulated geobodies. All geobodies erode the background facies by default.

Overlap rules: Overlap rules help constrain the fraction of volumetric overlap between two geobodies. The overlap is controlled by two parameters, minimum overlap and maximum overlap, which are bounded by [0, 1]. For each geobody, the user must specify an overlap rule with all previous geobodies. If the volumetric overlap between two geobodies is to be the same, then minimum and maximum overlap should be set equal.

To illustrate some end member overlap cases consider the example of a three facies training image - background, ellipsoid and cuboid - simulated in that order. Prior to any geobody simulation all grid nodes are set to background facies. The ellipsoid object is simulated first. No erosion or overlap rules need to be specified for the ellipsoid object because it is simulated first. The cuboid objects, which are simulated next (second), erode the ellipsoids. Consider the following four cases of overlap between the cuboid and ellipsoid objects: if, for the cuboid object, min overlap and max overlap are both set to 0, then the two geobodies will not be in contact (Figure A.4(a)). On the other hand, if min and max overlap are both set to 1, then cuboids will be completely contained within the ellipsoids (Figure A.4(b)). Setting min overlap to 0.01 will ensure that cuboids are attached to ellipsoids (Figure A.4(c)). If no specific overlap relationship exists between the two geobodies then set min overlap to 0 and max overlap to 1, which results in a random overlap (Figure A.4(d)).

Warning: It is the user's responsibility to ensure consistency between the different overlap rules. If one or more geobodies cannot be simulated due to inconsistent overlap criteria, then the simulation can be stopped by clicking Abort on the progress bar.

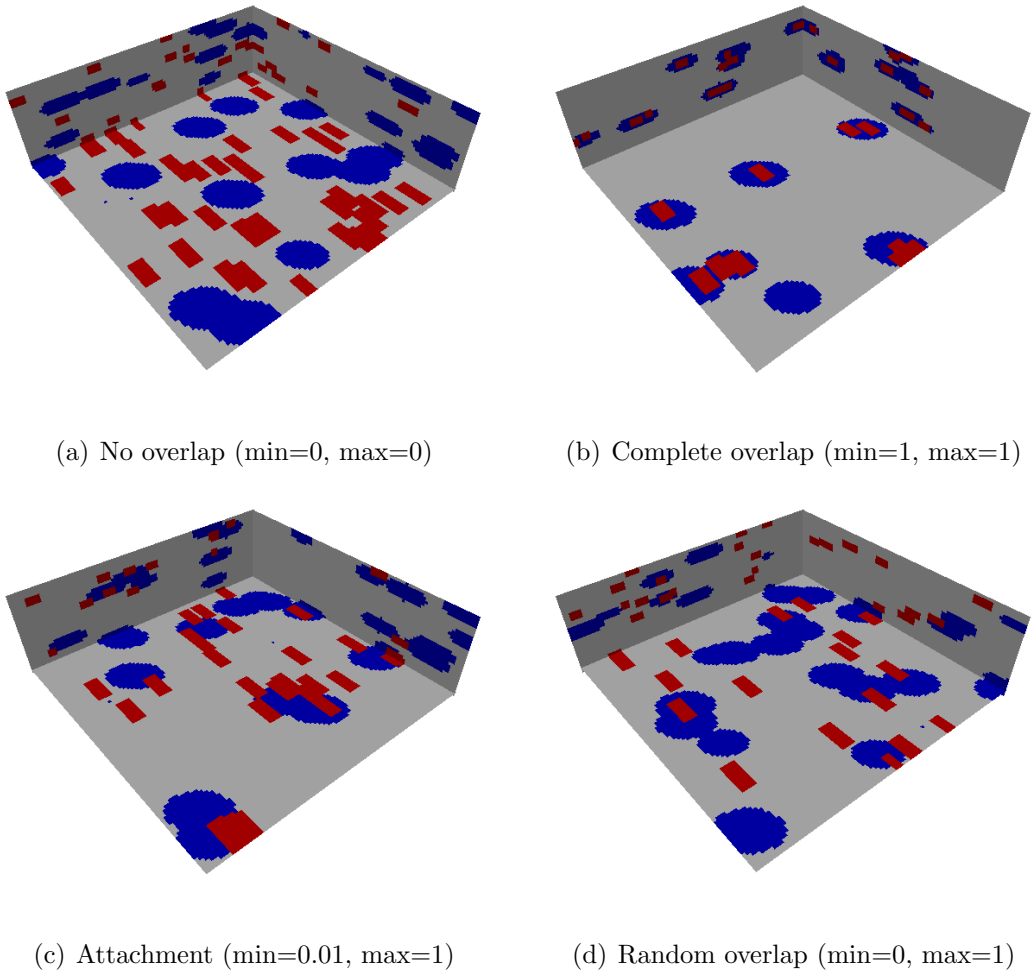

(a) No overlap (min=0, max=0)

(b) Complete overlap (min=1, max=1)

(c) Attachment (min=0.01, max=1)

(d) Random overlap (min=0, max=1)

Figure A.4: Examples of interaction between ellipsoid and cuboid objects using different values of minimum and maximum overlap values. The values specified are for the cuboid object.

A.2.2 Description of input parameters

The *TiGenerator* algorithm is activated from *Utilities* | *TiGenerator* in the algorithm panel. The main *TiGenerator* interface is given in Figure A.6(a), and the parameters are described below. The text inside [ ] is the corresponding keyword in the TiGenerator parameter file.

1. **Simulation Grid Name** [`ti_grid`]: The name the simulation grid.

2. **Property Name Prefix** [`ti_prop_name`]: Prefix for the simulation output. The suffix __real# is added for each realization.

3. **Nb of realizations** [`nb_realizations`]: Number of simulations to generate.

4. **Seed** [`seed_rand`]: Seed for the random number generator (should be a large odd integer).

5. **Nb of geobodies** [`nb_geobodies`]: Number of different geobody types to be simulated. Minimum value of this parameter is set to 1 (at least one geobody must be simulated). Total number of facies in the Ti is equal to the number of geobodies plus the background facies (index 0).

6. **Geobody information**: Information about a geobody is collected using a geobody selector [`geobodySelector`]. For each geobody the following input is required: geobody type [`gbType`], geobody parameters, proportion [`gbProp`], and interaction rules with all previously simulated geobodies. Note that the geobodies are simulated in the order in which they are specified. Select one geobody type from the drop-down menu and click on the adjacent push button to invoke the corresponding geobody dialog. The geobody parameters can either be set as constant or specified as a uniform or triangular distribution (Figure A.3). All dimensions should be specified in number of cells. Rotation for all geobodies, except the cuboid, is limited to the horizontal plane (Figure A.5(a)). The cuboid object can be rotated in both the horizontal (azimuth) and vertical (dip) planes (Figure A.5). The types of geobodies available in *TiGenerator* and a description of their parameters are as follows

Sinusoid The dimensions of the sinusoid object are determined by three parameters: length [sinLen], width [sinWid] and thickness [sinThk]. The horizontal sinuosity is specified by an amplitude [sinAmp] and a wavelength [sinWvl]. Horizontal orientation of the sinusoid [sinRot] is specified as clockwise rotation in degrees from North (y axis).

Ellipsoid The geometry of the ellipsoid object is determined by three radii: Max radius [ellipMaxr], Med radius [ellipMedr], and Min radius [ellipMinr]. Ellipsoid orientation [ellipRot] is specified as clockwise rotation in degrees from North (y axis).

Half-ellipsoid The half-ellipsoid object can be either a lower half ellipsoid [lhellip] or an upper half ellipsoid [uhellip]. Its geometry is determined by three radii: Max radius [hellipMaxr], Med radius [hellipMedr], and Min radius [hellipMinr]. Half-ellipsoid orientation [hellipRot] is specified as clockwise rotation in degrees from North (y axis).

Cuboid The cuboid object has three parameters: length [cubLen], width [cubWid] and height [cubHgt]. Cuboid orientation is specified through two angles: [cubRotStrike] is clockwise azimuth rotation in degrees from North (y axis), and [cubRotDip] is dip rotation in degrees from the horizontal plane.

User-defined User-defined shape refers to any rasterized shape provided by the user through a text file [filename]. The file should contain three columns and as many lines as number of points in the raster. Each line contains, separated by spaces, the i, j, and k coordinates of a point in the raster relative to a center location (0, 0, 0). The shape need not be symmetric. Orientation [udefRot] is specified as clockwise rotation in degrees from North (y axis). The user-defined shape can be scaled by providing scaling factors in x, y, and z directions [udefScal]; these factors should be greater than zero.

For any given geobody, the interaction with previous geobodies must be specified by invoking the Interaction dialog shown in Figure A.6(b). Three type of interaction rules are required.

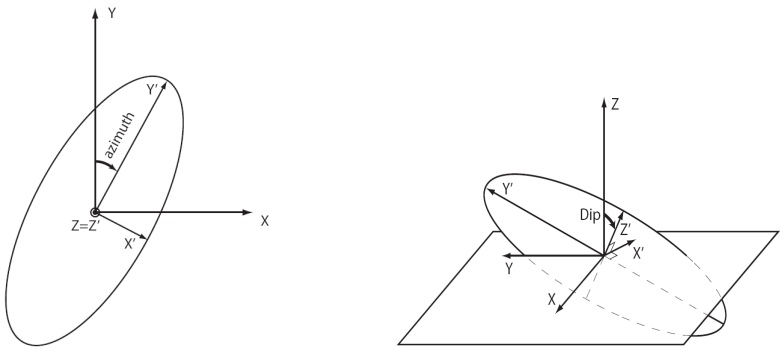

(a) Azimuth (b) Dip

Figure A.5: Rotation convention for the different geobodies.

7. **Erosion rules with previous geobodies**: The erosion rules are specified as a space-separated string of 0s and 1s. If the current geobody erodes a previous geobody, then the erosion value is 1 otherwise it is 0. For the first geobody this field should be left blank as there are no previously simulated geobodies.

8. **Overlap with previous geobodies**: The overlap rules control the fraction of volumetric overlap between two geobodies. It is specified as a pair of minimum [`min`] and maximum [`max`] overlap values, which are between [0, 1]. For the first geobody these fields should be left blank as there are no previously simulated geobodies. See Section A.2.1 for more information about overlap rules.

9. **No overlap with self**: The minimum and maximum overlap rules are for modeling overlap with previous geobodies. If no overlap is desired between geobodies of the same type (i.e. same index), then this box should be checked.

A.3 Examples of training images generated using *TiGenerator*

Some example training images and their corresponding parameters are presented in this section. The simulation grids in Figures A.7 and A.8 each contain 100 x 100 x

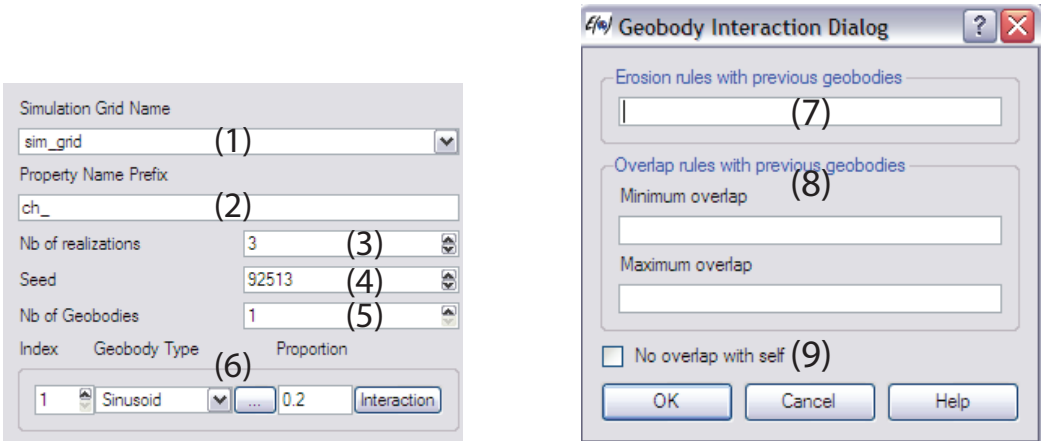

(a) Main interface

(b) Object interaction dialog

Figure A.6: User interface for the *TiGenerator*.

30 grid blocks.

Figure A.7(a) shows a channelized training image. Channels are modeled using the sinuosoid objects and all their parameters are kept constant. The horizontal channels are oriented at 15 degrees from North and are cut by fractures which are striking North and dipping at 45 degrees. Fractures are modeled using elongated cuboids and they erode the channels. The input channel proportion is 0.10; the simulated proportion in Figure A.7(a) is 0.09. Note that input geobody proportions may not be honored exactly due to erosion by other objects and discretization round-ups.

Figure A.7(b) depicts a three facies Ti with background, channels and crevasse splays simulated in that order. The channels are modeled using sinusoids, which are oriented at 15 degrees from North and all their parameters are kept constant. Crevasse splays are modeled by small ellipsoid objects which are oriented at 15 degrees. The crevasse splays are forced to be attached to the channels by specifying a minimum overlap of 0.01. To prevent excess overlap between the channels and the crevasse splays, their maximum overlap is set to 0.02. The simulated proportion of channels is smaller than the input proportion partly due to the erosion by crevasse splays. With some practice, the user should be able to factor-in the impact of such erosion and overlap on his input proportions. The parameters used for generating the training

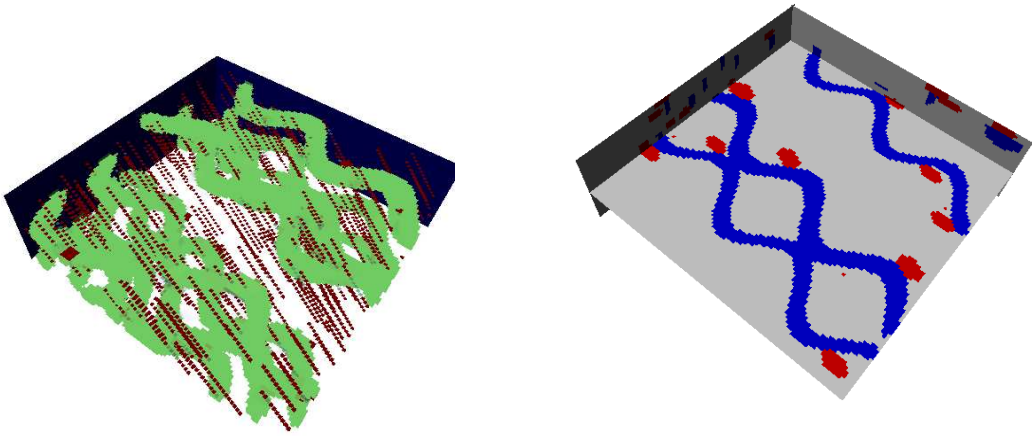

(a) Channels cut by fractures

(b) Channels with crevasse-like attachment

Figure A.7: Examples of parametric shapes generated using the *TiGenerator*.

images in Figure A.7 are given in Section A.5 (Figures A.11 to A.16).

Figure A.8(a) shows a training image generated using a user-defined template (Figure A.9). The file used for specifying this template is given in Section A.5. This feature adds great versatility to the type of shapes that can be generated with the *TiGenerator*. All object interaction rules described in Section A.2.1 are also applicable to the user-defined shapes. For example, Figure A.8(b) shows the non-parametric crevasse splays attached to channels. The user-defined shapes can be scaled as well as rotated (Figure A.10). Figure A.10(c) shows the user-specified crevasse striking at 45 degrees and stretched twice its original size (Figure A.10(a)). Note that some shapes may not maintain their original characteristics when rotated and scaled due to the discrete domain. In such cases it is better to provide a rotated or scaled raster as input shape. The parameters used for generating the training images in Figure A.8 are given in the Section A.5 (Figures A.12, A.17, and A.18).

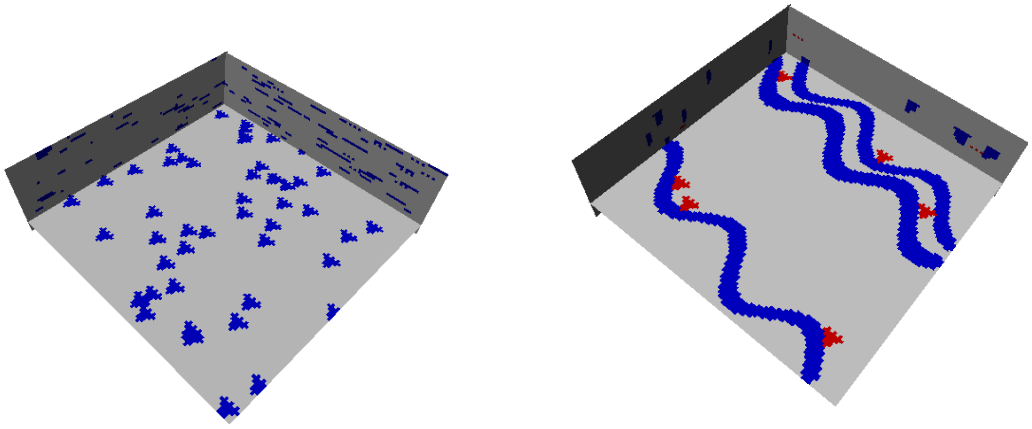

(a) User-defined shape

(b) Channels with crevasse-like attachment

Figure A.8: Examples of training images containing both parametric and user-defined shapes.

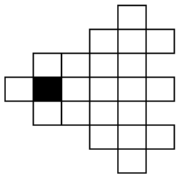

Figure A.9: Rasterized template of crevasse splays used in Figure A.8. The shaded node is the center (0,0,0); all other nodes are specified with respect to this center location. See Section A.5 for the location of all nodes.

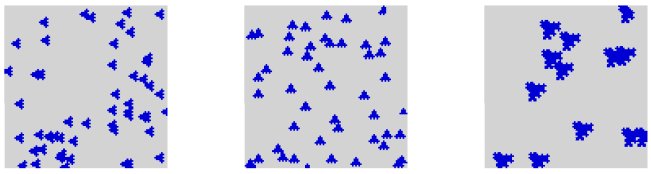

(a) Original raster

(b) 90^o rotation

(c) 45^o rotation; 0.5 scaling

Figure A.10: Rotation and scaling of user-defined shapes.

A.4 Adding new shapes and object interaction features

This section is intended for developers who would like to expand the existing capabilities of *TiGenerator* by adding new parametric shapes or object interaction features. The basic structure of the program is outlined and implementation of interaction rules is explained. Modifications required to the user interface is described briefly.

A.4.1 Adding new shapes

TiGenerator is designed using the object-oriented paradigm to take advantage of the inheritance mechanism of C++. The program lends itself particularly well to an object-oriented design. Each parametric shape in *TiGenerator* is a self-contained class, which is derived from an abstract base class called Geobody. Each class contains all information about a particular shape, including its interaction with other geobodies. The Geobody class contains an empty constructor, a destructor, and four additional functions:

- draw
- get_geobody_index
- get_rasterized_vol
- reset_rasterized_vol

To add a new parametric shape to *TiGenerator*, derive a new sub-class from the Geobody class for that shape. The constructor of the new class should initialize all the parameters relevant to the shape. For instance, the geometry parameters of the Cuboid class are different from those of the Ellipsoid class; hence, their constructors have different input parameters. In addition to implementing a constructor and a destructor, override the aforementioned four functions of the Geobody class. Additional helper functions may be added as necessary. Refer to the source code of currently available objects in the TiGenerator project as an example.

The structure of the main program was outlined in Algorithm 1 (see Section A.2). Each SGeMS plug-in contains an initialize and an execute function. All algorithm parameters are read from the graphical user interface and initialized in the initialize function. The main loop of the algorithm is implemented in the execute function of TiGenerator.cpp file in the TiGenerator project. Because of the object-oriented design, no change is required in the execute function when a new object or interaction feature is introduced. However, new function(s) to initialize the parameters of the new object must be implemented in the initialize function in the TiGenerator.cpp file.

A.4.2 Modifying the user interface

The name of the newly defined object must be added to the geobodySelector widget (Figure A.6(a)) so that the users can access it. This custom-made Qt widget was designed specifically for use with *TiGenerator*. It can be accessed in TiWidgets project, which is separate from the TiGenerator project. A new Qt dialog must be written for the new object for input of parameters. This dialog should pop-up when the new object is selected. New accessor functions need to be implemented in the ti_qtAccessors.cpp file to access and set the value of the parameters on the new dialog. Refer to any exisiting object dialog in the TiWidgets project as an example.

A.4.3 Implementing new object interaction rules

Currently, two types of interaction rules are available for the different geobodies: erosion rules and overlap rules. The erosion rules class is fairly simple; it stores the vector of erosion rules. Similarly, the overlap rules class stores the vectors of minimum and maximum overlap rules.

For each geobody, these classes are initalized from the values specified by the user and then passed to the geobody constructor. The task of enforcing the rules is delegated to the geobody. For instance, to enforce the overlap rules at a given location, before drawing itself, a geobody will check if the minimum and maximum overlap criteria with all previously simulated geobodies are satisfied or not. To add a

new geobody interaction rule, create a new class for that rule. Modify the Interaction Dialog in the TiWidgets project to input the parameters for the new interaction rules. Write new function(s) to initialize an object of this class and then pass it to the corresponding geobody constructor. Then modify the draw function of each geobody class so that the new interaction rule is honored while drawing that geobody.

A.5 Parameter files

Raster template corresponding to the user-defined shape shown in Figure A.9.

```
0 0 0
-1 0 0
1 0 0
0 -1 0
0 1 0
1 1 0
1 -1 0
2 0 0
2 1 0
2 -1 0
2 2 0
2 -2 0
3 0 0
3 1 0
3 -1 0
3 2 0
3 -2 0
3 3 0
3 -3 0
4 0 0
4 2 0
4 -2 0
```

Parameter files corresponding to the examples in Figures A.7 and A.8.

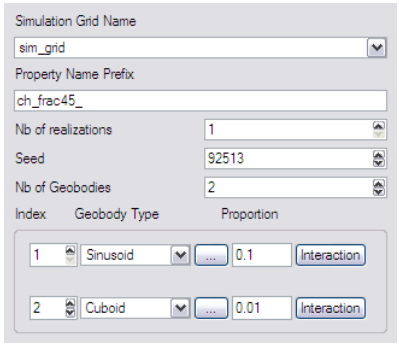

Figure A.11: Main interface parameters for the channel and fractures Ti shown in Figure A.7(a).

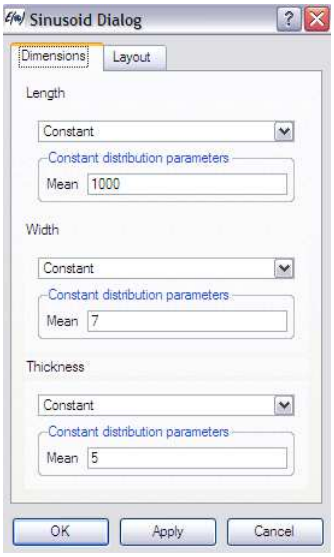

(a) Sinusoid dimensions

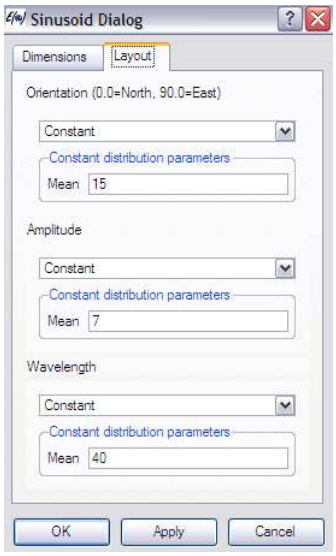

(b) Sinusoid horizontal layout

Figure A.12: Parameters for the sinusoid object in Figures A.7 and A.8. Interaction rules are left blank for the sinusoid object because it is simulated first in all examples.

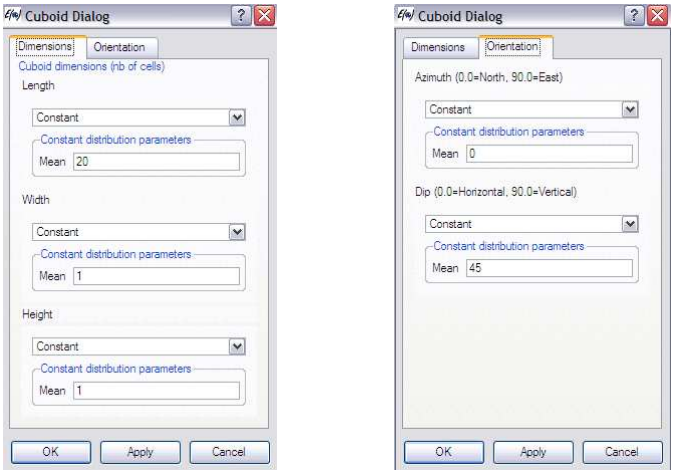

(a) Cuboid dimensions (b) Cuboid orientation

Figure A.13: Parameters for the cuboid object shown in Figure A.7(a).

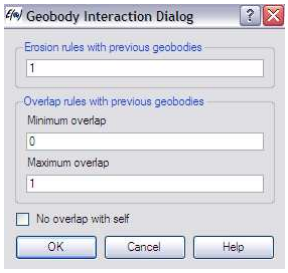

Figure A.14: Interaction rules for the cuboid object shown in the channel and fracture Ti of Figure A.7(a).

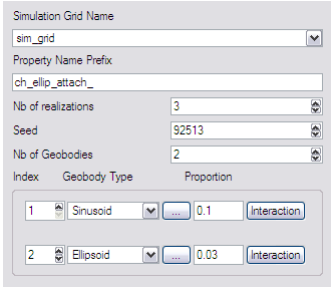

Figure A.15: Main interface parameters for the channel and ellipsoid Ti shown in Figure A.7(b).

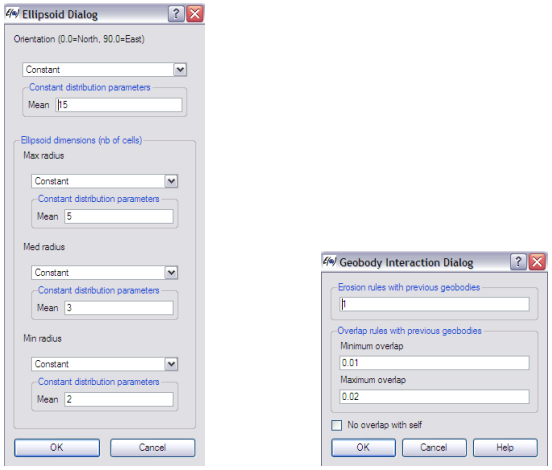

(a) Dimensions (b) Interaction rules

Figure A.16: Parameters for the ellipsoid object shown in Figure A.7(b).

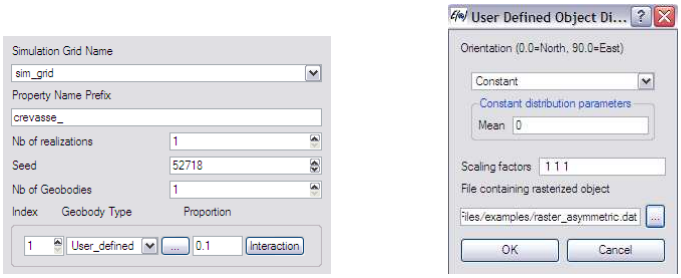

(a) Main interface (b) User-defined shape

Figure A.17: Main interface and parameters for the user-defined shape Ti shown in Figure A.8(a).

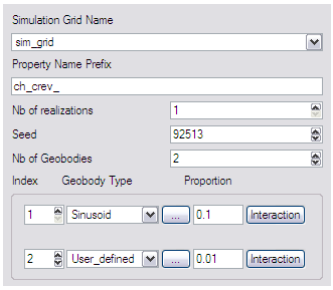

(a) Main interface

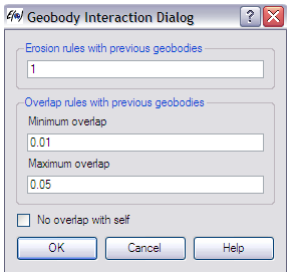

(b) User-defined shape interaction rules

Figure A.18: Main interface and interaction rules for the user-defined shape shown in Figure A.8(b). All other parameters for the user-defined shape in this Ti are similar to those given in Figure A.17(b).

Bibliography

Akamine, J. and Caers, J.: 2007, A workflow to account for uncertainty in well-log data in 3d geostatistical reservoir modeling, *20th Annual Report, Stanford Center for Reservoir Forecasting*, Stanford University.

Bassiouni, Z.: 1994, *GSLIB: Geostatistical Software Library and User's Guide*, Society of Petroleum Engineers, New York.

Bitanov, A. and Journel, A.: 2004, Uncertainty in n/g ratio in early reservoir development, *Journal of Pet. Sci.& Engr.* **44**(1-2), 115–131.

Biver, P., Haas, A. and Bacquet, C.: 2002, Uncertainties in facies proportion estimation, ii. application to geostatistical simulation of facies and assessment of volumetric uncertainties., *Mathematical Geology* **34**(6), 703–714.

Biver, P., Mostad, P. F. and Gillou, A.: 1996, An overview of different techniques to quantify uncertainties on global statistics for geostatistical modeling., *in* E. Y. Baafi and N. A. Schofield (eds), *Fifth Annual Geostatistics Congress Proceedings*, Vol. 1, Wollongong, South Africa, p. 573584.

Bowman, S. A. and Vail, P. R.: 1999, Interpreting the stratigraphy of the baltimore canyon section, offshore new jersey with phil, a stratigraphic simulator., *in* J. Harbaugh, W. Watney, E. Rankey, R. Slingerland, R. Goldstein and E. Franseen (eds), *Numerical Experiments in Stratigraphy: Recent Advances in Stratigraphic and Sedimentologic Computer Simulations*, SEPM Special Publication, p. 117138.

Caers, J.: 2006, A general algorithm for building 3d spatial laws from lower dimensional structural information, *19th Annual Report, Stanford Center for Reservoir Forecasting*, Stanford University, CA.

Caers, J. and Ma, X.: 2002, Modeling conditional distributions of facies from seismic using neural nets, *Mathematical Geology* **34**(2), 139–163.

Castro, S., Caers, J. and Mukerji, T.: 2005, The stanford vi reservoir, *18th Annual Report, Stanford Center for Reservoir Forecasting*, Stanford University.

Caumon, G. and Journel, A.: 2004, Reflections on early uncertainty assessment: Application to a hydrocarbon reservoir development, *Seventh Annual Geostatistics Congress Proceedings*, Banff, Alberta, Cananda.

Caumon, G., Strebelle, S., Caers, J. and Journel, A.: 2004, Assessment of global uncertainty for early appraisal of hydrocarbon fields, *In SPE Annual Technical Conference and Exhibition, SPE paper 89943*, Houston, TX.

Chiles, J. and Delfiner, P.: 1999, *Geostatistics*, John Wiley & Sons, Inc., New York.

Clapp, R.: 2001, Multiple realizations: Model variance and data uncertainty, *Stanford Exploration Project Report. 108*, Stanford, CA.

Clapp, R.: 2003, Multiple realizations and data variance: Successes and failures, *Stanford Exploration Project Report. 113*, Stanford, CA.

Cojan, I., Fouche, O., Lopez, S. and Rivoirard, J.: 2004, Processed-based reservoir modelling in the example of meandering channel, *Seventh Annual Geostatistics Congress Proceedings*, Banff, Alberta, Canada.

Damsleth, E., Tjolsen, C., Omre, K. and Haldorsen, H.: 1990, A two-stage stochastic model applied to a north sea reservoir., *In 65th SPE Annual Technical Conference and Exhibition*, New Orleans, LA, pp. 791–802.

Deutsch, C. and Journel, A.: 1998, *GSLIB: Geostatistical Software Library and User's Guide*, Oxford University Press, New York.

Deutsch, C. and Tran, T.: 2002, Fluvsim: a program for object-based stochastic modeling of fluvial depositional systems, *Computers and Geosciences* (28), 525–535.

Efron, B.: 1979, Bootstrap methods: Another look at the jackknife, *Ann. Stat.* **7**, 1–26.

Fournier, F. and Derain, J.: 1995, A statistical methodology for deriving reservoir properties from seismic data, *Geophysics* **60**(5), 1437–1450.

Goovaerts, P.: 1997, *Geostatistics for natural resources evaluation*, Oxford University Press, New York.

Haas, A. and Formery, P.: 2002, Uncertainties in facies proportion estimation, i. theoretical framework: the dirichlet distibution., *Mathematical Geology* **34**(6), 679702.

Haldorsen, H. and Chang, D.: 1986, Notes on stochastic shales: from outcrop to simulation model., *in* L. Lake and H. Caroll (eds), *Reservoir Characterization*, Academic Press, London, p. 445485.

Jones, T. and Larue, D.: 1997, Object-based modeling and deepwater depositional systems., *in* Pawlowsky-Glahn (ed.), *Proceedings of IAMG97*, p. 438443.

Journel, A. G.: 1993, Resampling from stochastic simulations, *Environ. Ecol. Stat* **1**, 63–83.

Lantuejoul, C.: 2002, *Geostatistical Simulation: Models and Algorithms*, Springer, New York.

Mackey, S. and Bridge, J.: 1992, A revised fortran program to simulate alluvial stratigraphy, *Computers and Geosciences* **18**(2), 119–181.

Maharaja, A.: 2005, Hierarchical simulation of multiple-facies reservoirs using multiple-point geostatistics, *In SPE Annual Technical Conference and Exhibition, SPE paper 97774*, Dallas, TX.

Maharaja, A.: 2006, Assessing uncertainty on net-to-gross at the appraisal stage: Application to a west africa deep-water reservoir, *19th Annual Report, Stanford Center for Reservoir Forecasting*, Stanford University.

Mallet, J.-L.: 2004, Space-time mathematical framework for sedimentary geology, *Mathematical Geology* **36**(1), 1–32.

Norris, R., Massonat, G. and Alabert, F.: 1993, Early quantification of uncertainty in the estimation of oil-in-place in a turbidite reservoir, *In SPE Annual Technical Conference and Exhibition, SPE paper 26490*, Houston, TX.

Pyrcz, M., Catuneanu, O. and Deutsch, C.: 2005, Stochastic surface-based modeling of turbidite lobes, *AAPG Bulletin* **89**(2), 177–191.

Remy, N., Boucher, A. and Wu, J.: 2008, *Applied Geostatistics with SGeMS: A User's Manual*. To be published.

Sheriff, R. and Geldart, L.: 1995, *Exploration Seismology*, second edn, Cambridge University Press, New York.

Shmaryan, L. and Deutsch, C.: 1999, Object-based modeling of fluvial / deepwater reservoirs with fast data conditioning: Methodology and case studies, *In SPE Annual Technical Conference and Exhibition, SPE paper 56821*, Houston, TX.

Strebelle, S.: 2002, Conditional simulation of complex geological structures using multiple-point statistics, *Mathematical Geology* **34**(7), 1161–1168.

Strebelle, S., Payrazyan, K. and Caers, J.: 2002, Modeling of a deepwater turbidite reservoir conditional to seismic data using multiple-point geostatistics, *In SPE Annual Technical Conference and Exhibition, SPE paper 77425*, San Antonio, Texas.

Sun, T., Paola, C., Parker, G. and Meakin, P.: 2002, Fluvial fan deltas: Linking channel processes with large-scale morphodynamics, *Water Resources Research* **38**(8), 10.

Tetzlaff, D. M. and Harbaugh, J. W.: 1989, *Simulating Clastic Sedimentation*, Van Nostrand Rheinhold, New York.

Zhang, T.: 2006, *Filter-based Training Pattern Classification for Spatial Pattern Simulation*, PhD thesis, Stanford University, CA.